Stellingen behorende bij het proefschrift

Design
of Fibre Reinforced Composite Panels
for Aerospace Applications

P.G. van Bladel

1. Onder drukbelasting zal de knikvorm van een rechthoekig, opgelegd, orthotroop paneel in een van de hoofdrichtingen altijd één halve golf hebben.

2. Een ontwerp van een sandwichpaneel voor drukbelasting waarbij de (stijve) buitenlagen net niet bezwijken, en waarbij de (lichtgewicht) kern net dik genoeg is om knik te voorkomen, is niet altijd het lichtste ontwerp.

3. Bij optimalisatie van composietpanelen is het nodig rekening te houden met de standaarddiktes van de materialen waaruit deze gemaakt zullen worden.

4. Discrete optimalisatie van laminaten en sandwichpanelen op de wijze zoals dat in dit proefschrift wordt uiteengezet, kan vele gelijkwaardige optima opleveren. Derhalve hoeft een ontwerper vaak geen toevlucht te nemen tot een "exotische" laminaatopbouw om een goed ontwerp te realiseren; een "gewoon" laminaat (0°,±45° en 90°) zal dan volstaan.

5. Discrete optimalisatie van gegolfde platen geeft in het algemeen geen gelijkwaardige optima. Wel kunnen lokale optima optreden die het moeilijk maken voor het optimalisatieproces om het globale optimum te vinden.

6. Naast geavanceerde rekenmodellen, die rekenintensief zijn en gedetailleerde resultaten geven, hebben ook eenvoudiger modellen bestaansrecht. Deze sluiten beter aan op de behoeften van de ontwerper die aan het begin van het ontwerptraject staat, en geven inzicht in de verschillende aspecten die een rol spelen bij het ontwerpen.

7. Donovan, Goland en Goodier stellen (in *J of Appl Mech* XII(1), March 1945) dat theoretische optimalisatie zin heeft. Weliswaar, zo stellen zij, worden er enkel theoretisch ideale resultaten mee bereikt, maar het is nuttig deze bovengrenzen, het maximaal haalbare te vinden. De hier beschreven computerprogramma's SAPANO en COPANO houden echter veel meer rekening met de concrete technische randvoorwaarden en hun resultaten hebben daarmee ook praktische waarde.

8. "La machine elle-même, plus elle se perfectionne, plus elle s'efface derrière son rôle. Il semble que tout l'effort industriel de l'homme, tous ses calculs, toutes ses nuits de veille sur les épures, n'aboutissent, comme signes visibles, qu'à la seule simplicité, comme s'il fallait l'expérience de plusieurs générations

STELLINGEN

pour dégager peu à peu la courbe d'une colonne, d'une carène, ou d'un fuselage d'avion, jusqu'à leur rendre la pureté élémentaire de la courbe d'un sein ou d'une épaule (...), jusqu'à ce qu'on ne la remarque plus (...) Il semble que la perfection soit atteinte non quand il n'y a plus rien à ajouter, mais quand il n'y a plus rien à retrancher. Au terme de son évolution, la machine se dissimule."
<div align="right">A. de Saint Exupéry, Terre des hommes, Éds. Gallimard 1939, p. 59-60
(vertaling: zie onderaan)</div>

9. Met het *Internet* is het als met de tv: het medium zelf heeft geen grenzen. Die moeten dus in de gebruiker aanwezig zijn.

10. Waar de christenen de sociale consequenties van het geloof dat God drie-één is, beseffen en weten te incarneren, zal een gemeenschapsleven ontstaan zoals dat van de eerste christenen beschreven staat, en dat verder gaat dan de privé sfeer.

11. De functie $y=1/x$ wordt groter naarmate x vanuit het positieve naar nul gaat. Zo verwezenlijkt de mens zich meer naarmate hij zich in zelfgave ontledigt.

Vertaling van stelling 8: "Hoe meer een machine zich perfectioneert, des te meer vervaagt zij achter haar functie. Het lijkt of alle industriële inzet van de mens, alle berekeningen, alle nachten gebogen over projectietekeningen, als enig zichtbaar resultaat de eenvoud zelf opleveren. Het is alsof we de ervaring van verschillende generaties nodig hebben gehad om beetje bij beetje de kromming van een pilaar, van een stroomlijn of van een vliegtuigromp te bevrijden, tot ze de elementaire zuiverheid hebben van de kromming van een borst of van een schouder (...), zodat men ze niet eens meer opmerkt (...) Het lijkt erop dat de perfectie niet bereikt wordt wanneer er niets meer toe te voegen valt, maar wanneer er niets meer af kan. In de limiet van zijn evolutie verbergt de machine zichzelf."

Design
of Fibre Reinforced Composite Panels
for Aerospace Applications

P.G. van Bladel

Faculty of Aerospace Engineering

Delft University of Technology

Acknowledgement

Table of Contents

Notation

a	[mm]	length of panel in x-direction
a_i, a_{ij}	[-]	coefficients in interpolations [i,j=0,1,2]†
A_{ij}	[N/mm]	submatrix of ABD-matrix of classical laminate theory [i,j=1,2,6]
A_{ii}	[N/mm]	elementary transverse shear stiffness [i=4,5]
A_{ii}^{τ}	[N/mm]	elementary transverse shear stiffness assuming constant transverse shear stress [i=4,5]
A, A_{mn}	[mm]	out-of-plane deformation amplitude
b	[mm]	width of panel in y-direction
b_i	[mm]	width of faces of corrugated panel [i=1,2]
B_{ij}	[N]	submatrix of ABD-matrix of classical laminate theory [i,j=1,2,6]
C_{ij}	[mm^2/N]	compliance matrix of classical laminate theory [i,j=1,2,6]
d	[mm]	corrugation depth
D_{ij}	[Nmm]	submatrix of ABD-matrix of classical laminate theory [i,j=1,2,6]
$D_{ij\,fk}$	[Nmm]	D_{ij}-matrix of face k [k=1,2]
D_{ij}^{*}	[Nmm]	reduced bending stiffness matrix [i,j=1,2,6]
D_{ij}^{**}	[Nmm]	alternative reduced bending stiffness matrix (assuming cylindrical bending) [i,j=1,2,6]
e	[mm]	eccentricity
E, E_i	[MPa]	Young's modulus [i=x,y]
$E_f{'}$	[MPa]	reduced Young's modulus of sandwich panel
E_{long}	[MPa]	laminate modulus of corrugated panel, perpendicular to corrugation
E_{short}	[MPa]	laminate modulus of corrugated panel, parallel to corrugation
f	[-]	sandwich knock-down factor for shear load buckling
$g_i(z)$	[N]	function describing distribution of τ_{iz} across the cross-section [i=x,y]
G_{xy}	[MPa]	in-plane shear modulus
G, G_{iz}	[MPa]	transverse shear modulus [i=x,y]
h	[mm]	overall height of corrugated panel

---

† text between square brackets indicates possible values of the suffixes

k	[-]	buckling coefficient
k_i	[-]	shear correction factor of the transverse shear stiffness [i=x,y]
k_0	[-]	shear load buckling coefficient, without transverse shear effect
m	[g/cm^2]	mass of panel per unit of surface
m	[-]	number of half waves in out-of-plane deformation, in x-direction
n	[-]	number of half waves in out-of-plane deformation, in y-direction
M_x	[N]	applied bending moment in x-direction
M_y	[N]	applied bending moment in y-direction
M_{xy}	[N]	applied torsion moment
N_x	[N/mm]	applied direct in-plane load, in x-direction
N_y	[N/mm]	applied direct in-plane load, in y-direction
N_{xy}	[N/mm]	applied in-plane shearing load
N_{iz}	[N/mm]	applied transverse shear load [i=x,y]
p	[mm]	pitch of corrugation
p_i	[N/mm]	compressive buckling load [i=x,y]
$p_{i\,ts}$	[N/mm]	compressive buckling load in transverse shear [i=x,y]
q	[N/mm]	shear buckling load
q_s	[N/mm]	shear buckling load of a panel (including transverse shear deformation)
q_0	[N/mm]	shear buckling load of a plate (no transverse shear deformation)
$Q_{ij}^{(k)}$	[MPa]	reduced in-plane stiffness of layer k of a laminate [i,j=1,2,6]
$Q_{ii}(k)$	[MPa]	transverse shear stiffness of layer k with respect to plate axes [i=4,5]
R	[-]	ratio of equivalent thickness to laminate thickness, for corrugated panel
s	[-]	transverse shear stiffness parameter
S_{iz}	[N/mm]	transverse shear stiffness of panel [i=x,y]
t	[mm]	thickness
U	[Nmm]	strain energy
w	[mm]	out of plane deformation
wb_i	[mm]	partial out of plane deformation, in bending [i=x,y]
ws_i	[mm]	partial out of plane deformation, in transverse shear [i=x,y]

W	[Nmm]	work of applied load
x	[mm]	lengthwise in-plane coordinate
y	[mm]	transverse in-plane coordinate
z	[mm]	thickness coordinate
$z_{na\,i}$	[mm]	z-coordinate of neutral axis [i=x,y]
α_i	[-]	coefficient in skewed sine wave out-of-plane deformation (local buckling of corrugated panel)
β	[deg]	corrugation angle
Γ	[mm^5]	warping restraint parameter, (overall buckling of corrugated panels)
ε_x	[-]	direct strain, in x-direction
ε_y	[-]	direct strain, in x-direction
γ_{xy}	[-]	in-plane shear strain
γ_{iz}	[-]	transverse shear strain [i=x,y]
η	[-]	efficiency
θ	[-]	shear buckling stiffness parameter (laminate)
κ_i	[1/mm]	bending curvature, in x-direction [i=x,y]
κ_{xy}	[1/mm]	torsion deformation
λ	[mm]	half-wavelength of the out-of-plane deformation (corrugated panel)
μ	[-]	Poisson's factor of corrugated panel (= 1-$v_{xy}.v_{yx}$)
μ_i	[-]	Poisson's ratio of corrugated panel in bending [i=x,y]
v_{xy}	[-]	Poisson's ratio
ξ, χ	[-]	overall buckling stffness parameter (corrugated panel)
ρ	[mm]	radius of gyration of corrugated panel
ρ	[g/mm^3]	specific density
σ_{ii}	[MPa]	direct stress [i=1,2]
$\overline{\sigma_i}$	[MPa]	allowable direct stress [i=c,t]
τ_{12}	[MPa]	in-plane shear stress
τ_{iz}	[MPa]	transverse shear stress [i=x,y]
$\overline{\tau}$	[MPa]	allowable shear stress
ϕ	[deg]	orientation of a layer with respect to the laminate axes
ψ	[-]	shear buckling stiffness parameter

ω [-]   dimensionless radius of gyration (corrugated panel)

sub-/superscripts:

b	bending
c,f	core, face of sandwich panel
c,t	compression, tension
cr	critical, associated with buckling
e	eccentricity
i	layer i of laminate
k,(k)	layer k of a laminate
L	local buckling of a corrugated panel
O	overall buckling of a corrugated panel
s,ts	transverse shear
w	wrinkling
x,y,z	with respect to coordinate axes
′	equivalent (for stress or thickness)
∞	very long (infinitely long) panel
*	optimum

1

Introduction

This thesis is a contribution to the *design of fibre composite panels*, in particular for *aerospace applications*. Rapid scientific progress is being made these days in the field of composite structures; for structural analysis many computer codes (i.e. finite element packages) allow fibre composite materials to be used. As composite structures are increasingly used in practice, experience is also gained in manufacture, maintenance and repair. However, the *preliminary design* of these structures, where only the loading and general requirements on the structure are given while the actual form and layup have yet to be defined, has not received as much attention. This has prompted the research leading to this thesis. Two specific types of panels are chosen as subjects of the research: sandwich panels and corrugated panels. As part of this work two computer programs have been developed as software tools for the designer: SAPANO for sandwich panels and COPANO for corrugated panels. This thesis can be seen as the theoretical manual for the programs, while separate user's manuals are available to assist in their use [Bladel94a, Bladel94b]. The aerospace application provides a frame work for the results and the computer programs. Still, these remain valid for other fields of engineering as well.

Composites are joining the standard range of materials used for aerospace structures. While in military aircraft composites were introduced during the second world war [Middleton92], introduction in commercial aircraft has happened more gradually from 1970 onwards [Walden90]. In space applications composite sandwich panels and corrugated panels are often used as central load carrying structures for satellites [ESA94]. The main differences compared to metallic materials are the pronounced anisotropy and inhomogeneity. This requires a totally different approach to design, which was not readily understood by the first designers that used composites. This resulted not infrequently in 'black metal' structures (a nickname for carbon fibre composite structures made according to design practice for metallic materials). The application of composite materials in aerospace structures reflects their strong points, such as high stiffness, resulting low structural weight and reduction in the total number of parts. On the other hand, composites have their own

specific problems, such as sensitivity to impact damage and a high degree of quality control required in manufacture. Composite materials will probably never entirely replace metallic materials but will rather be used alongside metals, each type having its own field of application.

In aerospace applications the composite generally consists of long fibres orientated in specific directions, embedded in a matrix material. Different forms of composite are available, ranging from dry fibres and dry cloths or weaves (to be drenched with matrix material at the manufacturing stage) to pre-impregnated fibre layers (to be stacked in a mould and cured in an autoclave). In this thesis composite panels are considered for which dry cloths or pre-impregnated fibres (so-called *prepreg*) are the most suited. A sandwich panel, or each individual flat part of a corrugated panel, is a *laminate*, i.e. a stack of fibre layers each having a specific thickness, fibre orientation and mechanical properties. The thickness and orientation are typically discrete variables; the panel can only be built up of an integer number of fibre layers, and in the manufacturing process the orientation can be defined only up to limited precision. Because of the relatively small loading intensity in aerospace applications, the panel is a thin-walled structure for which buckling is an essential failure mode. Unfortunately the stability analysis of a composite panel is more complicated than that of a panel made of isotropic material. Further relevant failure modes are material failure, both static failure and failure associated with delamination growth after impact damage.

As mentioned above, this thesis considers two specific types of composite panels: sandwich panels and corrugated panels. In a sandwich panel the laminate has a lightweight layer in the middle (the *core*), increasing the bending and torsional stiffnesses of the panel, but simultaneously introducing significant transverse shear deflections. (Because of the low mass of the core, it has low stiffness as well.) On the other hand, in the corrugated panel considered here, the laminate is in effect folded to form a series of narrow strips running from top to bottom of the panel. This increases its bending stiffness in one direction by some factors of ten. Note that the use of composite materials, as opposed to metallic materials, favours the occurrence of non-negligible transverse shear deflections anyhow (see chapter 3). The design of composite panels is more complicated than the design of similar panels of isotropic material because not only the shape of the cross-section and the wall thickness have to be defined, but also the laminate has many design variables that must be defined in the design process. With these two types of panels, the structural box of an aircraft wing can be defined, i.e. using the sandwich panel as top and bottom cover (with a

smooth outside surface exposed to the air flow) carrying mainly normal loads and using the corrugated panel as the web of the front and rear spar, carrying mainly shear loads.

Because preliminary design is the first phase of the design process, the key issue is to appreciate the design problem, and not extreme accuracy of the analysis. Refinements of the structure and of the analysis will be made at a later stage anyway. This is reflected in all elements of this thesis; it is not, for example, devoted to the development of analysis methods that extend the level of accuracy currently available; rather the existing analysis methods are used in a design environment. Still, many existing formulae and models had to be improved. The computer programs developed are especially tailored to the design task; they are interactive and allow a rapid assessment of the influence of all the parameters involved (loads, material selection, etc.). As mentioned above, many variables are present in the design problem, too many for the designer to determine by hand. A numerical optimization scheme is therefore included in the computer programs to assist the user in defining a good design by searching for the feasible design with the lowest mass. In the optimization *discrete* variables are used to obtain optimum composite panels for practical use.

The thesis is divided into four parts; the first part presents the various aspects of mechanical analysis required for the design of sandwich panels and corrugated panels. In increasing complexity the early chapters present formulae and results from the literature, elaborated and adapted to the scope of the present work. Chapter 2 presents basic concepts of laminate analysis. Most of these (classical laminate theory, material failure criterion, buckling of laminates) are taken from the literature and included as reference for later chapters. The cylindrical bending assumption (used in the derivation of reduced bending stiffnesses for asymmetric laminates) is worth mentioning, as it is also used in the following chapter for the calculation of transverse shear stiffness. Chapter 3 examines the effect of transverse shear, important for all composite structures and for sandwich panels in particular. This effect is modelled with first order shear theory, i.e. the panel is regarded as homogeneous and global out-of-plane stiffnesses are used in the various analyses. Due to this approach, some aspects of sandwich panel behaviour are neglected; chapter 4 presents additional analyses to compensate for inadequacy of the first order shear theory. A separate chapter on the buckling of composite corrugated panels in shear concludes the first part of the thesis. In the second part different aspects of the design of composite panels are presented; first, in chapter 6 the design of

composite sandwich panels and corrugated panels is examined in an analytical way. Next, chapter 7 presents the numerical method used for optimization. The use of discrete variables in the design presents the greatest challenge here. In the third part of the thesis, chapters 8 and 9, the computer codes SAPANO and COPANO are described. The fourth part presents in chapter 10 some relevant results obtained with the programs on the performance of optimum sandwich panels and corrugated panels. Chapter 11 draws some general conclusions on the results of the research.

part I

Composite Panel Analysis

2

Laminate Analysis
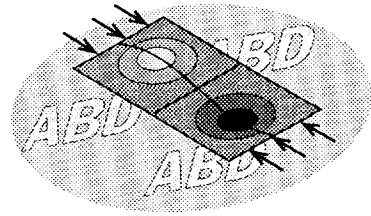
This chapter presents various formulae related to the analysis of flat laminates. A laminate is a thin plate composed of several individual layers, commonly used as the basic form of many fibre composite structures in aerospace applications, such as stiffened panels or sandwich panels. Then *prepregs* (thin layers of fibre pre-impregnated with a resin) or mats of fibres (to be impregnated during production) are used in the laminate to produce the various parts of the panel. Here only rectangular laminates without taper (i.e. of constant thickness) are considered, as illustrated in Figure 1.

Many of the formulae of this chapter are well known from the literature, but are presented here to build a reference frame for later chapters and for use in the computer programs to be developed in part three. The first paragraph presents the basic formulae of the classical laminate theory, introducing the nearly standard notation. The second and third paragraphs examine the subject
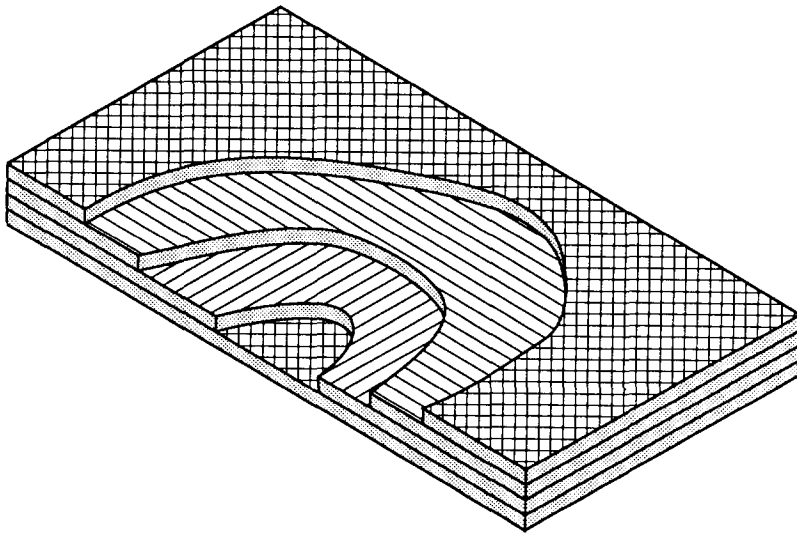
Figure 1 A typical laminate

of material failure, with a stress criterion and a criterion associated with delamination, respectively. The last paragraph deals with the buckling of rectangular laminated plates, both in compression and in shear.

2.1   Classical laminate theory

The classical laminate theory (CLT) is a simple framework providing the relationship between applied loads and overall deformations of a laminate, assuming plane stress and Kirchhoff-Love type deformation (i.e. a cross-section normal to the mid-plane of the laminate remains normal when load is applied)[Whitney87]. As such, CLT applies to *thin* plates. Note that, to apply the Kirchhoff-Love assumption, a composite laminate must have a greater length to thickness ratio than a metal plate, due to its reduced transverse shear stiffness. This is examined in the next chapter.

2.1.1 Formulation

Classical laminate theory defines a relation between the loads on the mid-plane of the laminate and the deformations based on the generalized Hooke's law in a state of plane stress. In this way the following set of linear equations is obtained:

$$
\begin{bmatrix} N_x \\ N_y \\ N_{xy} \\ - \\ M_x \\ M_y \\ M_{xy} \end{bmatrix} = \begin{bmatrix} A_{11} & A_{12} & A_{16} & | & B_{11} & B_{12} & B_{16} \\ A_{12} & A_{22} & A_{26} & | & B_{12} & B_{22} & B_{26} \\ A_{16} & A_{26} & A_{66} & | & B_{16} & B_{26} & B_{66} \\ - & - & - & - & - & - & - \\ B_{11} & B_{12} & B_{16} & | & D_{11} & D_{12} & D_{16} \\ B_{12} & B_{22} & B_{26} & | & D_{12} & D_{22} & D_{26} \\ B_{16} & B_{26} & B_{66} & | & D_{16} & D_{26} & D_{66} \end{bmatrix} \cdot \begin{bmatrix} \varepsilon_x \\ \varepsilon_y \\ \gamma_{xy} \\ - \\ \kappa_x \\ \kappa_y \\ \kappa_{xy} \end{bmatrix} \tag{1}
$$

By the reciprocal theorem the order of the subscripts in (1) is independent, e.g. $A_{12}=A_{21}$. The submatrices A_{ij}, B_{ij} and D_{ij} are defined by a summation through the thickness of the stiffness properties $Q_{ij}^{(k)}$ of every layer (with respect to the laminate axes):

$$A_{ij} = \int_{-t/2}^{t/2} Q_{ij}^{(k)} dz = \sum_{k=1}^{n} Q_{ij}^{(k)}(z_{k+1} - z_k)$$

$$B_{ij} = \int_{-t/2}^{t/2} Q_{ij}^{(k)} z \, dz = \sum_{k=1}^{n} \frac{1}{2} Q_{ij}^{(k)}(z_{k+1}^2 - z_k^2) \qquad (2)$$

$$D_{ij} = \int_{-t/2}^{t/2} Q_{ij}^{(k)} z^2 dz = \sum_{k=1}^{n} \frac{1}{3} Q_{ij}^{(k)}(z_{k+1}^3 - z_k^3)$$

where z is the thickness coordinate, measured with respect to the mid-plane of the laminate. The A_{ij} submatrix contains the in-plane stiffnesses, the D_{ij} submatrix the out-of-plane stiffnesses, and B_{ij} is a coupling matrix. For every layer k, the stiffness $Q_{ij}^{(k)}$ depends on the in-plane *material* stiffnesses $Q_{ij}^{'(k)}$ and the orientation ϕ (defined positive when rotating from the laminate axes to the material axes), as follows:

$$
\begin{aligned}
Q_{11}^{(k)} &= Q_{11}^{'(k)} \cdot \cos^4\phi + Q_{22}^{'(k)} \cdot \sin^4\phi + 2(Q_{12}^{'(k)} + 2Q_{66}^{'(k)}) \cdot \sin^2\phi \cdot \cos^2\phi \\
Q_{22}^{(k)} &= Q_{11}^{'(k)} \cdot \sin^4\phi + Q_{22}^{'(k)} \cdot \cos^4\phi + 2(Q_{12}^{'(k)} + 2Q_{66}^{'(k)}) \cdot \sin^2\phi \cdot \cos^2\phi \\
Q_{12}^{(k)} &= (Q_{11}^{'(k)} + Q_{22}^{'(k)} - 4Q_{66}^{'(k)}) \cdot \sin^2\phi \cdot \cos^2\phi + Q_{12}^{'(k)} \cdot (\sin^4\phi + \cos^4\phi) \\
Q_{66}^{(k)} &= (Q_{11}^{'(k)} + Q_{22}^{'(k)} - 2Q_{12}^{'(k)} - 2Q_{66}^{'(k)}) \cdot \sin^2\phi \cdot \cos^2\phi + Q_{66}^{'(k)} \cdot (\sin^4\phi + \cos^4\phi) \\
Q_{16}^{(k)} &= (Q_{22}^{'(k)} - Q_{12}^{'(k)} - 2Q_{66}^{'(k)}) \cdot \cos\phi \cdot \sin^3\phi - (Q_{11}^{'(k)} - Q_{12}^{'(k)} - 2Q_{66}^{'(k)}) \cdot \cos^3\phi \cdot \sin\phi \\
Q_{26}^{(k)} &= (Q_{22}^{'(k)} - Q_{12}^{'(k)} - 2Q_{66}^{'(k)}) \cdot \cos^3\phi \cdot \sin\phi - (Q_{11}^{'(k)} - Q_{12}^{'(k)} - 2Q_{66}^{'(k)}) \cdot \cos\phi \cdot \sin^3\phi
\end{aligned}
\qquad (3)
$$

For every layer, the material stiffnesses $Q_{ij}^{'(k)}$ are written in terms of the engineering constants E, G and ν as follows:

$$Q'^{(k)}_{11} = \frac{E^{(k)}_x}{1 - v^{(k)}_{xy} \cdot v^{(k)}_{yx}}$$

$$Q'^{(k)}_{22} = \frac{E^{(k)}_y}{1 - v^{(k)}_{xy} \cdot v^{(k)}_{yx}} \tag{4}$$

$$Q'^{(k)}_{12} = \frac{v_{xy} \cdot E^{(k)}_y}{1 - v^{(k)}_{xy} \cdot v^{(k)}_{yx}}$$

$$Q'^{(k)}_{66} = G^{(k)}_{xy}$$

With the help of the elements of the 6x6-matrix of (1) - the so-called ABD-matrix - a unique definition of the terms *orthotropic* and *symmetric* (which will be used frequently further on) is easily made. Both are related to the existence of a plane of symmetry in the laminate, and can be associated with a number of zeros in the ABD-matrix. A laminate is *symmetric* if the mid-plane is such a plane of symmetry, see Figure 2a. Then all B_{ij}-elements in (1) are zero; examining the equation it appears that no coupling exists between in-plane loads and out-of-plane deformations and vice versa. A laminate is called *orthotropic* if a plane of symmetry exists perpendicular to the xy-plane, see

a. symmetric laminate   b. orthotropic laminate
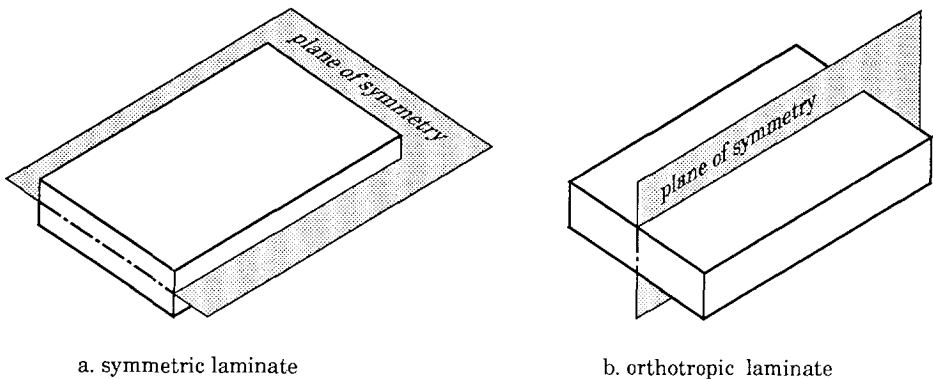
Figure 2 Orthotropy and symmetry of laminates

Figure 2b. In the literature the term *specially orthotropic* is reserved for laminates where this plane of symmetry coincides with the body axes of a rectangular plate, but here this situation will be called simply *orthotropic*. Then all elements with suffixes 16 and 26 in the ABD-matrix are zero. In literature the term *balanced* also exists; then there are as many layers in the laminate oriented at an angle $+\phi$ as there are at $-\phi$. Then at least the terms A_{16} and A_{26} in the ABD-matrix are zero.

2.1.2 Analysis of asymmetric laminates

Formula (1) is derived with the mid-plane of the laminate as datum. If the laminate is not symmetric about the mid-plane, some elements of the coupling matrix B_{ij} are not zero. Coupling will then occur between bending and stretching when a load is applied at the mid-plane of the laminate. However, in these cases as well, one would like to use the (buckling) formulae for symmetric laminates, that only apply D_{ij}. A reduced bending stiffness matrix D^* is then often used [Ashton69] (by introducing an approximation). D^* represents the relation between the moments M_i and the curvatures κ_j in the absence of normal loads; it is defined by a matrix algebra manipulation of (1) which can be rewritten as:

$$\begin{cases} N_i = A_{ij}.\varepsilon_j + B_{ij}.\kappa_j \\ M_i = B_{ij}.\varepsilon_j + D_{ij}.\kappa_j \end{cases} \tag{5}$$

Substituting ε_j from the first row into the second yields the following:

$$\begin{cases} \varepsilon_i = A_{ij}^{-1}.N_j - (A^{-1}.B)_{ij}.\kappa_j \\ M_i = (B.A^{-1})_{ij}.N_j + (D-B.A^{-1}.B)_{ij}.\kappa_j \end{cases} \tag{6}$$

In (6) the reduced bending stiffness matrix D^*_{ij} is visible as the factor of κ_j:

$$D^*_{ij} = (D-B.A^{-1}.B)_{ij} \tag{7}$$

Clearly, in (6) the coupling is removed when the in-plane loads N_i are zero; then, D^*_{ij} is indeed the relationship between M_i and κ_j.

However, sometimes significant errors arise when D^*_{ij} is used in buckling analyses ([Ewing88], [Leissa87]); in special cases even the main elements of D^*_{ij}

are less than zero[†].

An alternative is to derive another type of bending stiffness D^{**}_{ij}, assuming cylindrical bending. For example, assuming cylindrical bending in x-direction, the following conditions are imposed:

$$N_x = 0. \; , \; \varepsilon_y = \gamma_{xy} = 0. \; , \; \kappa_y = \kappa_{xy} = 0. \tag{8}$$

Substitution in (1) yields:

$$
\begin{bmatrix} 0. \\ N_y \\ N_{xy} \\ - \\ M_x \\ M_y \\ M_{xy} \end{bmatrix}
=
\left[\begin{array}{ccc|ccc}
A_{11} & A_{12} & A_{16} & B_{11} & B_{12} & B_{16} \\
A_{12} & A_{22} & A_{26} & B_{12} & B_{22} & B_{26} \\
A_{16} & A_{26} & A_{66} & B_{16} & B_{26} & B_{66} \\
\hline
B_{11} & B_{12} & B_{16} & D_{11} & D_{12} & D_{16} \\
B_{12} & B_{22} & B_{26} & D_{12} & D_{22} & D_{26} \\
B_{16} & B_{26} & B_{66} & D_{16} & D_{26} & D_{66}
\end{array} \right]
\cdot
\begin{bmatrix} \varepsilon_x \\ 0. \\ 0. \\ - \\ \kappa_x \\ 0. \\ 0. \end{bmatrix}
\tag{9}
$$

Compare this to the derivation of the reduced bending stiffness D^*_{ij}; the basic assumption is there to set the in-plane loads $N_i = 0$. Substitution in (5) yields:

$$
\begin{cases}
0. = A_{ij} \cdot \varepsilon_j + B_{ij} \cdot \kappa_j \\
M_i = B_{ij} \cdot \varepsilon_j + D_{ij} \cdot \kappa_j
\end{cases}
\tag{10}
$$

In both cases sufficient zeroes are introduced to eliminate some parameters from the set of equations. In particular, (9) leads to the following set of equations:

[†] A 2 layer laminate with fibres at $0°$ and $+45°$ typically has D^*_{11}, D^*_{22} and D^*_{12} all less than zero; see also Figure 3.

$$
\begin{bmatrix} N_y \\ N_{xy} \\ M_x \\ M_y \\ M_{xy} \end{bmatrix} =
\begin{bmatrix}
B_{12} - A_{12}\dfrac{B_{11}}{A_{11}} \\[2ex]
B_{16} - A_{16}\dfrac{B_{11}}{A_{11}} \\[2ex]
D_{11} - \dfrac{B_{11}{}^2}{A_{11}} \\[2ex]
D_{12} - B_{12}\dfrac{B_{11}}{A_{11}} \\[2ex]
D_{16} - B_{16}\dfrac{B_{11}}{A_{11}}
\end{bmatrix} \cdot \kappa_x
\tag{11}
$$

in which the equations for M_x, M_y and M_{xy} yield the first column of a new $D_{cyl.b.}$-matrix. Similar cylindrical bending assumptions in y-direction and in the xy-direction (the latter perhaps more mathematical than practical) yield the second and third columns of this matrix; the complete $D_{cyl.b.}$-matrix is then:

$$
[D_{ij}]_{cyl.b.} =
\begin{bmatrix}
D_{11} - \dfrac{B_{11}{}^2}{A_{11}} & D_{12} - B_{12}\dfrac{B_{22}}{A_{22}} & D_{16} - B_{16}\dfrac{B_{66}}{A_{66}} \\[3ex]
D_{12} - B_{12}\dfrac{B_{11}}{A_{11}} & D_{22} - \dfrac{B_{22}{}^2}{A_{22}} & D_{26} - B_{26}\dfrac{B_{66}}{A_{66}} \\[3ex]
D_{16} - B_{16}\dfrac{B_{11}}{A_{11}} & D_{26} - B_{26}\dfrac{B_{22}}{A_{22}} & D_{66} - \dfrac{B_{66}{}^2}{A_{66}}
\end{bmatrix}
\tag{12}
$$

Unfortunately, this matrix is not symmetric. However, by averaging the non-diagonal elements the following symmetric D**-matrix is obtained:

$$
D^{**}{}_{ij} =
\begin{bmatrix}
D_{11} - \dfrac{B_{11}{}^2}{A_{11}} & D_{12} - \dfrac{B_{12}(B_{11}A_{22} + B_{22}A_{11})}{2A_{11}A_{22}} & D_{16} - \dfrac{B_{16}(B_{11}A_{66} + B_{66}A_{11})}{2A_{11}A_{66}} \\[3ex]
(SYM) & D_{22} - \dfrac{B_{22}{}^2}{A_{22}} & D_{26} - \dfrac{B_{26}(B_{22}A_{66} + B_{66}A_{22})}{2A_{22}A_{66}} \\[3ex]
 & & D_{66} - \dfrac{B_{66}{}^2}{A_{66}}
\end{bmatrix}
\tag{13}
$$

The cylindrical bending assumption for the x- and y-direction is equivalent to bending with respect to the neutral axis in that direction. Therefore the associated bending stiffnesses (D^{**}_{11} and D^{**}_{22}) will never be less than zero, unlike the diagonal elements of D^{*}_{ij}.

To assess the validity of D^{*}_{ij} and D^{**}_{ij}, for several cases bending stiffnesses and buckling loads are compared. For an anisotropic two layer laminate [0°/ϕ] (every layer 1.mm thick) the bending stiffnesses D^{*}_{11} and D^{**}_{11} are given in Figure 3a, while Figure 3b presents these stiffnesses for an antisymmetric angle-ply [ϕ/-ϕ] (every layer 1.mm thick). In both cases D^{**}_{11} is larger than D^{*}_{11} (in the second case D^{**}_{11} is even equal to D_{11}). In the first case for some values of the layer angle ϕ the bending stiffness D^{*}_{11} is less than zero (as mentioned before). In the paper by Ewing et al. [Ewing88] the validity of the reduced bending stiffness D^{*}_{ij} is examined for asymmetric cross-ply and angle-ply laminates, because for these two types of laminates exact solutions (considering the full ABD-matrix, and not only bending stiffnesses) exist. The obtained buckling loads for cross-ply laminates are of great accuracy (within 1%), while for angle-ply laminates large errors can occur (above 20%). The obtained buckling loads are always conservative. When the cylindrical bending stiffnesses D^{**}_{ij} are used for the buckling calculation, for cross-ply laminates equally good results are obtained. For asymmetric angle-ply laminates (as mentioned above) D^{**}_{ij} is equal to D_{ij}; with respect to the exact solutions of [Ewing88], unconservative buckling loads are obtained.

Concluding, from the few cases considered, we can expect the *traditional* reduced bending stiffnesses D^{*}_{ij} to give conservative buckling loads, but for some cases negative stiffnesses occur on the diagonal of the D*-matrix (giving
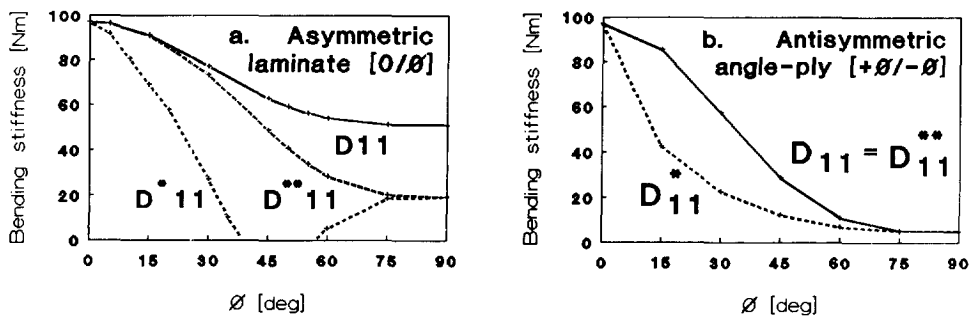
Figure 3   Reduced bending stiffnesses for two types of asymmetric laminates (2 layers of equal thickness t=1.mm)

negative buckling loads). The *cylindrical bending* reduced bending stiffnesses D^{**}_{ij} on the other hand may give unconservative buckling loads, but negative stiffnesses will never occur. This last advantage makes D^{**}_{ij} more suitable for application in the envisaged computer program, even if it is unconservative[†]. Whichever method is selected, it must not be forgotten that in the end, both reduced bending stiffness methods remain *approximations* to the real situation.

2.2   Material failure

Failure of composite materials is a complex matter because of its heterogeneous composition. This is reflected in the large number of failure criteria available. However, these can be grouped into failure criteria covering what might be called static failure and other criteria covering failure following impact damage of the laminate. For both types of failure modes an appropriate criterion is presented.

2.2.1 Static failure

This concerns the static over-stressing of the laminate, causing either fibre or matrix failure. Here the Tsai-Hill criterion is used, in a modified form [Jong84]. It is an extension of the von Mises yield criterion for isotropic materials. Failure occurs if the following inequality in terms of the stress components is satisfied:

$$(\frac{\sigma_{11}}{X})^2 - \frac{\sigma_{11}.\sigma_{22}}{X.Y} + (\frac{\sigma_{22}}{Y})^2 + (\frac{\tau_{12}}{S})^2 \geq 1. \tag{14}$$

where X, Y and S are the appropriate material strength values obtained from tests (i.e. for X the tensile value for the strength in x-direction is substituted if σ_{11} is larger than zero, etc.). The modification is in the denominator of the cross term in $\sigma_{11}.\sigma_{22}$, which is here X.Y and not X^2, as in the original formulation of the Tsai-Hill criterion. The main advantage of this criterion is that it agrees well with test data, while the disadvantage is that it does not reflect a true failure mechanism, being simply an analogy of the isotropic yield criterion of von Mises.

[†] For cross-ply laminates, for example, the error is very small; whether the approximation is then conservative or not, is of small influence.

2.2.2 Impact damage

Damage caused by the impact of foreign objects on a composite is often delamination. This decreases the strength of the laminate, without necessarily causing immediate failure. However, under cyclic loading the damage can grow to a level that does cause failure of the laminate. There is a certain level of impact energy above which this damage becomes visible. It has to be assumed that structures exposed to impact of foreign objects do have damage below this threshold of *barely visible damage*. Tests have shown that if the compressive strain in the laminate remains below a certain value (typically 0.4% for carbon fibre composites), then the delamination associated with barely visible impact damage will not cause progressive delamination and subsequent failure. An engineering approach is therefore to limit the compressive strain level in the structure to a certain value. Here this is done on a ply by ply basis in the reference direction of each ply.

2.3   Stability of rectangular orthotropic simply-supported laminates

The buckling of rectangular orthotropic plates is a well-documented subject [Leissa87]. Here the basic formulae are presented in terms of an energy method, as a reference for further chapters. The energy method is based on the formulae for strain energy U and the work of the applied load W during the buckling deformation. Both U and W are functions of the out-of-plane displacement function w:

$$U = \int_0^a \int_0^b \frac{1}{2}\left(D_{11} w_{,xx}^2 + 2 D_{12} w_{,xx} w_{,yy} + D_{22} w_{,yy}^2 + 4 D_{66} w_{,xy}^2\right) dx\,dy$$

$$W = \int_0^a \int_0^b \frac{1}{2}\left(N_x w_{,x}^2 + N_y w_{,y}^2 + 2 N_{xy} w_{,x} w_{,y}\right) dx\,dy$$

$$(15)$$

where the comma denotes partial differentiation with respect to the parameter or parameters following the comma. The structure is in a state of equilibrium (although not necessarily stable equilibrium) if the total energy (U-W) is stationary with respect to the deflection parameters. Therefore, setting the partial derivative of the total energy (U-W) with respect to the deflection parameters equal to zero yields the buckling equation. Equations for compression and shear buckling are defined separately below. Unfortunately there are different approaches to the two problems. Therefore a single equation for the combined compression and shear buckling cannot be found. However, a

parabolic interaction formula exists for combined compression and shear [Bleich52] for long isotropic plates. In chapter 3 it will be shown that the same formula is also valid for orthotropic plates as well.

For all buckling formulae of this and subsequent chapters the plate is considered simply-supported on all four sides. For the applications considered (design computer programs for composite sandwich panels and corrugated panels) this is an appropriate boundary condition, because in these applications the edges cannot introduce bending moments into the structure.

2.3.1 Compression buckling

If only direct loads are acting on the laminate, the term in the shear load N_{xy} in (15) vanishes. For a plate which is simply-supported on all four sides, a double sine wave with amplitude A (and with m half waves in the x-direction and n half waves in the y-direction) is a suitable buckling deflection that satisfies rigorously the boundary conditions:

$$w = A \, \sin\frac{m\pi x}{a} \, \sin\frac{n\pi y}{b} \tag{16}$$

Using (16) the integrals of (15) can be evaluated; this yields the following formulae for U and W:

$$U = A^2 \cdot \frac{ab}{8} \left(D_{11}(\frac{m\pi}{a})^4 + D_{22}(\frac{n\pi}{b})^4 + (2D_{12} + 4D_{66})(\frac{m\pi}{a})^2(\frac{n\pi}{b})^2 \right)$$

$$W = A^2 \cdot \frac{ab}{8} \left(N_x(\frac{m\pi}{a})^2 + N_y(\frac{n\pi}{b})^2 \right) \tag{17}$$

Putting:

$$\frac{\partial(U-W)}{\partial A} = 0. \tag{18}$$

gives:

$$A\frac{ab}{4} \left(D_{11}(\frac{m\pi}{a})^4 + D_{22}(\frac{n\pi}{b})^4 + (2D_{12} + 4D_{66})(\frac{m\pi}{a})^2(\frac{n\pi}{b})^2 - N_x(\frac{m\pi}{a})^2 - N_y(\frac{n\pi}{b})^2 \right) = 0. \tag{19}$$

This condition is satisfied if either A=0. (the trivial solution, implying no buckling deformation) or else if:

$$p_x(\frac{m\pi}{a})^2 + p_y(\frac{n\pi}{b})^2 = D_{11}(\frac{m\pi}{a})^4 + D_{22}(\frac{n\pi}{b})^4 + 2(D_{12} + 2D_{66})(\frac{m\pi}{a})^2(\frac{n\pi}{b})^2$$

(20)

This is the required buckling equation; if it is satisfied a non-zero buckling amplitude A exists. Note that the integer parameters m and n, indicating the number of half waves, remain undefined; the buckling load is obtained by calculating the loads p_x, p_y with (20) for different m and n. The lowest set of loads will be the actual buckling loads. In paragraph 3.2.3 possible combinations of m and n are investigated, proving the well-known assumption that always either m=1 or n=1. Note the use of p_x, p_y for *buckling* loads to distinguish these from simply the applied loads N_x, N_y.

For anisotropic plates (D_{16}, $D_{26} \neq 0$.) there is no exact solution. Moreover various investigations have resulted in conflicting results [Leissa87]. For moderate values of D_{16}, D_{26} the effect of anisotropy on the compression buckling load p_x can be evaluated by the approximation developed by Wiedeman, reported by Wiggenraad [Wiggenraad77]; good results are obtained for aspect ratio's a/b over 2 or 3.

2.3.2 Shear buckling

For buckling of a simply-supported rectangular laminate in shear a double sine wave (16) does not adequately represent the buckling deformation, because of the skew nature of the buckling mode. A truncated Fourier series, which can represent any type of deformation, is generally used. However, for sufficient accuracy many terms are needed in the Fourier series. Solving the buckling equation for the buckling load q_0 would then require much computation time. Therefore this approach is discarded (in view of the application of the formulae, see chapter 1). Another approach is the use of a skewed sine wave buckling deformation, as suggested by Lekhnitskii [Lekhnitskii68] and others. While this approach works well for very long plates, it is less good for rectangular plates, because the skewed sine wave does not adequately represent the buckling mode at the edges in that case. Furthermore, this approach gives a buckling equation in which the skew angle and the wavelength are variable, like m and n in (20). But while m and n are parameters that can take only integer values (1,2,...), the skew angle and wavelength are real variables and minimization of q_0 with respect to these variables is again a lengthy process.

Therefore, an interpolation scheme has been devised [Bladel88] on the basis of the results given in the ESDU data item 80023, which uses a truncated Fourier

series deformation (with 36 displacement terms). The results given in the ESDU item are presented in graphical form, as a function of two orthotropic stiffness parameters ψ and θ. By suitable curve fitting procedures the following formula in these two parameters is obtained:

$$q_0 = \frac{(D_{11} D_{22})^{1/2}}{a\,b} k_0$$

$$k_0 = \begin{bmatrix} \dfrac{1}{\psi^2} & \dfrac{1}{\psi} & 1 \end{bmatrix} \cdot \begin{bmatrix} 1.121 & -.699 & 3.828 \\ -4.829 & 11.109 & 15.260 \\ 3.200 & 34.110 & 29.008 \end{bmatrix} \cdot \begin{bmatrix} \theta^2 \\ \theta \\ 1 \end{bmatrix}$$

$$\psi = \left(\frac{a\,D_{22}}{b\,D_{11}} \right)^{1/4}$$

$$\theta = \frac{D_{12} + 2D_{66}}{(D_{11} D_{22})^{1/2}}$$

$$(21)$$

The accuracy of (21) is apparent in Figure 4, where the results of formula (21) are compared with its source [ESDU80] and with results of NASA TN D-7996 [Housner75] which applies a radically different approach (a finite difference scheme especially devised for the buckling of orthotropic plates). Note that (21) (which is derived for rectangular laminates) is accurate for length to width ratio's of up to 5 ([Bladel88], by comparison with the approach of Lekhnitskii mentioned above [Lekhnitskii68] for very long panels).

For moderate values of D_{16}, D_{26} the reference [Wiggenraad77] provides an approximation to include the effect of the anisotropy (in the same way as for compression buckling).
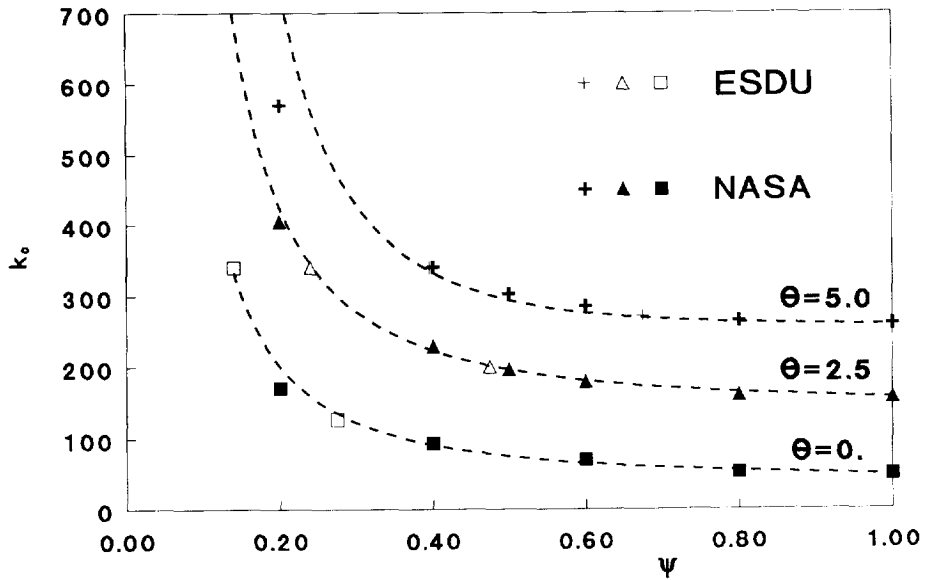
Figure 4 Shear buckling coefficient k_0 of rectangular orthotropic plates as a function of the orthotropic stiffness parameters ψ and θ. Comparison of developed formula (dotted line) with literature (marked points)

3

Transverse Shear Effects
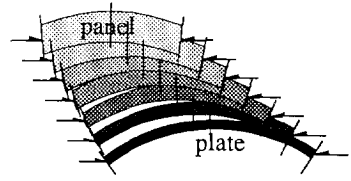
The analysis of the previous chapter supposed the Kirchhoff-Love assumption to hold (a cross-section of the laminate, normal to the mid-plane in the undeformed state, remains normal in the deformed state). However, because composite materials have much lower transverse shear stiffnesses (G_{xz} and G_{yz}) than metals, even for relatively thin composite panels this assumption may no longer hold ([Whitney69], [Noor92]). Accordingly a distinction will be made between the words *plate* and *panel*; *plate* is used when transverse shear effects are disregarded, and *panel* when these are included. To illustrate the different behaviour, in Figure 5 the buckling load of a panel (calculated by a formula that will be derived in 3.2.1) is compared with the buckling load of a plate, showing that only if a/t>30. is the error in compressive buckling load less than 10%. For metal plates, on the other hand, the Kirchhoff-Love assumption already holds for a/t>10. For composite materials it is generally necessary, therefore, to use
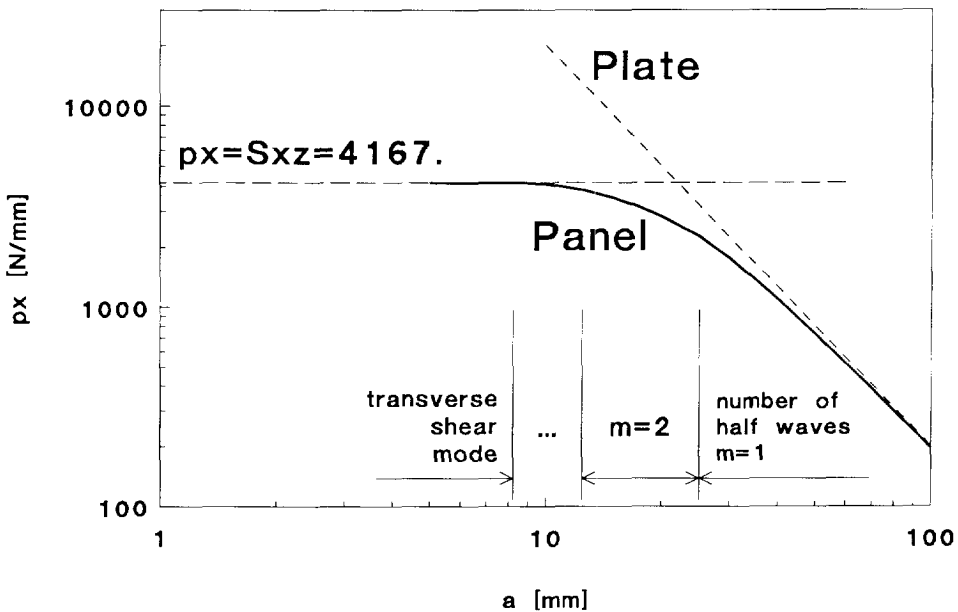
Figure 5 Influence of the transverse shear stiffness on the compressive buckling load of a simply-supported square CFRP ±45° panel of 2.mm thickness

analysis methods that include transverse shear effects.

In the literature, several models that include transverse shear effects are available (for a review see [Noor89]). Because the present application deals with the gross response characteristics of a composite panel (in particular the buckling load) a first order shear theory is sufficiently accurate, if appropriate transverse shear stiffnesses are used [Noor89]. A first order shear theory implies the Reissner-Bollé-Mindlin assumption: a cross-section, normal to the mid-plane in the undeformed state, remains straight but not necessarily normal in the deformed state (see Figure 6b). The composite panel is treated as homogeneous and overall *transverse shear* stiffnesses S_{xz} and S_{yz} are calculated (just as in the previous chapter the ABD-matrix was defined in terms of the *in-plane* stiffness properties of the layers).

Note that in this chapter transverse shear effects for composite panels in general are considered, not focusing in particular on sandwich panels. Nevertheless, a sandwich panel can very conveniently be modelled as a laminate that contains a thick and light, but very flexible, layer somewhere near the middle, so the formulae of this chapter do apply to sandwich panels as well. Behaviour specific to the sandwich panel (for example, the effect of bending of the faces) will be dealt with in the following chapter.

a. no transverse   b. first order   c. higher order
   shear effect   shear theory   shear theory
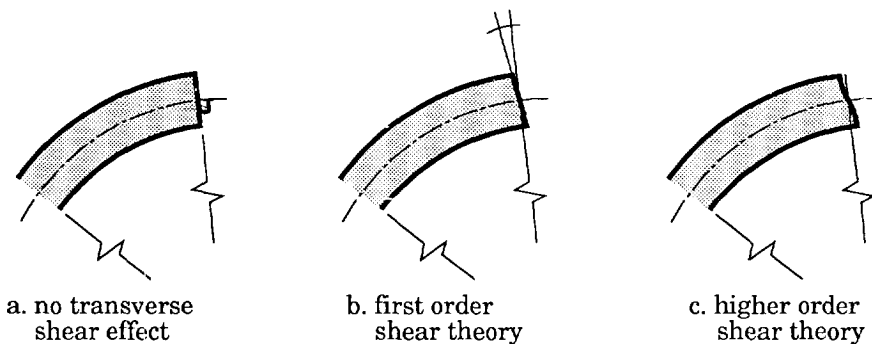
Figure 6 Plate theories with and without transverse shear

Transverse shear stiffnesses S_{xz} and S_{yz} are first defined based on the laminate stiffness parameters and then buckling formulae for composite panels in compression and shear are deduced. Finally, the interaction between compression and shear buckling for panels with transverse shear effects is examined.

3.1 Transverse shear stiffness definition

Many different approaches are available for the definition of transverse shear stiffnesses (TSS). These approaches differ in the assumptions on the transverse shear strains (γ_{xz}, γ_{yz}) and the transverse shear stresses (τ_{xz}, τ_{yz}); for example, often either the transverse shear *strains* or the transverse shear *stresses* are assumed constant through the thickness (see Figure 7). Here, another approach is used, based on the assumption of cylindrical bending of the panel; the TSS are then deduced from the internal deformation energy in the process. But first, for comparison purposes, well-known transverse shear stiffnesses A_{44} and A_{55} are calculated following the constant shear strain approach.

a. constant transverse
   shear strain angle $\overline{\gamma}_{xz}$

b. constant transverse
   shear stress τ_{xz}
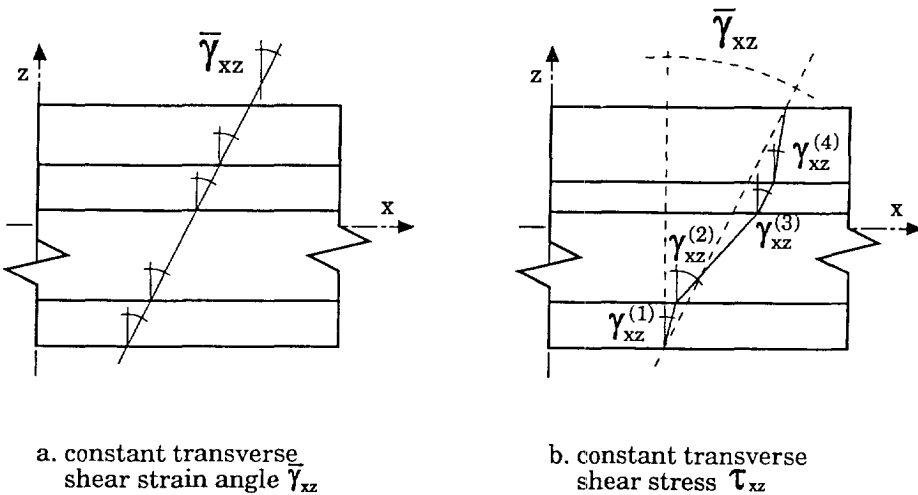
Figure 7 Elementary transverse shear stiffness definitions

3.1.1 Elementary transverse shear stiffnesses A_{44} and A_{55}

The *elementary* TSS A_{44} and A_{55} are calculated with a summation similar to that of the classical laminate theory for the in-plane stiffnesses A_{ij} (i,j=1,2,6) (this is, of course, the reason for using the same symbol A). A_{44} is the relation between an applied transverse shear load N_{xz} and the resulting overall transverse shear strain $\overline{\gamma_{xz}}$:

$$N_{xz} = A_{44} \cdot \overline{\gamma_{xz}} \tag{22}$$

N_{xz} is associated with the transverse shear stress in the layer $\tau_{xz}^{(k)}$, as follows:

$$N_{xz} = \sum_{k=1}^{n} t^{(k)} \cdot \tau_{xz}^{(k)} \tag{23}$$

where superscript '(k)' denotes 'of layer k'. For every $\tau_{xz}^{(k)}$:

$$\tau_{xz}^{(k)} = Q_{44}^{(k)} \cdot \overline{\gamma_{xz}} \tag{24}$$

Substitution of (24) and (23) in (22) yields:

$$A_{44} \cdot \overline{\gamma_{xz}} = \sum_{k=1}^{n} t^{(k)} \cdot Q_{44}^{(k)} \cdot \overline{\gamma_{xz}} \tag{25}$$

or, simplified:

$$A_{44} = \sum_{k=1}^{n} t^{(k)} \cdot Q_{44}^{(k)} \tag{26}$$

In (26) the shear stiffness A_{44} is given in terms of the layer stiffness $Q_{44}^{(k)}$. This layer stiffness is defined with respect to the panel axes x and y. Because the various layers in the laminate may have different orientations, $Q_{44}^{(k)}$ is defined in terms of the material shear moduli $G_{xz}^{(k)}$ and $G_{yz}^{(k)}$, and the orientation $\phi^{(k)}$ of that layer with respect to the panel axes. Matrix algebra yields:

$$Q_{44}^{(k)} = \frac{1}{\dfrac{\cos^2(\phi)}{G_{xz}^{(k)}} + \dfrac{\sin^2(\phi)}{G_{yz}^{(k)}}}$$

$$Q_{55}^{(k)} = \frac{1}{\dfrac{\cos^2(\phi)}{G_{yz}^{(k)}} + \dfrac{\sin^2(\phi)}{G_{xz}^{(k)}}} \tag{27}$$

3.1.2 Improved transverse shear stiffnesses S_{xz} and S_{yz}

With a model similar to that used by other researchers ([Vlachoutsis92], [Chow71]) improved TSS S_{xz} and S_{yz} are derived based on equivalent shear strain energy in cylindrical bending. Only the derivation for S_{xz} is given below, the derivation of S_{yz} being similar.

A state of cylindrical bending in the x-direction implies no deformation in the y-direction. If the classical shear stress formula of engineering bending theory is applied, τ_{xz} is given by the following formula, where the standard parameters are substituted by stiffness parameters of classical laminate theory:

$$\tau_{xz}(z) = \frac{-N_{xz} \cdot g_x(z)}{D_{11}^{**}} \qquad (28)$$

where:

$$g_x(z) = \int_{-t/2}^{z} Q_{11}(z) \cdot (z - z_{na\ x}) dz$$

$$D_{11}^{**} = D_{11} - \frac{B_{11}^2}{A_{11}} \qquad (29)$$

$$z_{na\ x} = \frac{B_{11}}{A_{11}}$$

The variable $z_{na\ x}$ is the z-coordinate of the neutral axis in a cross-section perpendicular to the x-axis. For a homogeneous laminate, (28) yields a parabolic shear stress distribution through the thickness. Note that in (29), because of the integral sign, $Q_{11}(z)$ is written as a function of z (actually, its value is constant in every layer of the laminate; therefore $Q_{11}(z)$ and $Q_{11}^{(k)}$ are two notations identifying the same quantity). The variable $z_{na\ x}$ and D11**, the latter taken from 2.1.2, both confirm the cylindrical bending assumption, because these parameters (together with $Q_{11}(z)$) are used when Poisson's effects (saddle bending etc.) are restrained. The use of (28), with τ_{xz} varying through the thickness, is the essential difference of this approach with respect to the *elementary* TSS calculation of 3.1.1. Here τ_{xz} satisfies elementary mechanical conditions, such as zero shear stress at the top and bottom (free) surfaces of the laminate, and maximum shear stress at the position of the neutral axis, see Figure 8.

With this assumption for the deformations, the transverse shear stiffness S_{xz} can be derived. First, the internal deformation energy in transverse shear U is given in terms of the transverse shear load N_{xz} and the overall transverse shear

strain $\overline{\gamma_{xz}}$:

$$U = \frac{1}{2} N_{xz} \cdot \overline{\gamma_{xz}}$$ (30)

S_{xz} can be introduced with the following formula:

$$N_{xz} = S_{xz} \cdot \overline{\gamma_{xz}}$$ (31)

Substitution of $\overline{\gamma_{xz}}$ of (31) in (30) yields:

$$U = \frac{N_{xz}^2}{2S_{xz}}$$ (32)

Solving for S_{xz} yields:

$$S_{xz} = \frac{N_{xz}^2}{2U}$$ (33)
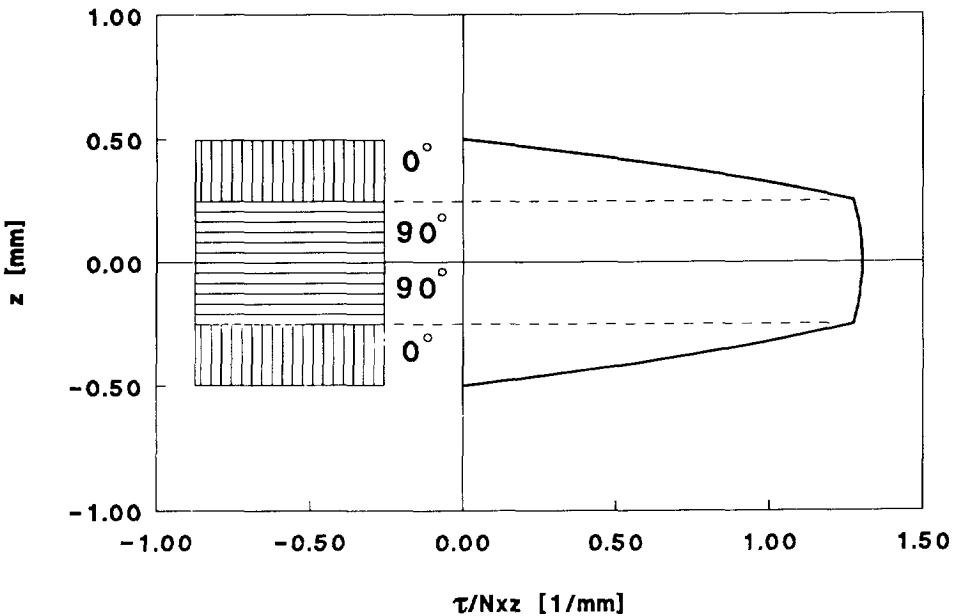
Figure 8 Transverse shear stress distribution through the thickness of a symmetric CFRP 0°/90° laminate of 1.mm thickness

For U, the strain energy in transverse shear, the following holds:

$$U = \frac{1}{2} \int_{-t/2}^{t/2} \tau_{xz}(z) \cdot \gamma_{xz}(z)\, dz = \frac{1}{2} \int_{-t/2}^{t/2} \frac{\tau_{xz}^2(z)}{Q_{44}(z)}\, dz \tag{34}$$

Substituting τ_{xz} from (28) yields:

$$U = \frac{N_{xz}^2}{2D_{11}^{**2}} \int_{-t/2}^{t/2} \frac{g_x^2(z)}{Q_{44}(z)}\, dz \tag{35}$$

Substituting of U into (33) yields:

$$S_{xz} = \frac{D_{11}^{**2}}{\displaystyle\int_{-t/2}^{t/2} \frac{g_x^2(z)}{Q_{44}(z)}\, dz} \tag{36}$$

Equation (36) gives the transverse shear stiffness S_{xz} in terms of the laminate parameters. It can be related to the elementary TSS A_{44} with a well-known *shear correction factor* k_x ([Vlachoutsis92], [Chow71], [Whitney70]), as follows:

$$k_x \cdot A_{44} = S_{xz} \tag{37}$$

Note that for homogeneous isotropic laminates a value $k_x = 5/6$ is obtained.

3.2   Overall buckling under compressive load

In chapter 2 the energy method was used to derive the stability equation of a rectangular simply-supported orthotropic plate under compressive load. This method is used again here, now including transverse shear effects. First the buckling equation is derived, then the results are compared with results from the literature.

3.2.1 Derivation of the buckling equation

To include transverse shear effects means introducing more flexibility into the system. Extra deformations, the transverse shear deformations ws_x and ws_y, are defined, acting in addition to the bending deformations wb_x and wb_y. These four 'partial deformations' relate to the total out-of-plane deformation w as follows:

$$w = wb_x + ws_x = wb_y + ws_y \qquad (38)$$

The out-of-plane deformation w and its components wb_x, ws_x, wb_y, ws_y are all defined as double sine waves for a given number of half waves m and n along and across the panel, to satisfy rigorously the boundary conditions of simple support:

$$
\begin{aligned}
w &= A \, \sin\frac{m\pi x}{a} \, \sin\frac{n\pi y}{b} \\
wb_x &= Ab_x \, \sin\frac{m\pi x}{a} \, \sin\frac{n\pi y}{b} \\
ws_x &= As_x \, \cdots \\
wb_y &= Ab_y \, \cdots \\
ws_y &= As_y \, \cdots
\end{aligned}
\qquad (39)
$$

With (38) and (39) two of the five unknowns A, Ab_x, As_x, Ab_y, As_y can be eliminated:

$$A = Ab_x + As_x = Ab_y + As_y \qquad (40)$$

In chapter 2 the plate had only bending strain energy Ub, expressed in terms of w. Now Ub is written in terms of wb_x and wb_y:

$$
Ub = \int_0^a \int_0^b \frac{1}{2}\Big(D_{11}\,wb_{x,xx}^2 + D_{22}\,wb_{y,yy}^2 + \\
+ 2D_{12}\,wb_{x,xx}wb_{y,yy} + D_{66}(wb_{x,xy}+wb_{y,xy})^2 \Big) \, dx\,dy
\qquad (41)
$$

Furthermore, the transverse shear strain energy Us is introduced (see [Libove48] and [Plantema66]):

$$
Us = \int_0^a \int_0^b \frac{1}{2}\Big(S_{xz}\,ws_{x,x}^2 + S_{yz}\,ws_{y,y}^2 \Big) \, dx\,dy
\qquad (42)
$$

For the work of the applied loads W (15) still holds.

The solution to the problem, i.e. values for the remaining three deflection parameters A, As_x, As_y, is found by the theorem of stationary total potential. This states that in a state of equilibrium the change in total potential of the system (Ub+Us-W) is zero:

$$\frac{\partial(Ub+Us-W)}{\partial A} = 0. \quad , \quad \frac{\partial(Ub+Us-W)}{\partial As_x} = 0. \quad , \quad \frac{\partial(Ub+Us-W)}{\partial As_y} = 0. \quad (43)$$

A condensed notation is introduced, as follows:

$$D16 = D_{11}(\frac{m\pi}{a})^4 + D_{66}(\frac{m\pi}{a})^2(\frac{n\pi}{b})^2$$

$$D26 = D_{22}(\frac{n\pi}{b})^4 + D_{66}(\frac{m\pi}{a})^2(\frac{n\pi}{b})^2$$

$$D126 = (D_{12}+D_{66})(\frac{m\pi}{a})^2(\frac{n\pi}{b})^2$$

$$SX = S_{xz}(\frac{m\pi}{a})^2 \quad (44)$$

$$SY = S_{yz}(\frac{n\pi}{b})^2$$

$$PXY = p_x(\frac{m\pi}{a})^2 + p_y(\frac{n\pi}{b})^2$$

Evaluation of (43) yields the following set of three linear equations in A, As_x, As_y:

$$\begin{bmatrix} D16+D26+2.D126-PXY & -(D16+D126) & -(D26+D126) \\ -(D16+D126) & D16+SX & D126 \\ -(D26+D126) & D126 & D26+SY \end{bmatrix} \cdot \begin{bmatrix} A \\ As_x \\ As_y \end{bmatrix} = \begin{bmatrix} 0. \\ 0. \\ 0. \end{bmatrix} \quad (45)$$

This homogeneous set of equations has a non-zero solution only if the determinant of the coefficient matrix is zero. This condition yields the buckling equation:

$$PXY = \frac{(SX+SY).(D16.D26-D126^2) + SX.SY.(D16+D26+2.D126)}{(SX+D16).(SY+D26) - D126^2} \quad (46)$$

As in chapter 2, the integer parameters m and n, representing the number of

half waves in each direction, have to be varied to obtain the smallest critical load. Figure 5 shows the buckling load for unidirectional compression; in that case always n=1, while the value of m depends on the parameters of the problem. When the size of the panel is decreased, larger m are found. At a certain size the number of half-waves m increases without limit, while p_x decreases asymptotically to S_{xz}. This is explained in detail below.

An interesting phenomenon occurs when the transverse shear stiffnesses S_{xz} and S_{yz} are small compared with the ratio of bending stiffnesses to panel dimensions. Then the panel will buckle in a 'transverse shear mode', for which the waveform is undefined and, if compression is applied in only one direction, the buckling load is equal to the transverse shear stiffness in the direction of the applied load. Figure 5 shows this clearly for the case of uniaxial compression; as the panel becomes smaller, the buckling load diverts from that of a *plate* (without transverse shear deformation) towards the transverse shear stiffness S_{xz}. This is also recognizable in (46); when D16, D26 and D126 are large compared with SX and SY, and taking p_y=0., (46) simplifies to:

$$PXY = SX + SY$$
$$p_{xts}(\frac{m\pi}{a})^2 = S_{xz}(\frac{m\pi}{a})^2 + S_{yz}(\frac{n\pi}{b})^2 \tag{47}$$
$$p_{xts} \to S_{xz} \quad , m \to \infty, n=1$$

where $p_{x\,ts}$ is the compression buckling load in transverse shear mode.
For laminates this transverse shear buckling behaviour is well possible; for sandwich panels it is less realistic, as will be shown in chapter 4, because then the transverse shear mode is prevented by the bending stiffnesses of the separate faces.

3.2.2 Verification of the buckling equation

In the previous paragraph a buckling equation is derived on the basis of the energy method, using a first order shear theory model of the panel, with an improved transverse shear stiffness definition. In this paragraph the validity of this approach is examined by comparison with buckling loads obtained by more refined analyses [Noor75]. This reference contains buckling results using 3-D linear elasticity theory, for a large number of (symmetric and non-symmetric) composite panels of unidirectional (UD) material in alternate layers at 0° and 90°. Material stiffness data are as follows:

Table 1 Material data

E_x [MPa]	E_y [MPa]	G_{xy} [MPa]	G_{xz} [MPa]	G_{yz} [MPa]	v_{xy} [-]
300000.	10000.	6000.	6000.	5000.	0.25

The buckling loads are compared below for various cases (all simply-supported), identified by the quantity NL (taken from [Noor75]) indicating the number of distinct layers in the laminate. Table 2 gives the laminate stacking associated with the values of NL. Note that all the laminates have 60 plies at 0° and 60 plies at 90°, giving a constant total thickness of 120 plies (or 12.mm) in each case.

Table 2 Laminate composition

NL	laminate stacking
a) symmetric laminate	
3	$[0°_{30}/90°_{30}]_s$ [†]
5	$[0°_{15}/90°_{30}/0°_{15}]_s$
9	$[0°_{10}/90°_{15}/0°_{10}/90°_{15}/0°_{10}]_s$
b) non-symmetric laminate	
2	$[0°_{60}/90°_{60}]_t$ [‡]
4	$[0°_{30}/90°_{30}]_{2t}$
6	$[0°_{15}/90°_{15}]_{4t}$
10	$[0°_{12}/90°_{12}]_{5t}$

† meaning of the notation: from the top to the mid-plane first 30 plies at 0° and then 30 plies at 90°; the 's' stands for 'symmetric', and the number of plies is only given for the upper half of the laminate.
‡ from top to bottom first 60 plies at 0° and then 60 plies at 90°; the 't' stands for 'total'.

First, the influence of orthotropy is examined by varying E_x while the other material data are held constant; the results, in terms of E_x/E_y, are given in table 3. The main parts a) and b) of the table contain results for the present (first order shear) theory and 3-D linear elasticity theory (results from

[Noor75]). A third part c) of the table contains buckling coefficients for the laminate NL=10 when the *plate* buckling formula of chapter 2 is used.

Table 3 Buckling load coefficient $\dfrac{p_x \cdot b^2}{E_y \cdot t^3}$ of square plates in terms of E_x/E_y; material data from table 1, except E_x (modified to obtain the required value of E_x/E_y); b/t=10.

NL	E_x/E_y
	3.	10.	20.	30.	40.
a) first order shear theory
3	5.39	9.91	15.21	19.51	23.08
5	5.40	10.14	16.00	21.01	25.33
9	5.41	10.18	16.13	21.25	25.69
2	4.77	6.22	7.91	9.44	10.85
4	5.23	9.08	13.79	17.80	21.27
6	5.33	9.69	15.10	19.74	23.77
10	5.38	10.02	15.80	20.78	25.10
b) 3-D linear elasticity theory
3	5.30	9.76	15.02	19.30	22.88
5	5.33	9.96	15.65	20.47	24.59
9	5.34	10.04	15.92	20.96	25.34
2	4.69	6.12	7.82	9.37	10.82
4	5.17	9.02	13.74	17.78	21.28
6	5.27	9.61	15.00	19.64	26.67
10	5.32	9.91	15.67	20.63	24.96
c) plate buckling theory
10	5.72	11.29	19.25	27.21	35.15

There is good agreement between parts a) and b) throughout; the difference is in only four cases more than 2%, and never more than 3%. The *plate buckling*

results for NL=10, on the other hand, are 7.5% to 41% higher than the results of b).

Next, the influence of thickness is examined by comparing results for short, thicker (square) panels. These are given in table 4.

Table 4 Buckling load coefficient $\dfrac{p_x.b^2}{E_y.t^3}$ for thick square panels (b/t=5.), with

material data of table 1

NL	first order shear theory	3-D el. theory
3	10.54	10.38
9	11.54	12.14
2	6.73	6.66
10	10.63	12.07

For some cases, considerable differences are found. Note that for some, but not all, laminates the first order shear theory gives *lower* buckling loads than the 3-D theory.

Subsequently, the influence of the length to width ratio a/b is examined; results of present first order shear theory and of the 3-D linear elasticity theory of [Noor75] are given in table 5 (again for a thickness ratio of b/t=10.), showing a good agreement throughout.

Table 5 Buckling load coefficient $\dfrac{p_x \cdot b^2}{E_y \cdot t^3}$ for different length to width ratio's;

material data of table 1; (b/t=10.)

NL	a/b						
	0.3	0.5	1.0	1.5	2.0	2.5	3.0
a) first order shear theory							
2	21.60	13.91	9.435	10.07	9.435	9.616	9.435
4	28.78	22.37	17.80	18.18	17.80	17.70	17.80
10	34.61	26.56	20.78	21.33	20.78	20.71	20.78
b) 3-D linear elasticity theory[†]							
2	22.2	13.9	9.5	10.0	9.3	9.3	9.3
4	30.0	22.3	17.6	18.2	17.7	17.4	17.4
10	34.8	26.5	20.6	21.1	20.3	20.6	20.4

† only one decimal digit, because values are read from a graph

3.2.3 Possible values for waveform parameters m and n

In formula (46) for the direct buckling loads p_x and p_y the parameters m and n, indicating the number of half-waves along and across the panel, have to be varied to find the lowest possible combination of p_x and p_y. Knowing which combinations of values for m and n are feasible, and which combinations can be excluded a priori, would eliminate several calculations and therefore shorten computation time. In this respect, it is worth mentioning that in many publications on direct buckling loads of orthotropic plates and panels the results are always given for either m=1 or n=1 without, however, proving this (eg. [Wittrick52]).

A solution is presented in two steps. In the first place, it is known from literature that for every *orthotropic plate* an equivalent *isotropic plate* can be defined with the same compression buckling load (reported in [Wittrick52]). Next, below it is proved that isotropic *panels* (with finite transverse shear

stiffness) will indeed buckle with m=1 or n=1. Combining the two cases it can be assumed that this will hold for an orthotropic *panel* (with finite transverse shear stiffness) as well.

Assuming isotropic bending and transverse shear behaviour of the panel the parameters of formula (46) can be simplified as follows, introducing the stiffness parameters D and S:

$$D = D_{11} = D_{22} = D_{12} + 2D_{66}$$
$$S = S_{xz} = S_{yz} \tag{48}$$

Because the buckling wave form parameters m and n always appear in connection with the panel dimensions a and b, the following parameters M and N are introduced:

$$M = \frac{m\pi}{a}, \qquad N = \frac{n\pi}{b} \tag{49}$$

which are considered real values for now (i.e. not integer, or discrete).
Substituting the introduced parameters D, S, M and N formula (46) can be rewritten as:

$$p_x = \frac{D(M^2+N^2)^2}{M^2(1+\dfrac{D}{S}(M^2+N^2))} - p_y\frac{N^2}{M^2} \tag{50}$$

To prove that in buckling either m=1 or n=1, it is shown that the regions where the partial derivatives of p_x in (50) with respect to M and N are less than zero do not overlap. If they would overlap, in that region higher values of M and N would produce lower buckling loads; but they do not, and therefore the lowest physically possible value of either M or N will yield the lowest value for p_x.

Partial derivation of p_x in (50) with respect to M yields:

$$\frac{\partial p_x}{\partial M} = \frac{2p_y N^2}{M^3} + \frac{2D}{M^3(1+\frac{D}{S}(M^2+N^2))^2}\left[(M^2+N^2)(M^2-N^2(1+\frac{D}{S}(M^2+N^2)))\right] \tag{51}$$

And with respect to N:

$$\frac{\partial p_x}{\partial N} = \frac{-2p_y N}{M^2} + \frac{2ND}{M^2(1+\frac{D}{S}(M^2+N^2))^2}\left[(M^2+N^2)(2+\frac{D}{S}(M^2+N^2))\right] \tag{52}$$

If the following two conditions were to hold:

$$\begin{cases}\dfrac{\partial p_x}{\partial M} < 0 \\[2mm] \dfrac{\partial p_x}{\partial N} < 0\end{cases} \tag{53}$$

the following condition would hold as well (with M, N$\geq$0):

$$(\frac{\partial p_x}{\partial M}*M + \frac{\partial p_x}{\partial N}*N) < 0 \tag{54}$$

Substituting (51) and (52) into (54) yields the following condition in which terms in p_y are eliminated:

$$\frac{2D(M^2+N^2)^2}{M^2(1+\frac{D}{S}(M^2+N^2))^2} < 0 \tag{55}$$

With M, N, D, S all greater than zero the last inequality is never satisfied. Returning to the basic assumption it is therefore proved that there do not exist values for M and N for which both partial derivatives are less than zero. Therefore taking either M or N at its minimum value will produce the lowest buckling load in formula (50). The minimum values of M and N correspond, of course, to m=1 and n=1 respectively, hence this traditional assumption is now proven.

This is an interesting conclusion that allows all evaluations of the buckling load for which both m and n are greater than 1 to be eliminated a priori. Furthermore if the buckling loads p_x for various values of m, while n=1, produces a minimum p_x for m>1, it is not anymore necessary to verify p_x for n>1 (m=1) because it has just been proved that if $\delta p_x/\delta m<0$, then always $\delta p_x/\delta n>0$ (here m and n are improperly used, as if these were real numbers).

3.3 Overall buckling under shear load

Similar to 3.2, a buckling formula is first derived, which is then compared to results in literature.

3.3.1 Buckling formula

Unfortunately the plate buckling formula of 2.3.2 cannot be expanded to include transverse shear flexibility, because this formula was obtained by interpolation of graphical data. Therefore a knock-down factor f is defined, analogous to that of Plantema [Plantema66]. That source refers to Kuenzi et al. [Kuenzi60] as the origin of the knock-down formula. [Kuenzi60] applies an energy method to obtain the buckling equation, using a truncated Fourier series for the out-of-plane displacement w. Unfortunately, it appears that this method would require a computing time beyond what can be allowed in the present application. Therefore this method, and its resulting design curves, are left aside in favour of the knock-down factor f, similar to that of Plantema (modified to allow for orthotropic TSS):

$$q_s = f.q_0$$

$$\text{where: if } \left[s \geq 1 + (\frac{b}{a})^2\right] \text{ then: } f = \cfrac{1}{1+\cfrac{k_0-1-(\frac{b}{a})^2}{s}}$$

$$\text{else: } f = \frac{s}{k_0}$$

$$\text{and where: } \quad k_0 = (\frac{b}{\pi})^2\frac{q_0}{\sqrt{D_{11}D_{22}}} \tag{56}$$

$$s = (\frac{b}{\pi})^2\sqrt{\frac{S_{xz}S_{yz}}{D_{11}D_{22}}}$$

Figure 9 shows the buckling load obtained with (56); notice the similarity with Figure 5 for compression buckling.

The difference between (56) and the knock-down factor of Plantema is in the definition of s; in Plantema, restricted to isotropic TSS, this was defined as:

$$s_{Plantema} = (\frac{b}{\pi})^2 \frac{S_{xz}}{\sqrt{D_{11}D_{22}}} \qquad (57)$$

Then, as Plantema explains, for $s<(1+(b/a)^2)$, buckling occurs in a transverse shear mode, with $q_{ts}=S_{xz}$. Here, on the other hand, with s defined as in (56), the transverse shear mode yields the following buckling load:

$$q_{ts} = \sqrt{S_{xz}.S_{yz}} \qquad (58)$$

(where 'ts' stands for transverse shear).

This buckling load q_{ts} is equal to the transverse shear buckling load $q_{ts\infty}$ for *infinitely long* panels with orthotropic TSS, derived by the author [Bladel88]. In [Bladel88] (58) is derived for infinitely long orthotropic panels with an energy method and a skewed sine wave buckling displacement, applying only
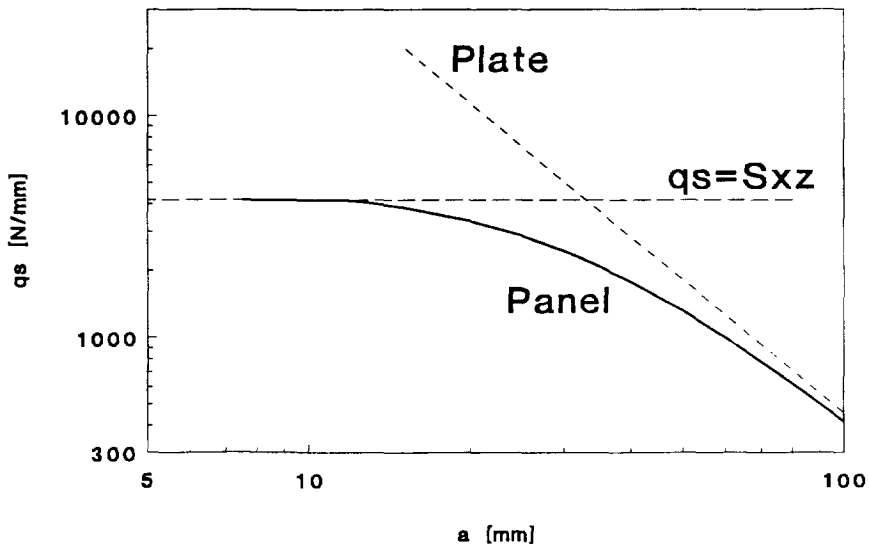
Figure 9 Shear buckling of an orthotropic panel, including transverse shear effects

transverse shear deformation. The use of $q_{ts\infty}$ for *rectangular* panels as well is justified by the fact that the equation (58) for $q_{ts\infty}$ in [Bladel88] is obtained without any condition on the wavelength.

3.3.2 Comparison of results with literature

[Kuenzi60], previously referred to in 3.3.1, also gives some experimental results. Although restricted to square isotropic panels, they are used here to validate (56). Figure 10 compares the test results of [Kuenzi60] with the numerical results of (56). Reasonable agreement is found, although there is considerable scatter in the experimental results.

The bending stiffness of the faces (considered further in chapter 4) is not included in the analysis. This results in conservative calculated buckling loads. This might explain why, in Figure 10, in the region s<2. where transverse shear mode buckling occurs (see (56)), the prediction is so conservative. Unfortunately, Kuenzi does not report whether transverse mode shear buckling has in fact occurred in any of the experiments.
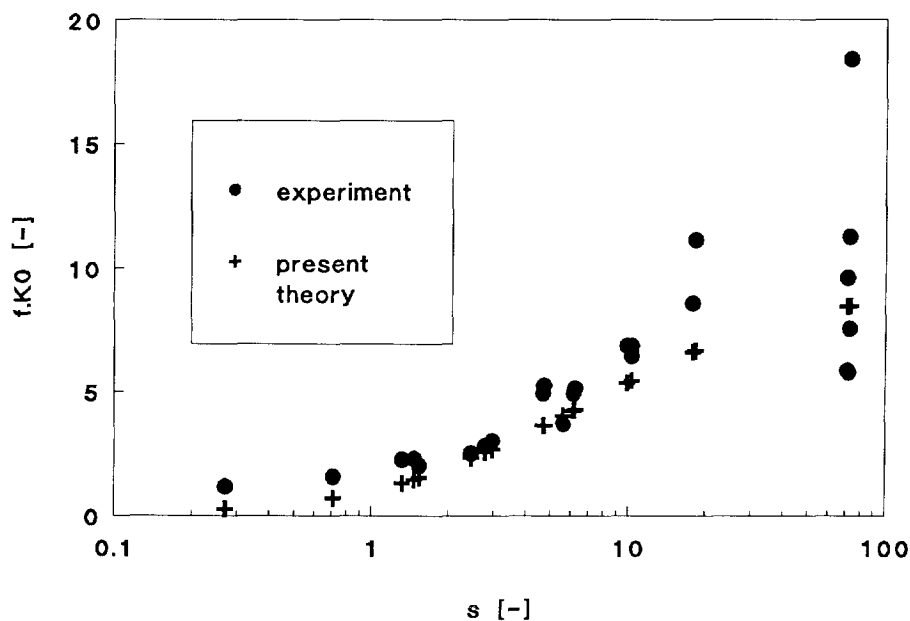
Figure 10 Comparison of use of knock-down factor f with experimental results of [Kuenzi60]

3.4   Interaction of compression and shear loads

For isotropic plates a well-known interaction formula for buckling under combined compression and shear loads exists [Bleich52]:

$$\frac{N_x}{p_x} + \left(\frac{N_{xy}}{q}\right)^2 \geq 1. \tag{59}$$

Buckling will occur if (59) is satisfied, in other words when the combination of the applied loads N_x and N_{xy} is such to make the left-hand side of (59) equal to or higher than one. In [Bladel88] this formula was examined for use with orthotropic plates, including transverse shear effects, showing it to be applicable in this more general case as well.

4
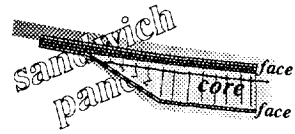
Sandwich Panel Analysis

Two aspects of the compression buckling behaviour of sandwich panels, beyond those dealt with in chapter three, are considered in this chapter: the effect of bending of the faces, and the influence of an asymmetric layup. Shear load is not covered, because the associated formulae of chapter three cannot be adapted for these effects. It should be recalled that the analysis methods presented here are intended for use in an interactive computer program for the designer; therefore, while adequate accuracy must be achieved, the required calculations should not be too elaborate or time consuming.

4.1 Effect of face bending on the compression buckling load

By the term *face bending* is meant bending of the faces as two independent plates. Although the bending stiffnesses D_{ij} do include the bending stiffnesses of the faces with respect to their own mid-planes, in chapter three these stiffnesses are only associated with the overall *bending* deformation of the panel wb. In this chapter, on the other hand, the face bending effect is not associated with the overall bending deformation wb, but rather with the total out-of-plane deformation of the panel w, as illustrated in Figure 11. This figure presents on the left-hand side the out-of-plane deformation of a panel according to the first

a. first order   b. sandwich panel
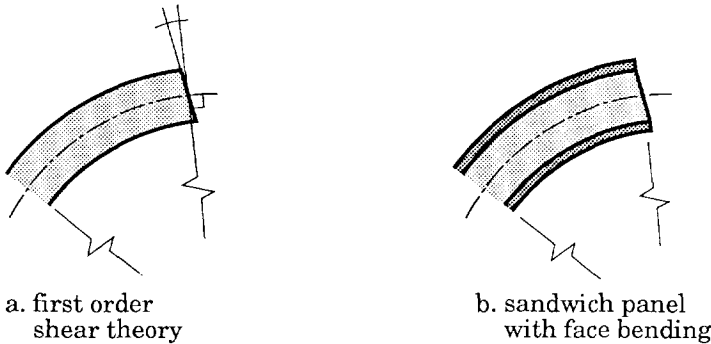   shear theory   with face bending

Figure 11 Face bending of sandwich panels

order shear theory of chapter three, and on the right-hand side a more realistic out-of-plane deformation of a sandwich panel where the face bending is associated with the total out-of-plane deformation w. The two models presented here to include face bending in the compression buckling load of rectangular, orthotropic sandwich panels are approximations extending the first order shear theory.

The influence of this effect on the compression buckling load will be large when the faces of the sandwich panel are thick, and when the panel is short.

4.1.1 Face bending included in the energy formulation

A first method is similar to that of [Allen69]. It defines the strain energy associated with bending of the faces separately and includes this in the energy method of chapter three.

As mentioned above, the essence of this method is to associate the face bending stiffnesses (written as D_{ijf1} and D_{ijf2} for faces 1 and 2, respectively) also with the shear deformation ws, and not only with the bending deformation wb (as is done implicitly in chapter three, through D_{ij}). This is done by introducing the strain energy contribution Uf, associated with bending of the faces, in terms in D_{ijf} and ws. The strain energy U of the sandwich panel, including face bending, is now given as the sum of Ub, Us and Uf:

$$U = Ub + Us + Uf$$

$$Ub = \int_0^a \int_0^b \frac{1}{2}\left(D_{11}\,wb_{x,xx}^2 + D_{22}\,wb_{y,yy}^2 + \right.$$
$$\left. + 2D_{12}\,wb_{x,xx}wb_{y,yy} + D_{66}(wb_{x,xy}+wb_{y,xy})^2\right)\,dx\,dy \qquad (60)$$

$$Us = \int_0^a \int_0^b \frac{1}{2}\left(S_{xz}\,ws_{x,x}^2 + S_{yz}\,ws_{y,y}^2\right)\,dx\,dy$$

$$Uf = \int_0^a \int_0^b \frac{1}{2}\left((D_{11f1}+D_{11f2})\,ws_{x,xx}^2 + (D_{22f1}+D_{22f2})\,ws_{y,yy}^2 + \right.$$
$$\left. + 2(D_{12f1}+D_{12f2})\,ws_{x,xx}ws_{y,yy} + (D_{66f1}+D_{66f2})(ws_{x,xy}+ws_{y,xy})^2\right)\,dx\,dy$$

Note that the correct approach would be to subtract the face bending stiffnesses from D_{ij} in the formula for Ub and include terms in wb in the face bending strain energy Uf. The terms in the bending stiffness D_{11} and related face bending stiffnesses D_{11f1} and D_{11f2} in (60) would then be:

$$\text{contribution to Ub: } (D_{11} - D_{11f1} - D_{11f2}) \, wb_{x,xx}^2 \qquad (61)$$
$$\text{contribution to Uf: } (D_{11f1} + D_{11f2})(wb_{x,xx} + ws_{x,xx})^2$$

The difference between (60) and (61) is only in the cross terms:

$$(D_{11f1} + D_{11f2}) \, 2 \, wb_{x,xx} \, ws_{x,xx} \qquad (62)$$

Because with (60) the resulting formula is simpler the representation of (60) is retained here.

The buckling equation is derived in the same way as in chapter three. After substitution of double sine wave deformations for w, wb_x, ws_x, wb_y, ws_y and evaluation of integrals and derivatives, the buckling equation is the condition for which the determinant of the set of equations in the coefficients A, As_x and As_y becomes zero. As in chapter three a condensed notation is defined:

$$D16 = D_{11}(\frac{m\pi}{a})^4 + D_{66}(\frac{m\pi}{a})^2(\frac{n\pi}{b})^2$$
$$D16F = (D_{11f1} + D_{11f2})(\frac{m\pi}{a})^4 + (D_{66f1} + D_{66f2})(\frac{m\pi}{a})^2(\frac{n\pi}{b})^2$$
$$D26 = D_{22}(\frac{n\pi}{b})^4 + D_{66}(\frac{m\pi}{a})^2(\frac{n\pi}{b})^2$$
$$D26F = (D_{22f1} + D_{22f2})(\frac{n\pi}{b})^4 + (D_{66f1} + D_{66f2})(\frac{m\pi}{a})^2(\frac{n\pi}{b})^2$$
$$D126 = (D_{12} + D_{66})(\frac{m\pi}{a})^2(\frac{n\pi}{b})^2 \qquad (63)$$
$$D126F = (D_{12f1} + D_{12f2} + D_{66f1} + D_{66f2})(\frac{m\pi}{a})^2(\frac{n\pi}{b})^2$$
$$SX = S_{xz}(\frac{m\pi}{a})^2$$
$$SY = S_{yz}(\frac{n\pi}{b})^2$$
$$PXY = p_x(\frac{m\pi}{a})^2 + p_y(\frac{n\pi}{b})^2$$

The following buckling equation is then obtained, in which the stability equation (46) can clearly be recognized:

$$PXY = \frac{(SX+D16F+SY+D26F+2.D126F).(D16.D26-D126^2) + \\ + ((SX+D16F).(SY+D26F)-D126F^2).(D16+D26+2.D126)}{(SX+D16F+D16).(SY+D26F+D26) - (D126+D126F)^2} \quad (64)$$

As in chapter three, the number of half waves m and n are free variables in (64) and have to be chosen to obtain the lowest buckling load. There is no reason to believe that the comments on possible values of m and n (paragraph 3.2.3) should not be applicable to the present case (including face bending) as well.

Figure 12 shows the effect of face bending on the compressive buckling load of a square sandwich panel with ±45°-faces and a honeycomb core, by comparison with the formula of chapter three. For large panels (large width to thickness ratio a/t), the method described above and that of chapter three give the same results, whereas for small panels the present method yields significantly higher buckling loads. While the formula of chapter three, for small panels, yields a transverse shear mode of buckling with a buckling load equal to the transverse shear stiffness S_{xz} (as discussed in chapter three), the present method does not. This is because, for the transverse shear mode buckling to occur, the number of half waves along the panel m has to grow towards infinity. This is prevented in the present case by the strain energy associated with bending of the faces, which would have to grow accordingly.
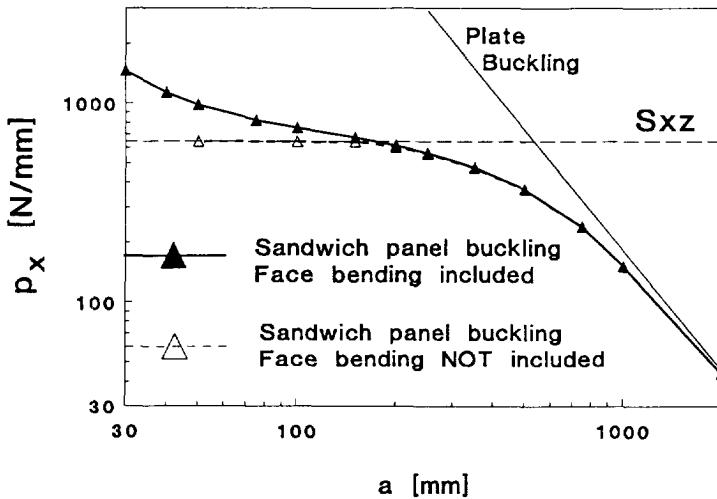
Figure 12 Effect of face bending on compression buckling load p_x of sandwich panels (square ±45°CFRP panel; two 1.mm faceplates and a 10.mm honeycomb core)

4.1.2 Face bending included in equivalent transverse shear stiffnesses

Another approach to include the face bending stiffnesses in the compressive buckling load of sandwich panels is described fully in [Bladel89a]; the idea behind the method is to use the buckling load in a transverse shear mode to obtain equivalent $S_{xz\ ts}$ and $S_{yz\ ts}$ (*ts* stands for transverse shear), which can then be used in Formula (46). This is explained briefly below.

First, a buckling load $p_{x\ ts}$ is calculated in a particular transverse shear mode where no *overall* bending of the panel, but only bending of the *faces*, is present, see Figure 13; at the edges of the panel the mid-planes of the two faces and the core in both undeformed and deformed states are constrained to lie in a vertical plane. With the energy method a compression buckling load $p_{x\ ts}$ can be derived, for every number of half waves m and n along and across the panel. Substituting this buckling load in the transverse shear mode formula (47) of chapter three, further assuming $S_{xz\ ts} = S_{yz\ ts}$, defines the equivalent transverse shear stiffnesses $S_{xz\ ts}$ and $S_{yz\ ts}$ for every m and n. This can be used in the buckling equation (46) of chapter three. In this way, the buckling formula of chapter three is improved by using *equivalent* transverse shear stiffnesses that include the effect of face bending.

The results of this approach are similar to those of paragraph 4.1.1. Nevertheless the method of paragraph 4.1.1 is to be preferred, because the resulting equation (64) can be easily used when the face bending effect is not to be included, simply by substituting zero face bending stiffnesses D_{ijf1} and D_{ijf2}. Furthermore, for every m and n only one buckling analysis is done in the method of paragraph 4.1.1, while in paragraph 4.1.2 an extra transverse shear buckling analysis is always performed.
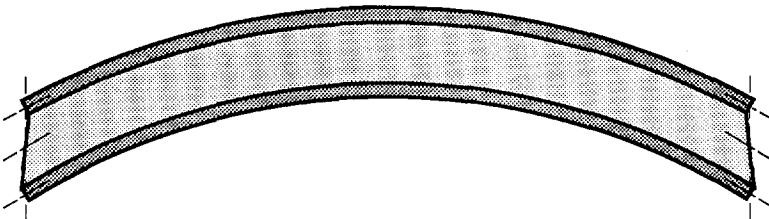
Figure 13 Transverse shear mode buckling without overall bending deformation

4.2   Effect of eccentricities in sandwich panels

In practice, eccentricities are hard to avoid in sandwich panels loaded in compression. First, the panel itself might not be symmetric with respect to its mid-plane; then even if the compressive load is applied on the mid-plane, in effect an eccentricity will occur. Also, when the edges of the sandwich panel are not built into a spacious fitting, but rather crushed to obtain flat, easily fastened edges (see for example Figure 14), the in-plane loading will be applied eccentrically. In this paragraph shear loads are not considered, because these would make the analysis much more involved; then the contributions of all the different waveforms (sine waves along and across the panel) to the total out-of-plane deflection are coupled.

When an eccentricity is present, a compressive load will induce a bending moment that can easily lead to premature failure of the panel. Two approaches can be followed to prevent this from happening; first of all, one can simply try to reduce the eccentricity itself by choosing a layup such that its neutral axis is near to the plane of loading, perhaps creating a sandwich panel with one 'stiff' face - where the load is applied - and one meant to provide stability. The advantage of this approach is its simplicity, while the disadvantage is that it is not possible to judge the influence of the possible remaining (small) eccentricity. Therefore, additionally, the second approach defines the effect of the eccentricity in terms of stresses in the laminate, checking whether these remain within allowable bounds. This approach gives more information and defines a suitable upper bound for the value of the eccentricity, but it is much more involved and implemented here only in an approximate way. Below, the calculations required to obtain the value of the eccentricity are given, and then the associated stresses are calculated.
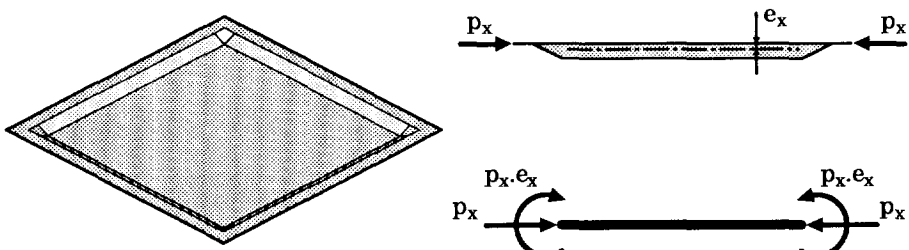
Figure 14 Sandwich panel with flattened edges creates an eccentricity for compressive loads

4.2.1 Definition of eccentricity

The value of the eccentricity e_x and e_y is the difference between the vertical position of the applied load and the vertical position of the neutral axis in that direction. Figure 14 shows this for the case of the sandwich panel with flattened edges.

The vertical position of the applied load can be found by considering how the load is applied to the panel at its edges; a compressive load will be introduced here via fasteners or the adhesive layer with which the panel is attached to the rest of the structure. This compressive load will be carried principally by the layers of the laminate that are stiff in compression. A first approximation is therefore to consider it to be applied at the middle of these 'stiff' layers.

The vertical position of the neutral axis can easily be derived from the ABD-matrix of the classical laminate theory, with the following result:

$$z_{na\ x} = \frac{B_{11}}{A_{11}} \quad ; \quad z_{na\ y} = \frac{B_{22}}{A_{22}} \tag{65}$$

Note that the definition of neutral axes means adopting cylindrical bending assumptions (recall that also in chapters two and three cylindrical bending is used). Because a composite panel is generally not homogeneous or isotropic, the position of the neutral axis in x- and y-directions may not coincide.

4.2.2 Evaluation of stresses associated with eccentricity

Stresses induced by eccentricity are defined in two steps; first, the out-of-plane deformations are defined with the energy method, and then the classical laminate theory (CLT) is used to calculate the stresses associated with these deformations. A failure criterion can then be used to check against failure of the structure. [Bladel89b] presents this method in detail; here, only the main features are reported.

The energy method is used to obtain the out-of-plane deformation of the panel. The formulation of the energy equation is similar to that of chapter three, except that now there is an extra contribution to the work of the applied load, associated with the eccentricity, We. This contribution can be derived with the help of Figure 15; for a strip, infinitesimally narrow in the y-direction, the work associated with the eccentricity dWe becomes:

$$dWe = N_x e_x \left(wb_{x,x}(x=a) - wb_{x,x}(x=0.) \right) dy$$
$$dWe = N_x e_x \left(\int_0^a wb_{x,xx} dx \right) dy \qquad (66)$$

The most accurate formulation would be to use a truncated Fourier series for the out-of-plane displacement function w and its components wb_x and wb_y:

$$w = \sum_{m,n} A \sin(\frac{m\pi x}{a}) \sin(\frac{n\pi y}{b}) \qquad (67)$$

However, after substitution and evaluation of the integrals there is no coupling between terms in different m and n. Therefore, it is possible simply to use a double sine wave formulation for w for only one m and n (as is done in chapter three). The actual out-of-plane deflection is then obtained by summing up all partial deflections for specific m and n.

When w is defined by a double sine wave for a single waveform (m and n), after integration over the whole panel, the work associated with the eccentricity becomes:

$$We = \frac{ab}{8} \left(-N_x e_x (\frac{m\pi}{a})^2 \frac{32}{mn\pi^2} Ab_x - N_y e_y (\frac{n\pi}{b})^2 \frac{32}{mn\pi^2} Ab_y \right) \qquad (68)$$

(where only odd m and n yield non-zero values of We).
The resulting deflection under a given load N_x and N_y is that for which the total energy (Ub+Us-W-We) is stationary. As in chapter three the derivatives are taken with respect to the coefficients A, As_x and As_y of the displacement
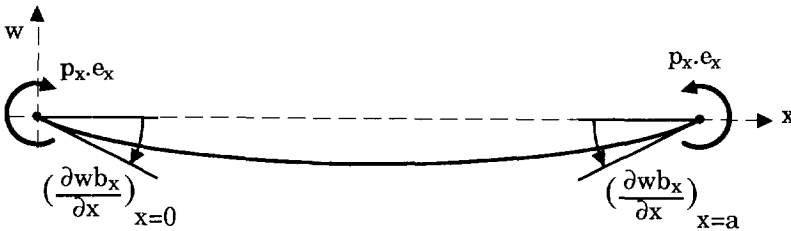
Figure 15 Derivation of the work We of the eccentric compressive load

function. In addition to the condensed notation of (63) the following parameters are defined:

$$NXY = N_x(\frac{m\pi}{a})^2 + N_y(\frac{n\pi}{b})^2$$

$$E_x = e_x(\frac{m\pi}{a})^2 \frac{16}{mn\pi^2}$$

$$E_y = e_y(\frac{n\pi}{b})^2 \frac{16}{mn\pi^2}$$

(69)

The following set of three equations is then obtained:

$$\begin{bmatrix} D16+D26+2.D126-NXY & -(D16+D126) & -(D26+D126) \\ -(D16+D126) & D16+SX & D126 \\ -(D26+D126) & D126 & D26+SY \end{bmatrix} \cdot \begin{bmatrix} A \\ As_x \\ As_y \end{bmatrix} = \begin{bmatrix} -N_x.E_x-N_y.E_y \\ N_x.E_x \\ N_y.E_y \end{bmatrix}$$

(70)

The left hand sides of the equations are identical to those of (46) of chapter 3. But here, the set of equations is not homogeneous, hence for every given value of the applied load, non-zero values for the displacement coefficients A, As_x and As_y are found (for the m and n in question) simply by solving the set of equations. Note that when the applied load is increased to the buckling load, the deflections will increase to infinity.

Just as in the buckling analysis it is interesting here to know *a priori* which values for m and n are important. Although only odd m and n are feasible here, the question is more complicated than in case of buckling because the analysis requires curvatures rather than the plain deflections. This aspect is covered in the paragraph below.

4.2.3 Selection of waveform parameters m and n

The selection of relevant values for m and n for the eccentricity analysis is more involved than that for buckling. Because in the end the stresses associated with the out-of-plane deflection are calculated, the curvatures rather than the plain deflections have to be defined (see Equation (1)). These are defined as:

$$\kappa_x = (-1)\sum_{m,n} \left(\frac{m\pi}{a}\right)^2 A \sin(\frac{m\pi}{a}) \sin(\frac{n\pi}{b})$$

$$\kappa_y = (-1)\sum_{m,n} \left(\frac{n\pi}{b}\right)^2 A \sin(\frac{m\pi}{a}) \sin(\frac{n\pi}{b}) \qquad (71)$$

$$\kappa_{xy} = 2\sum_{m,n} \left(\frac{m\pi}{a}\frac{n\pi}{b}\right) A \cos(\frac{m\pi}{a}) \cos(\frac{n\pi}{b})$$

where both m and n can only take odd values.

Notice that in (71) the coefficient A appears multiplied by m^2, n^2 or m*n, which is the reason the selection of important m and n is so involved. While the coefficient A itself decreases rapidly as m or n increases (after possibly an initial increase), because of the factors m^2, n^2 or m*n the contribution of that waveform to the total curvature does not decrease rapidly. As an example a sandwich panel of Figure 12, with a=b=250.mm is analysed for a compressive load N_x=-250. N/mm applied at the bottom face; the deflection coefficients given in Table 6 are obtained:

Table 6 Out-of-plane deflection coefficients A (square CFRP±45° sandwich panel; a=b=250.mm; two 1.mm faceplates and a 10.mm honeycomb core; N_x=-250.N/mm applied at the bottom face)

	n=1	n=3	n=5	n=7	n=9
m=1	.6823	.0013	.0001	.0000	.0000
m=3	.0559	.0135	.0007	.0001	.0000
m=5	.0116	.0044	.0019	.0003	.0001
m=7	.0042	.0015	.0010	.0005	.0001
m=9	.0020	.0007	.0005	.0003	.0002

The contribution of the different deflections to the curvature κ_x at the middle of the panel is then as given in Table 7:

Table 7 Contribution to curvature κ_x at the middle of the panel (square CFRP±45° sandwich panel; a=b=250.mm; two 1.mm faceplates and a 10.mm honeycomb core; N_x=-250.N/mm applied at the bottom face)

	n=1	n=3	n=5	n=7	n=9
m=1	.6823	-.0013	.0001	-.0000	.0000
m=3	-.5032	.1215	-.0065	.0007	-.0001
m=5	.2909	-.1113	.0463	-.0075	.0014
m=7	-.2053	.0744	-.0490	.0240	-.0066
m=9	.1588	-.0557	.0368	-.0269	.0146

Because of the alternating signs in the contributions (which makes the smaller contributions cancel each other) and the decreasing contribution when both m≠1 and n≠1, here it is proposed, as in the buckling analysis, to include only contributions of waveforms with either m=1 or n=1. In that case the additional problem of defining the critical position in the panel where the eccentricity effect is greatest, is made much easier as well, because if either m=1 or n=1, these maximum locations all lie on the lines x=a/2 and y=b/2. A good reference point is therefore the middle of the panel (a/2,b/2).

Even when only contributions with m=1 or n=1 are included, the total curvature κ_x does not converge rapidly as the number of included waveforms increases, as Figure 16 shows. Therefore instead of the total curvature, the average of the last two computed curvatures is computed when an even number of (odd) waveforms have been included (ie. at m=3,7,11 etc.). When this value is adequately converged the procedure stops.

With the curvature and the in-plane strain known the total strain at any through-the-thickness coordinate is known. With (1) the stresses can be computed and a failure criterion can then be used to check whether failure will occur. Notice that in the middle of the plate (x,y)=(a/2,b/2) the torsion κ_{xy} is always zero.

4.3   Wrinkling of sandwich panels

Wrinkling is a local form of instability, associated with compression of a stiff face supported by a relatively flexible core. Being a *local* instability, the panel dimensions can probably be neglected; as a matter of fact many formulae in literature do so. The literature presents many models for the wrinkling analysis of sandwich panels, from completely empirical to very theoretical ([Wiedemann86], [Allen69], [Stamm74], [Pearce72], [Zelst85], [Sullins69]). In this context, the following well-known formula [Wiedemann86] is used:

$$\sigma_w = 0.5 \sqrt[3]{E_f \ E_c \ G_c} \qquad (72)$$

where the parameters with the subscript 'c' refer to the core; E_c is the compressive modulus in z-direction and G_c the core transverse shear modulus in the panel direction of interest. E_f is the Young's modulus of the face in the direction of interest; it is derived from the D-matrix of the face in question.

Because the nature of the deformation is local, with short waves, it can be assumed that there is no interaction between wrinkling in x- and y-directions; short waves in both x- and y-direction would produce very pronounced short
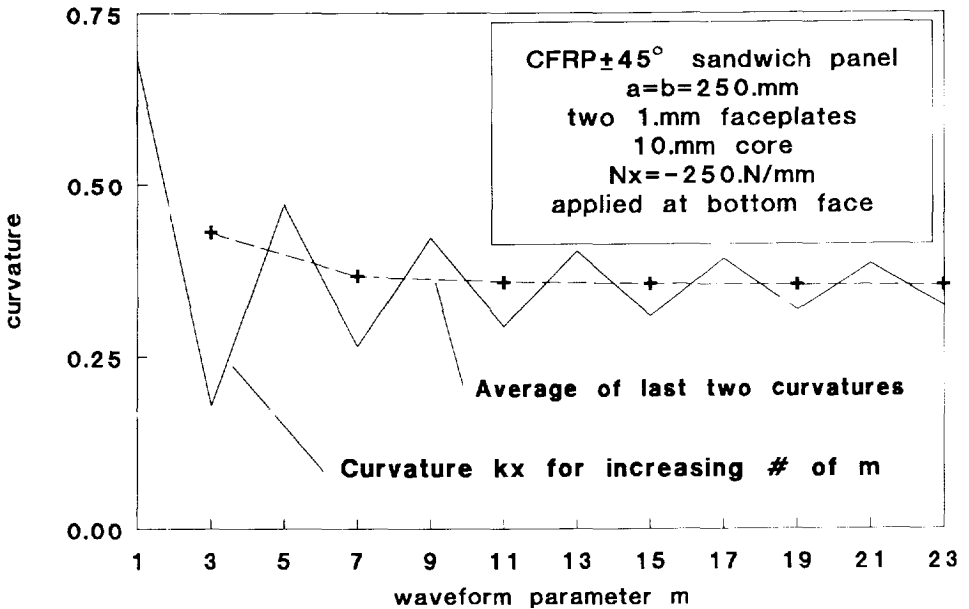
Figure 16 Curvature κ_x of a square sandwich panel for an increasing number of half waves m

cups in a face, a situation unlikely to occur. Therefore when direct loads in x- and y-direction are present, they are examined separately. When shear loads are present, the *applied* load-case (given with respect to the panel axes) is transformed into the *principal* load-case (at a certain angle with respect to the panel axes) with only direct loads (the *principal* loads). These principal loads are checked against the wrinkling loads in that direction.

Equation (72) only gives the wrinkling *stress* σ_w; in order to check for wrinkling the wrinkling *load* P_w should be known. For symmetric sandwich panels, the wrinkling *load* P_w is simply the wrinkling *stress* σ_w multiplied with twice the face thickness. In asymmetric panels however, the load carried by any of the two faces is inversely proportional to the vertical distance between that face and the neutral axis in that direction. The position of the neutral axis is derived from the cylindrical bending model, see paragraph 2.1.2. When the principal loads are at an angle to the panel axes, this calculation is lengthier but straightforward.
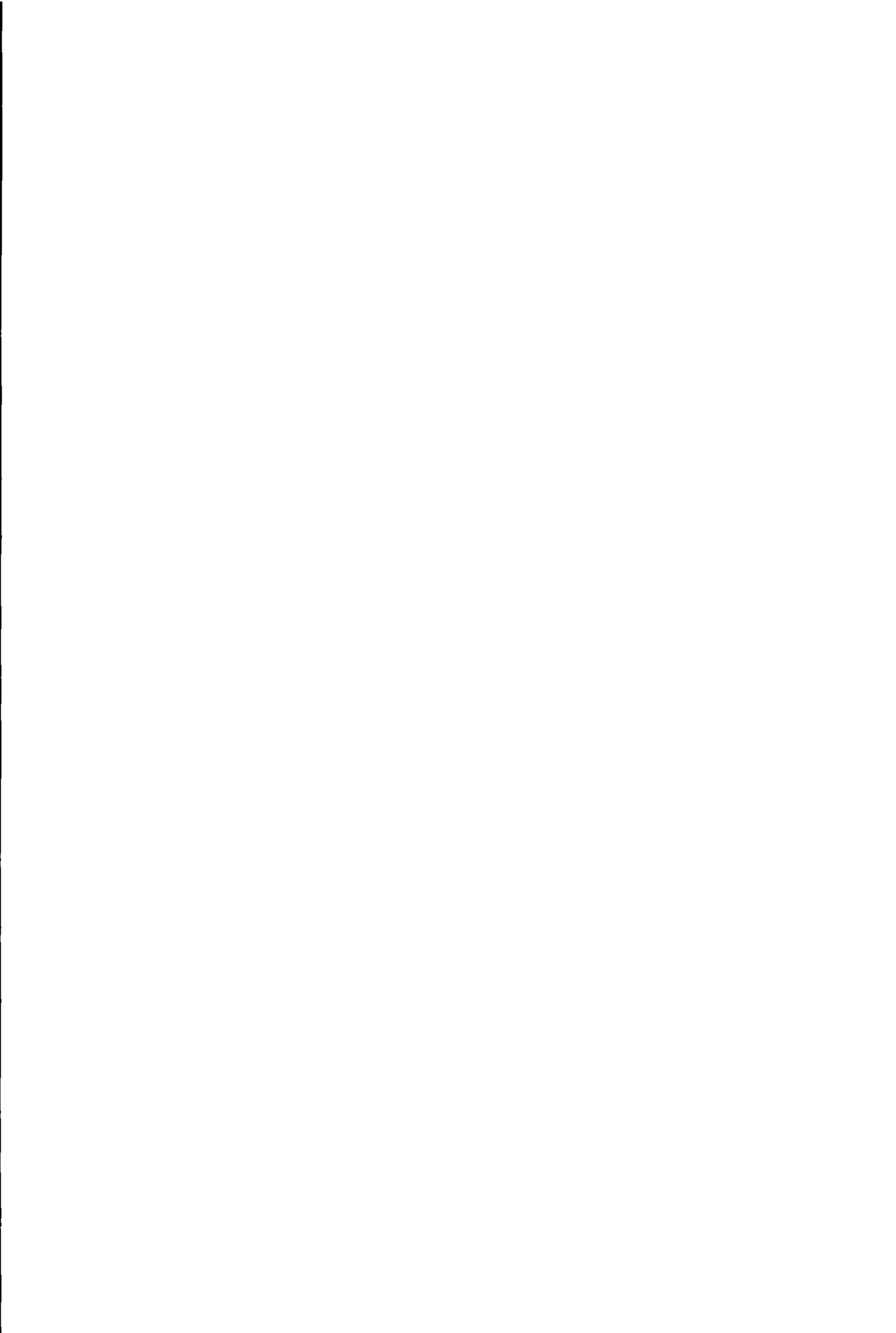
5
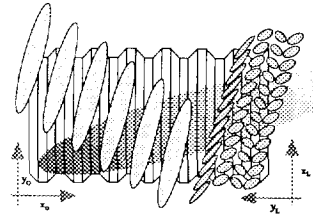
Composite Corrugated Panel Analysis

This chapter presents analytical formulae for the shear buckling of composite corrugated panels, of the type shown in Figure 17. The panel is defined by the layup of the laminate (which is the same in every part of the cross-section), the width of the two faces b_1 and b_2 (the term *face* is used here to denote the separate flat surfaces of the panel) and the angle β between the faces. The panel itself is of width h, and is assumed to be relatively long. It can be made of isotropic or orthotropic material. When the material is orthotropic, it is considered a laminate, as defined in chapter two.

The buckling analysis presented in this chapter considers two basic buckling modes of a corrugated panel, see Figure 18: first, an *overall* mode with a deformation pattern that largely ignores the presence of the corrugation. The corrugation serves only to increase the bending stiffnesses of the panel. The second buckling mode is a *local* one, where the deformation is confined to the separate faces. The angle where the two faces meet then forms a nodal line for the buckling deformation. Note in Figure 18 the distinct coordinate systems (x_O, y_O) and (x_L, y_L) for overall and local buckling respectively.
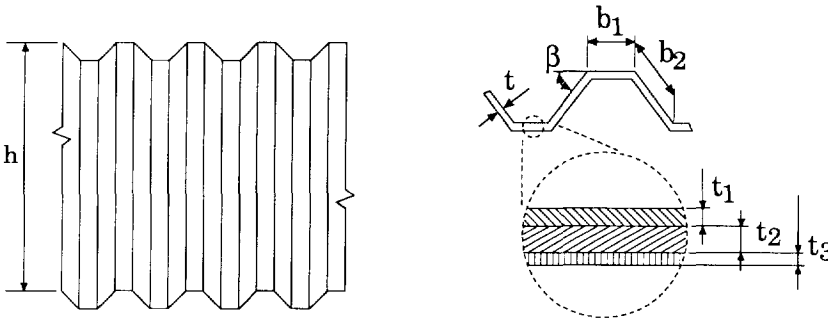
Figure 17 Definition of the corrugated panel

Because the resulting analytical formulae should be concise, these buckling modes are considered separately. However, interaction between the two modes might occur, especially if it is considered that the formulae will be used in a design program that searches for an optimum form of the corrugated panel, because this process favours corrugated panels with coincident local and overall buckling loads. Therefore it is necessary to investigate to what extent interaction of the two modes does occur. An additional paragraph presents the results of such an investigation, with the help of a finite element program, indicating that mode interaction does indeed occur for some panels. A parameter is developed to distinguish those panels that do exhibit mode interaction.

Finally, it is verified that the interaction formula for combined compression and shear loads, as presented earlier, also holds for corrugated panels.

a. Overall buckling   b. Local buckling
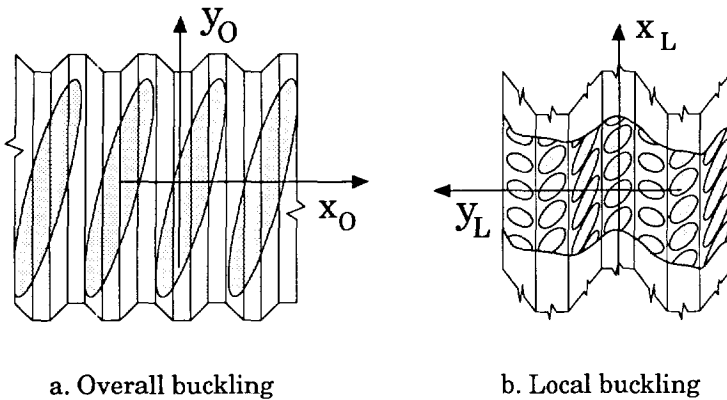
Figure 18 Buckling modes of the corrugated panel under shear load

5.1   Overall buckling of corrugated panels under shear load

For corrugated panels of isotropic material the overall buckling mode is described in [Peterson60], [Timoshenko63] and other references. There is, however, an essential difference between [Peterson60] and [Timoshenko63]; in [Peterson60] the differential equation describing buckling contains a term for the internal warping restraint that significantly increases the effective twisting stiffness of corrugated sheet, whereas the formula of [Timoshenko63] does not. Therefore [Peterson60] is considered more accurate. However, because here orthotropic material can be used, some modifications are still necessary. In [Bladel93] these are described, with a high quality approximation that eliminates the use of graphs or the numerical procedure of [Peterson60]. The following differential equation is considered in [Peterson60]:

$$\bar{D}_1 \frac{\partial^4 w}{\partial x_O^4} + 2\bar{D}_{12} \frac{\partial^4 w}{\partial x_O^2 \partial y_O^2} + \bar{D}_2 \frac{\partial^4 w}{\partial y_O^4} - E\Gamma \frac{\partial^6 w}{\partial x_O^2 \partial y_O^4} + 2q \frac{\partial^2 w}{\partial x_O \partial y_O} = 0. \tag{73}$$

where the term in $E\Gamma$ accounts for the internal warping restraint offered by the corrugation. Note the use of the symbol $\bar{D}$ instead of D to indicate the bending stiffness of the corrugated panel as a whole, not that of the laminate. In [Peterson60] only isotropic material is considered, for which the stiffnesses are given by:

$$\bar{D}_1 \approx \frac{Et^3}{12R}$$

$$\bar{D}_2 \approx ERt\rho^2 \tag{74}$$

$$\bar{D}_{12} = \frac{\mu_x \bar{D}_2 + \mu_y \bar{D}_1}{2} + \bar{D}_{xy}$$

where:

$$R = \frac{b_1 + b_2}{b_1 + b_2 \cos\beta} \tag{75}$$

is a factor to represent the extra mass in the panel (per unit of running length) due to the corrugation, as compared to a flat plate. Also:

$$\rho = \sqrt{\frac{\sin^2\beta \, (b_1 b_2^2 + \frac{b_2^3}{3})}{4(b_1 + b_2)}} \tag{76}$$

is the radius of gyration of the corrugated section. In [Peterson60] the stiffness $\bar{D}_{12}$ is neglected compared with $\bar{D}_1$ and $\bar{D}_2$; however, for orthotropic material $\bar{D}_{12}$ is best retained.

When orthotropic material is used, the bending stiffnesses are given by:

$$\bar{D}_1 \approx \frac{E_{long} t^3}{12R}$$
$$\bar{D}_2 \approx E_{short} R t \rho^2 \tag{77}$$
$$\bar{D}_{12} = 2D_{66}$$

where:

$$R = \frac{b_1 + b_2}{b_1 + b_2 \cos\beta}$$

$$\rho = \sqrt{\frac{\sin^2\beta (b_1 b_2^2 + \frac{b_2^3}{3})}{4(b_1 + b_2)}} \tag{78}$$

$$E_{long} = \frac{12}{t^3} D_{22}$$

$$E_{short} = \frac{1}{C_{11}}$$

Note that the terms E_{long} and E_{short} relate to the stiffnesses in the direction perpendicular to the corrugation (in which the corrugated panel is very long) and parallel to the corrugation (in which the panel is relatively short) respectively. E_{long} is obtained from the laminate bending stiffness D_{22} because in this direction the stiffness of the panel is obtained from *bending* of the faces. E_{short}, on the other hand, is obtained from the compliance C_{11} because in that direction the stiffness is obtained from *stretching* of the separate faces.

A high quality approximation for the buckling load is developed in [Bladel93]; it yields the following buckling formula:

$$q_O = k_O \frac{\sqrt[4]{\bar{D}_1 \bar{D}_2^3}}{h^2}$$

where: $\quad k_O = [1. \; \xi \; \xi^2] . \begin{bmatrix} 8.186 & 5.685 & -.7429 \\ 12.94 & -2.148 & .02857 \\ -2.700 & .3789 & .2857 \end{bmatrix} . \begin{bmatrix} 1. \\ \chi \\ \chi^2 \end{bmatrix}$

$$\xi = \frac{4 E_{short} \Gamma}{h^2 \sqrt{\bar{D}_1 \bar{D}_2}} \qquad 0. < \xi < 1.0 \qquad\qquad (79)$$

$$\chi = \frac{2 D_{66}}{\sqrt{\bar{D}_1 \bar{D}_2}} \qquad 0. < \chi < 0.2$$

$$\Gamma = d^4 t \left(.01 \left(\frac{p}{d} \right)^2 - .0476 \frac{p}{d} + .1366 \right) \qquad 2.0 < \frac{p}{d} < 4.6$$

$$p = 2(b_1 + b_2 \cos\beta)$$

$$d = b_2 \sin\beta$$

The limits on ξ, χ and p/d include the common range of corrugated panels and are associated with the definition of the coefficients in (79).

5.2 Local buckling of corrugated panels under shear load

Local buckling is a buckling mode of the faces rather than of the panel as a whole, see Figure 18b. The simplest model to analyse this mode would treat the faces separately, as if they were independent long plates; a more accurate but more complex model considers the faces to be linked together. The regular form of the corrugated panel is such that local buckling of *two* linked faces is an accurate model of the situation. In [Bladel93] an energy method is described for the shear buckling of linked orthotropic plates. This method is, however, abandoned because when one face becomes narrow the buckling load rises sharply while actually, when a face becomes very narrow, the buckling load should equal that of a single simply-supported strip. Therefore, also in [Bladel93] another method is proposed, using the shear buckling loads (obtained from the literature) of *single* long plates (in both simply-supported and clamped

conditions) as limit cases for buckling of two *linked* strips. In fact, the buckling load of *two coupled* strips that are equally wide is equal to that of a *single* strip of the same width, simply-supported at its sides, because there is no mutual stiffening. And when a face is narrower than the other, the narrow face will provide some kind of edge support for the wider face, which is *stiffer than simple-support*, but *less stiff than the clamped condition*. Therefore, initially the buckling load will tend towards that of the wider strip, in the clamped condition. As mentioned before, when a face becomes very narrow, the buckling load will decrease again to that of a single, simply-supported strip.

In this way, the buckling load of a single, long plate in both simply-supported and clamped condition is used in an interpolation scheme for the buckling of two linked strips. A third condition (that improves the quality of the interpolation), discussed in [Bladel93], is the gradient of the buckling load with respect to the width ratio b_2/b_1 at $b_2/b_1=1.0$. When the data from ESDU data sheet 80023 (containing shear buckling loads of long orthotropic strips) [ESDU80] are used for the buckling loads of the single faces, the following high quality approximation can be obtained [Bladel93]:

$$(80)$$

$$q_L = k_L \frac{\sqrt[4]{D_{11}D_{22}^3}}{b_{max}^2}$$

$$\text{where:} \quad k_L = \left[1. \frac{b_{min}}{b_{max}}\left(\frac{b_{min}}{b_{max}}\right)^2\right]\begin{bmatrix} 60.64 & 28.86 & -1.499 \\ -21.73 & 3.184 & -.5010 \\ -5.730 & -11.74 & .8336 \end{bmatrix}\begin{bmatrix} 1. \\ \dfrac{D_{12}+2D_{66}}{\sqrt{D_{11}D_{22}}} \\ \dfrac{(D_{12}+2D_{66})^2}{D_{11}D_{22}} \end{bmatrix}$$

Note that b_{min}/b_{max} is used instead of b_2/b_1 to limit the range of the interpolation, i.e. it is no longer significant which face is of width b_1 and which of width b_2. As already mentioned, if b_{min}/b_{max} decreases to near zero, (80) is no longer valid; then the buckling load of a single simply-supported strip should be obtained, while (80) (like the energy method tried at first) yields that of a single clamped strip. However, this error only occurs near $b_{min}/b_{max}=0$, and the computer program for which (80) is developed is not likely to prefer panels with $b_{min}/b_{max}<0.6$. Figure 19 compares the energy method referred to above and the interpolation scheme (both applicable to orthotropic materials) with results of

ESDU data sheet 74022 (for isotropic materials) [ESDU74]. For width ratios b_{min}/b_{max} around 1.0 there is a good agreement. For $b_{min}/b_{max} < 0.6$ (panels probably discarded anyway, as mentioned before) the agreement is bad, and the curve in Figure 19 is only drawn to show that it tends towards the buckling coefficient of a single clamped strip for $b_{min}/b_{max} \rightarrow 0$.

5.3   Mode interaction of local and overall buckling

The overall and local buckling modes described above may interact with each other, as mentioned in the introduction. A series of finite element (FEM) analyses using the finite element package *Abaqus* is performed to examine this possibility. In many cases a good agreement was found between the analytical prediction and the finite element result, both in buckling load and in buckling mode. However, for a number of panels buckling occurred in another mode, with in some cases a considerable reduction in buckling load. Paragraph 5.3.1 describes the finite element analysis and the results.

The phenomenon of buckling mode interaction is too complex to be described by
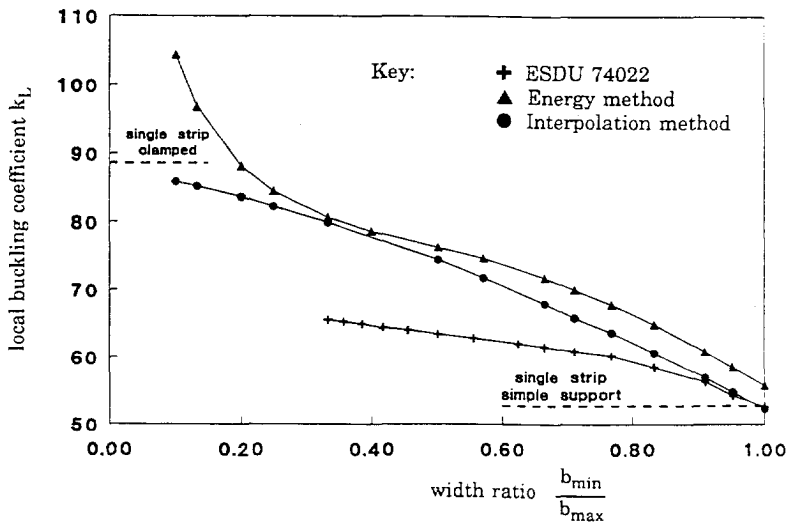
Figure 19   Local buckling coefficients of linked orthotropic strips made of isotropic material; comparison with results of ESDU data sheet 74022

a simple analytical formula; it therefore falls outside the scope of this research. However, it is possible to define a parameter (based on the properties of the corrugated panel) the value of which predicts whether mode interaction will or will not occur. This is also covered in the next paragraph.

5.3.1 FEM analysis of corrugated panels

Figure 20 shows a finite element model, typical of that used in the current investigation. It was made by a model generator (Patran); each face is modelled with 9 shell elements (quadratic 9 node elements with 5 degrees of freedom) and the complete model spans 7 complete corrugations. In this way a model with 7000 degrees of freedom is obtained. All edges are simply-supported, as shown in Figure 20. Shear load is applied by a prescribed edge displacement, creating a uniform shear stress throughout the structure (this was one test to check the results of the FEM analysis). An eigenvalue calculation is then performed, and the first eight eigenvalues are calculated. No problems of convergence were encountered. The buckling load of one corrugated panel has been checked by mesh refinement, showing a decrease of 7% when a finer mesh is used.

In total 82 corrugated panels were analysed, made of isotropic material. Table 8 describes all the panels and gives the results of the finite element analysis, and also the local and overall buckling loads obtained by the analytical formulae of
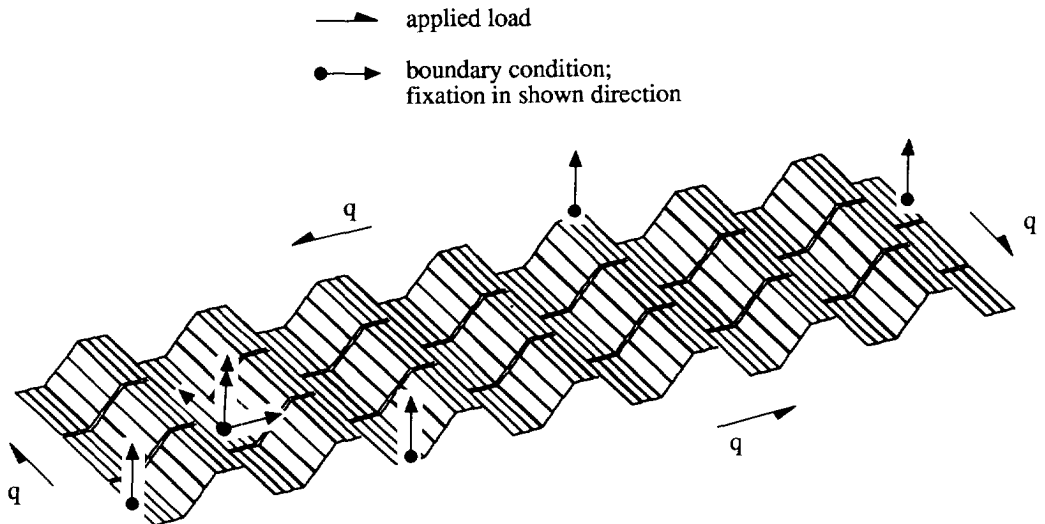
Figure 20 Finite element model of the corrugated panel

this chapter. In a number of cases the analytical formulae and the FEM analysis give markedly different results. In particular, the analytical formulae significantly *under*estimate the buckling load only when overall buckling is critical (i.e. the overall buckling load is lower than the local buckling load), see for example cases 5, 9 and 13 of Table 8. This phenomenon is also reported in ESDU data sheet 74022 [ESDU74], where predicted overall buckling loads of corrugated panels of isotropic material (using [Peterson60]) come out lower than the experimental overall buckling loads. On the other hand, when local buckling is critical (according to the analytical formulae), or when both modes occur simultaneously (i.e. when the buckling loads of both modes differ by less than 10%), the analytical formulae sometimes significantly *over*estimate the buckling load, as compared with the FEM result, see for example cases 11, 15 and 67 of Table 8.

Figure 21 shows the three distinct buckling deformation patterns, resulting from the FEM analyses: in Figure 21a an overall buckling mode is drawn, clearly recognisable from the buckling pattern that crosses the separate faces of the panel; in Figure 21b a local buckling mode is shown, recognisable from the buckling pattern confined to the separate faces. Figure 21c finally shows an interaction mode, clearly distinct from both the overall and local modes.

5.3.2 Stiffness parameter to restrict mode interaction

Mode interaction is a complex matter. It cannot therefore be treated as a third buckling mode in the present research, which is aimed at finding accurate but simple analytical formulae. However, a simple mechanical model can be developed to examine whether the intersection of two faces of the corrugated panel will act as a nodal line for the local buckling mode or whether it will not, in the latter case causing a buckling mode that is neither local nor overall but some kind of interaction mode.

There are two reasons underlying the association of the mechanical model with the *local* buckling mode: first, the FEM analyses give lower buckling loads (associated with the peculiar buckling mode of Figure 21c) than predicted by the analytical formulae of this chapter only in certain cases where the local buckling mode is critical. Furthermore, a basic condition for the local buckling mode to exist is precisely the existence of a nodal line at the intersection of two faces. Therefore it is appropriate to define a mechanical model to examine the possibility of 'breakdown' of the nodal line (as visible in the buckling deformation of Figure 21c) in the local mode.

The mechanical model assumes that the nodal line (and therefore the local buckling mode) is maintained when the strain energy that would be required to deform the smaller of the two faces is large enough compared with the strain energy required to deform the wider face; in other words, the narrower face has to be stiff enough in its plane to prevent the wider face (bending out of plane) from causing nodal line breakdown. This model is illustrated in Figure 22; note the assumed nodal line deformation (sinusoidal with half-wavelength λ) and the associated deformations of the two adjacent faces, the smaller face bending *in plane*, the wider face bending *out of plane*.

The strain energy Un in the smaller face bending in-plane is:

2a overall buckling mode

2b local buckling mode

2c interaction mode
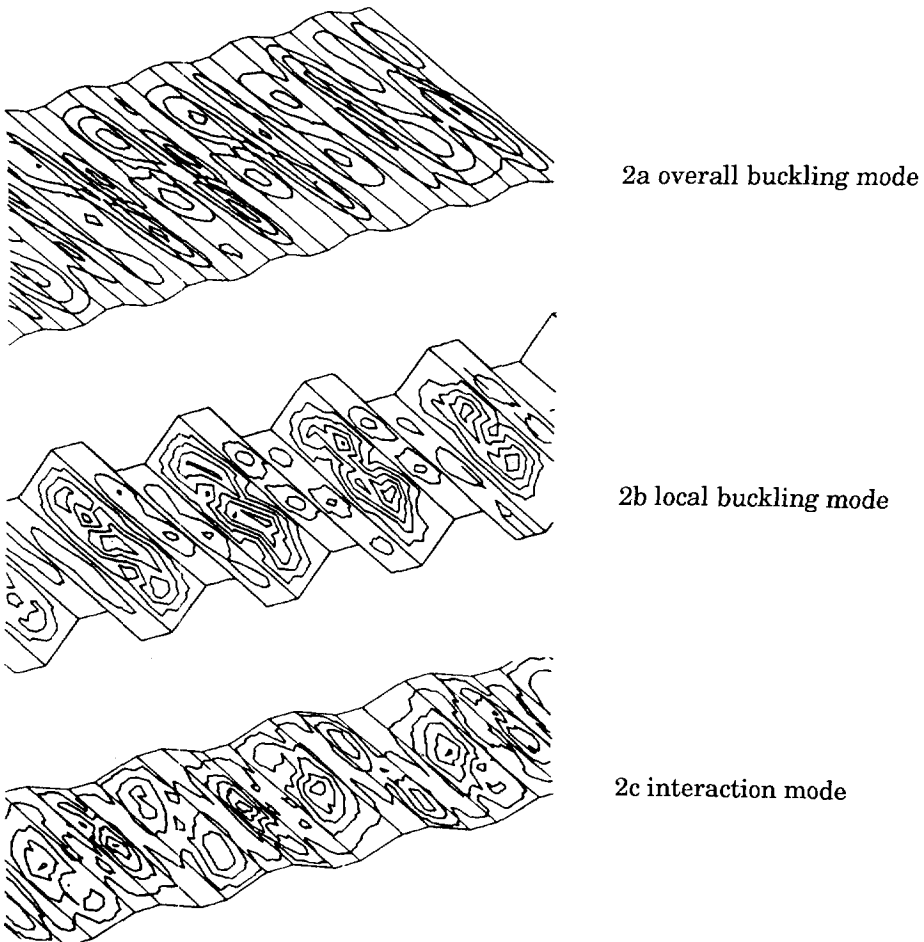
Figure 21 Shear buckling deformation patterns, as obtained by FEM analysis

$$Un = \frac{1}{2} \int_0^\lambda E_{short} I_i \, \vartheta^2 \, dx \tag{81}$$

where E_{short} is the Young's modulus of the plate in the x_L-direction, and where I_i is the second moment of area of the narrow face, bending in-plane. In (81) the specific bending curvature ϑ becomes:

$$\vartheta = \frac{\partial^2 w}{\partial x^2} = \frac{-\pi^2 w_{max} \sin\theta}{\lambda^2} \sin(\frac{\pi x}{\lambda}) \tag{82}$$

$$\text{where:} \quad w = (w_{max} \sin\theta) \sin(\frac{\pi x}{\lambda})$$

Substitution of ϑ and evaluation of the integral yields for the strain energy Un:

$$Un = \frac{E_{short} t b_{min}^3 (w_{max} \sin\theta)^2}{\lambda^3} \frac{\pi^4}{96} \tag{83}$$

To obtain the strain energy Uw of the wider face bending out of plane first the strain energy dUw in an infinitesimal strip dx is derived with the help of bending theory:
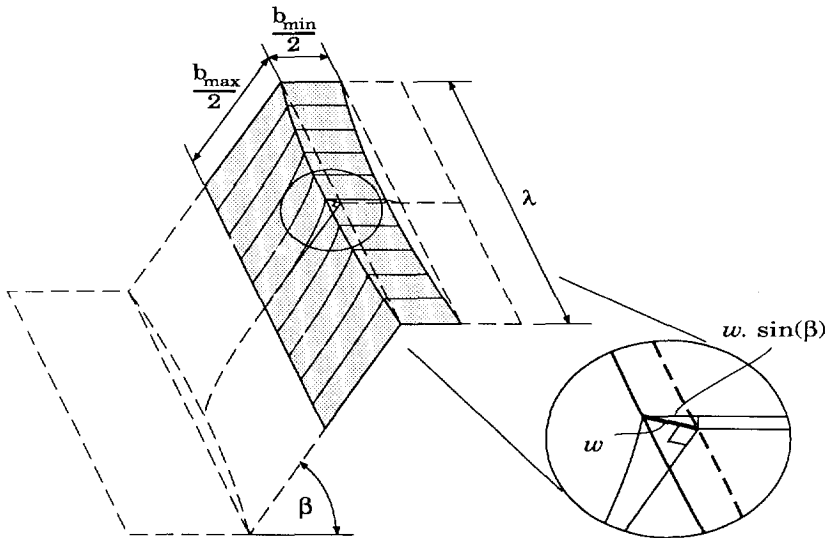
Figure 22 Model of nodal line break-down

$$dUw = \frac{1}{2}Pw$$

$$\text{where:} \quad w = \frac{P(\frac{b_{max}}{2})^3}{3E_{long}I_o} \tag{84}$$

$$I_o = \frac{t^3 dx}{12}$$

Elimination of P and integration over a half-wavelength λ yields:

$$Uw = \int_0^\lambda \frac{E_{long}t^3}{b_{max}^3} (w_{max}\sin\frac{\pi x}{\lambda})^2 dx$$

$$= \frac{E_{long}t^3}{b_{max}^3} w_{max}^2 \frac{\lambda}{2} \tag{85}$$

The stiffness parameter SP is now defined as the ratio of Un to Uw. SP becomes, after omission of numerical constants:

$$SP = \frac{E_{short}}{E_{long}} \frac{b_{min}^3 b_{max}^3}{t^2} \frac{\sin^2\beta}{\lambda^4} \tag{86}$$

To eliminate the half-wavelength λ it is related to the width of the faces. From the results of the local buckling analysis with the energy method mentioned in paragraph 5.2 (although the energy method is not used for the local buckling *load*, it is used here for the wavelength), it can be deduced that the half-wavelength λ is related to the face widths b_{min} and b_{max}:

$$\lambda = C \sqrt{b_{min}b_{max}} \tag{87}$$

Substitution of (87) in (86) yields the final formula for SP:

$$SP = \frac{E_{short}}{E_{long}} \frac{b_{min}b_{max}}{t^2} \sin^2\beta \tag{88}$$

The parameter SP can now be used to distinguish those panels for which buckling mode interaction occurs, see Figure 23; the buckling load ratio (ratio of

the analytically predicted load to the FEM buckling load), given in Table 8, is plotted against the value of SP, for all 82 investigated panels. Note that it is indeed possible to define a limiting value (SP=1500.) above which there is good agreement between the analytical prediction and the FEM-analysis. From Figure 23 it is also evident that below SP=1500. both the local and overall buckling predictions are not accurate.

5.4   Interaction of compression and shear for corrugated panels

In addition to shear load, there may also be compressive load in the y_0-direction in a corrugated panel. In the formulae derived above (for overall and local buckling) it was not possible to include the effect of compressive load. However, there exists a well-known interaction formula for combined compression and shear in long, flat plates (both isotropic and orthotropic) [Lekhnitskii68]:

$$\frac{N_x}{p_x} + \left[\frac{N_{xy}}{q}\right]^2 \geq 1. \tag{89}$$
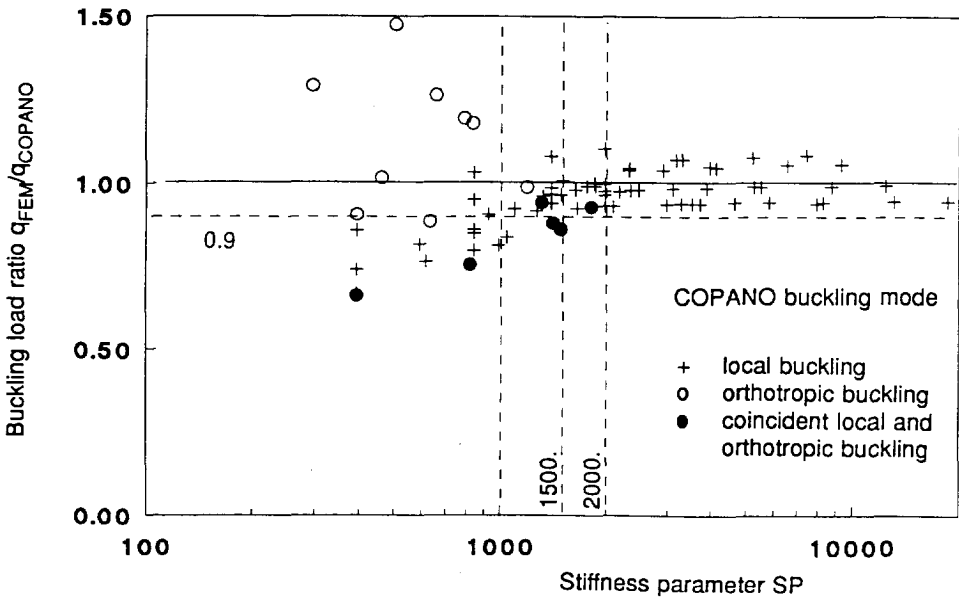
figure 23 Definition of a limit value for SP

In paragraph 3.4 it is found that this formula, although originally intended for plates, could also be applied to orthotropic sandwich panels. As discussed in previous paragraphs, corrugated panels buckle in two modes: local and overall buckling. For local buckling under combined shear and compression (89) may readily be used because the individual buckling loads for both compression and shear can be obtained for a local buckling mode. For overall buckling the situation is different; the shear buckling analysis includes internal warping restraint, while the compression buckling analysis does not. Nevertheless, a simple check was performed with an orthotropic flat plate analysis [ESDU73] (not including the internal warping restraint) to examine the overall buckling behaviour of corrugated panels. Figure 24 gives the results of the analysis for two corrugated panels, and the parabolic interaction formula (89). It shows that (89) is conservative up to 10%.

Figure 24 Interaction between compression and shear for corrugated panels

Table 8 Analytical and numerical shear buckling load of corrugated panels

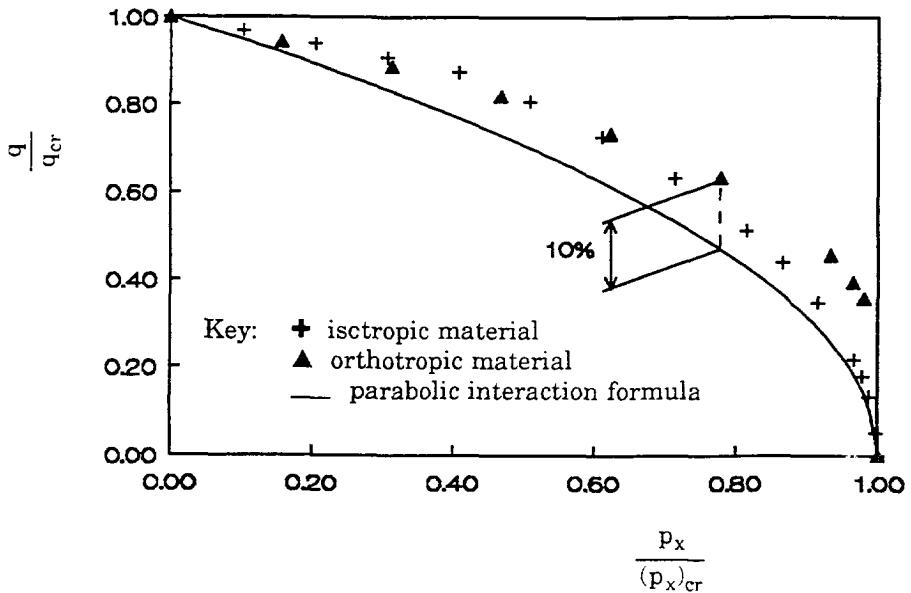| #	h	t	b_1	b_2	β	FEM	Buckling formula		buckling load ratio	Stiff. Param. SP
						q_{cr}	q_L	q_0		
	[mm]	[mm]	[mm]	[mm]	[deg]	[N/mm]	[N/mm]	[N/mm]	[−]	[−]
1	415.	0.5	22.5	22.5	50.	73.8	87.4	74.5	0.99	1188.
2	415.	0.5	22.5	28.1	50.	64.4	66.6	117.	0.97	1484
3	415.	0.5	22.5	37.5	50.	41.6	42.5	231.	0.98	1981.
4	415.	0.5	22.5	56.3	50.	19.5	20.8	557.	0.94	2973.
5	415.	0.5	22.5	22.5	40.	63.8	87.4	54.0	1.18	837.
6	415.	0.5	22.5	28.1	40.	55.9	66.6	82.0	0.84	1045.
7	415.	0.5	22.5	37.5	40.	41.2	42.5	153.	0.97	1394.
8	415.	0.5	22.5	56.3	40.	19.4	20.8	394.	0.93	2094.
9	415.	0.5	22.5	22.5	30.	52.1	87.4	35.3	1.48	506.
10	415.	0.5	22.5	28.1	30.	46.6	66.6	52.6	0.89	632.
11	415.	0.5	22.5	37.5	30.	36.2	42.5	94.0	0.85	844.
12	415.	0.5	22.5	56.3	30.	19.1	20.8	238.	0.92	1267.
13	415.	0.5	22.5	22.5	20.	31.6	87.4	19.0	1.66	237.
14	415.	0.5	22.5	28.1	20.	36.1	66.6	27.9	1.29	296.
15	415.	0.5	22.5	37.5	20.	28.2	42.5	48.7	0.66	395.
16	415.	0.5	22.5	56.3	20.	17.0	20.8	120.	0.82	593.
17	415.	0.4	22.5	22.5	50.	44.5	44.8	56.3	0.99	1857.
18	415.	0.4	22.5	28.1	50.	35.5	34.1	90.2	1.04	2319.
19	415.	0.4	22.5	37.5	50.	21.5	21.8	181.	0.99	3095.
20	415.	0.4	22.5	56.3	50.	10.0	10.6	398.	0.94	4646.
21	415.	0.4	22.5	22.5	40.	38.3	44.8	40.6	0.94	1307.
22	415.	0.4	22.5	28.1	40.	33.5	34.1	62.9	0.98	1633.
23	415.	0.4	22.5	37.5	40.	21.3	21.8	120.	0.98	2179.
24	415.	0.4	22.5	56.3	40.	9.97	10.6	290.	0.94	3271.
25	415.	0.4	22.5	22.5	30.	31.7	44.8	26.5	1.20	791.
26	415.	0.4	22.5	28.1	30.	27.8	34.1	40.1	0.82	988.
27	415.	0.4	22.5	37.5	30.	21.0	21.8	73.5	0.96	1319.
28	415.	0.4	22.5	56.3	30.	9.90	10.6	182.	0.93	1979.
29	415.	0.4	22.5	22.5	20.	22.1	44.8	14.2	1.56	370.
30	415.	0.4	22.5	28.1	20.	21.5	34.1	21.1	1.02	462.
31	415.	0.4	22.5	37.5	20.	16.7	21.8	37.7	0.78	617.
32	415.	0.4	22.5	56.3	20.	9.62	10.6	93.4	0.91	926.
33	415.	0.3	22.5	22.5	50.	20.3	18.9	39.8	1.07	3301.
34	415.	0.3	22.5	28.1	50.	15.1	14.4	65.3	1.05	4122.
35	415.	0.3	22.5	37.5	50.	9.10	9.18	132.	0.99	5501.
36	415.	0.3	22.5	56.3	50.	4.23	4.48	259.	0.94	8260.
37	415.	0.3	22.5	22.5	40.	19.8	18.9	28.6	1.05	2324.
38	415.	0.3	22.5	28.1	40.	15.0	14.4	45.2	1.04	2903.
39	415.	0.3	22.5	37.5	40.	9.07	9.18	87.5	0.99	3874.
40	415.	0.3	22.5	56.3	40.	4.23	4.48	188.	0.94	5815.
41	415.	0.3	22.5	22.5	30.	16.3	18.9	18.5	0.88	1406.

Table 8 contd.

#	h	t	b_1	b_2	β	FEM q_{cr}	Buckling formula q_L	q_0	buckling load ratio	Stiff. Param. SP
	[mm]	[mm]	[mm]	[mm]	[deg]	[N/mm]	[N/mm]	[N/mm]	[−]	[−]
42	415.	0.3	22.5	28.1	30.	14.3	14.4	28.6	0.99	1756.
43	415.	0.3	22.5	37.5	30.	9.01	9.18	53.6	0.98	2344.
44	415.	0.3	22.5	56.3	30.	4.21	4.48	124.	0.94	3519.
45	415.	0.3	22.5	22.5	20.	12.4	18.9	9.8	1.27	658.
46	415.	0.3	22.5	28.1	20.	10.9	14.4	14.9	0.76	822.
47	415.	0.3	22.5	37.5	20.	8.49	9.18	27.4	0.92	1097.
48	415.	0.3	22.5	56.3	20.	4.15	4.48	66.1	0.93	1646.
49	415.	0.2	22.5	22.5	50.	6.08	5.60	24.9	1.09	7427.
50	415.	0.2	22.5	28.1	50.	4.51	4.26	41.8	1.06	9275.
51	415.	0.2	22.5	37.5	50.	2.71	2.72	80.2	1.00	12378.
52	415.	0.2	22.5	56.3	50.	1.26	1.33	141.	0.95	18584.
53	415.	0.2	22.5	22.5	40.	6.05	5.60	17.8	1.08	5229.
54	415.	0.2	22.5	28.1	40.	4.50	4.26	28.8	1.06	6531.
55	415.	0.2	22.5	37.5	40.	2.70	2.72	55.3	0.99	8715.
56	415.	0.2	22.5	56.3	40.	1.26	1.33	102.	0.95	13085.
57	415.	0.2	22.5	22.5	30.	6.01	5.60	11.4	1.07	3164.
58	415.	0.2	22.5	28.1	30.	4.48	4.26	18.2	1.05	3952.
59	415.	0.2	22.5	37.5	30.	2.70	2.72	34.3	0.99	5273.
60	415.	0.2	22.5	56.3	30.	1.25	1.33	67.4	0.94	7917.
61	415.	0.2	22.5	22.5	20.	4.83	5.60	6.0	0.86	1480.
62	415.	0.2	22.5	28.1	20.	4.27	4.26	9.4	1.00	1849.
63	415.	0.2	22.5	37.5	20.	2.67	2.72	17.6	0.98	2467.
64	415.	0.2	22.5	56.3	20.	1.25	1.33	37.1	0.95	3705.
65	200.	0.5	22.5	37.5	20.	36.5	42.5	360.	0.86	395.
66	300.	0.5	22.5	37.5	20.	31.5	42.5	119.	0.74	395.
67	400.	0.5	22.5	37.5	20.	28.5	42.5	53.8	0.67	395.
68	500.	0.5	22.5	37.5	20.	27.1	42.5	29.9	0.91	395.
69	200.	0.5	22.5	37.5	30.	44.	42.5	671.	1.04	844.
70	300.	0.5	22.5	37.5	30.	40.5	42.5	234.	0.95	844.
71	400.	0.5	22.5	37.5	30.	36.6	42.5	104.	0.86	844.
72	500.	0.5	22.5	37.5	30.	34.0	42.5	57.2	0.80	844.
73	200.	0.5	22.5	37.5	40.	46.	42.5	1015.	1.08	1394.
74	300.	0.5	22.5	37.5	40.	42.	42.5	381.	0.99	1394.
75	400.	0.5	22.5	37.5	40.	41.2	42.5	170.	0.97	1394.
76	500.	0.5	22.5	37.5	40.	40.0	42.5	91.9	0.94	1394.
77	200.	0.5	22.5	37.5	50.	47.	42.5	1384.	1.11	1981.
78	300.	0.5	22.5	37.5	50.	42.5	42.5	568.	1.00	1981.
79	400.	0.5	22.5	37.5	50.	41.6	42.5	257.	0.98	1981.
80	500.	0.5	22.5	37.5	50.	41.1	42.5	137.	0.97	1981.
81	1000.	0.8	47.	51.	44.	69.8	75.3	75.5	0.93	1807.
82	1000	3.1	138.	120.	69.	634.	626.	6690.	1.01	1502.

part II

Optimum Composite Panels

6

Composite Panel Design
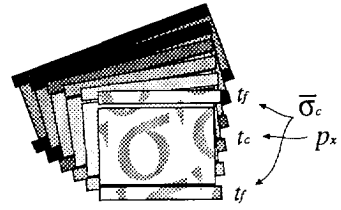
In this chapter some expressions to be used in optimization are introduced, and analytical formulae are obtained for the performance of composite sandwich panels and corrugated panels.

Whether analytical or numerical, an optimization process searches for the extreme (minimum or maximum) value of a target or *objective function* by varying some properties (the *variables*) of the subject. This process can be performed with or without conditions (*constraints*) that have to be satisfied. In this research an optimization for least mass is performed. The variables used to obtain the optimum are the cross-sectional dimensions; for sandwich panels these are the thicknesses of the different layers in the laminate and their orientation with respect to the laminate axes. For corrugated panels, as well as the definition of the laminate, also the shape of the cross-section (lengths of the two faces b_1 and b_2 and the corrugation angle β, see Figure 17) can be varied. Typical constraints are material failure and buckling.

In this chapter optimization will be performed *analytically*, aimed at finding formulae to define the *performance* of sandwich or corrugated panels satisfying some selected constraints. Then the objective function is not explicitly present in the process. Rather, it is implicitly assumed that by sizing the panel on the basis of the selected constraints, an optimum panel is obtained. In other words, the panels are *designed* by these constraints. For example, for a sandwich panel one can suppose that by using a minimum thickness for face and core such that material failure and buckling are marginally satisfied, an optimum panel will be obtained. In fact, the results of this chapter show that this reasoning is not always true. In the next chapter, on the other hand, optimization is performed *numerically*. Then a numerical iteration process is used to find the optimum, taking into account the constraints. Contrary to the analytical process of this chapter, it is then not known at the beginning which constraints will define the optimum configuration; the constraints merely serve as borders of a *design space* that contains all *feasible designs* (i.e. the designs that satisfy all constraints).

Performance is quantified by the *equivalent stress* (σ' for compression loaded panels and τ' for shear loaded panels). This is the applied load divided by an equivalent thickness t'; a small equivalent thickness t' means a low mass and results in a high equivalent stress and high performance. The two following paragraphs obtain formulae for the equivalent stress for sandwich panels in compression and corrugated panels in shear, in terms of the *structural index* (a parameter indicating the intensity of the applied load) and material parameters, but without the design variables. The formulae are derived taking into account a number of constraints, such as buckling and material failure; they provide insight into the behaviour of these composite panels and serve as a reference for the computer results of part 4 of this work.

6.1   Performance of sandwich panels under compression

In the literature there are many references to the design of sandwich panels, loaded in-plane, made of *isotropic* material ([Flügge51], [Bijlaard52], [Kovařík72]). For composite sandwich panels [Allen69] contains valuable information and will be cited further on. Other interesting work ([Wiedemann89]), also cited below, compares many different structural types. However, none of these references cover the subject in the detail required here.

In this paragraph two formulae are presented that describe the equivalent stress σ' of sandwich panels in compression. The panel is assumed symmetric, with two equal faces (of thickness t_f) and a core (of thickness t_c). To calculate σ' first the equivalent thickness t' of a sandwich panel is defined; it is the thickness of a (massive) plate, made of the face material, having the same mass as the sandwich panel. Equating the two masses yields:

$$\rho_f t' = 2\rho_f t_f + \rho_c t_c$$

$$t' = \frac{2\rho_f t_f + \rho_c t_c}{\rho_f} \tag{90}$$

$$t' = 2t_f + \frac{\rho_c}{\rho_f} t_c$$

The equivalent direct stress σ' is then:

$$\sigma' = \frac{N_x}{t'} = \frac{N_x\, \rho_f}{\rho_c t_c + 2\rho_f t_f} \tag{91}$$

Note that in this paragraph, for simplicity, a compressive load is considered positive. The first formula for σ' to be derived considers only *buckling* of the panel. It is obtained by maximizing the buckling load for a given mass, by a suitable distribution of mass between faces and core. The two conditions that serve to eliminate t_f and t_c are therefore *buckling* and the condition that the buckling load is *maximal* for a given mass. For the buckling condition formula (20) of chapter 2 is used, rewritten to introduce a buckling coefficient k, independent of t_f and t_c:

$$p_x(\frac{\pi}{a})^2 = D_{11}(\frac{\pi}{a})^4 + D_{22}(\frac{\pi}{b})^4 + (2.D_{12}+4.D_{66})(\frac{\pi}{a})^2(\frac{\pi}{b})^2$$

$$p_x = \frac{D_{11}}{ab}\left(\pi^2(\frac{b}{a}) + \frac{D_{22}}{D_{11}}(\frac{a}{b})^3 + \frac{2.D_{12}+4.D_{66}}{D_{11}}(\frac{a}{b})\right) \tag{92}$$

$$p_x = \frac{D_{11}k}{ab}$$

Unfortunately, in this way transverse shear effects are neglected here. However, if Equation (46) of chapter 3 were used to include these effects, the buckling coefficient k could not be made independent of t_f and t_c. If only the faces provide bending stiffness, D_{11} is given by:

$$D_{11} = (\frac{E_x}{1-\nu_{xy}\nu_{yx}})\, 2t_f\, (\frac{t_f+t_c}{2})^2$$

$$= \frac{1}{2}\, E_f'\, t_f\, (t_f+t_c)^2 \tag{93}$$

where the reduced modulus E_f' for the face material is:

$$E_f' = \frac{E_x}{1-\nu_{xy}\nu_{yx}} \tag{94}$$

With (93), (92) can be written as:

$$p_x = \frac{E_f' \, t_f \, (t_f + t_c)^2 \, k}{2ab} \tag{95}$$

The mass of the panel m (per unit area) is given by:

$$m = 2\rho_f t_f + \rho_c t_c \tag{96}$$

Substituting (96) in (95) to eliminate t_f yields:

$$p_x = \frac{E_f' k}{2ab} \frac{m - \rho_c t_c}{2\rho_f} \left(\frac{m - \rho_c t_c}{2\rho_f} + t_c \right)^2 \tag{97}$$

The highest buckling load with respect to t_c is that for which:

$$\frac{\partial p_x}{\partial t_c} = 0. \tag{98}$$

This condition yields the following equation in t_c:

$$m^2 (4\rho_f - 3\rho_c) + t_c 2m(2\rho_f - \rho_c)(2\rho_f - 3\rho_c) + t_c^2 (-3\rho_c)(2\rho_f - \rho_c)^2 = 0. \tag{99}$$

This is a second order equation with two solutions:

$$[t_c]_1 = \frac{-m}{2\rho_f - \rho_c}$$

$$[t_c]_2 = m \frac{4\rho_f - 3\rho_c}{3\rho_c(2\rho_f - \rho_c)} \tag{100}$$

$[t_c]_1$ is a negative root to be discarded here, leaving $[t_c]_2$ as the only physically relevant solution; examination of (97) reveals that at $[t_c]_2$ p_x is at a *maximum*, therefore at $[t_c]_2$ we do have an optimum configuration. Eliminating m in (96) with (100) yields:

$$\frac{t_f}{t_c} = \frac{\rho_c}{4\rho_f - 3\rho_c} \tag{101}$$

In other words, the panel with the highest buckling load for a given mass has a thickness ratio of face to core as given in (101)[†]. Combining (95) with (101) gives for t_f and t_c:

$$t_f = \left(\frac{p_x \, a \, b}{2E_f' \, k} \right)^{\frac{1}{3}} \left(\frac{\rho_c}{2\rho_f - \rho_c} \right)^{\frac{2}{3}}$$

$$t_c = (4\rho_f - 3\rho_c) \left(\frac{p_x \, a \, b}{2E_f' \, k \, \rho_c} \right)^{\frac{1}{3}} \left(\frac{1}{2\rho_f - \rho_c} \right)^{\frac{2}{3}}$$

(102)

Combining (91) and (102) a formula for σ' is obtained in terms of the structural index, which in the case of a compression loaded member is given by N_x/b, and material parameters, without the variables t_f and t_c. Note that here p_x can be replaced by N_x, because the design condition is that the applied load N_x equals the buckling load p_x:

$$\sigma' = \eta (E_f')^{\frac{1}{3}} \left(\frac{N_x}{b} \right)^{\frac{2}{3}}$$

$$\text{where:} \quad \eta = \frac{1}{3} \frac{\rho_f}{\rho_c} \left(\frac{2ak\rho_c}{b(2\rho_f - \rho_c)} \right)^{\frac{1}{3}}$$

(103)

This formula is a so-called *efficiency formula* because it contains the dimensionless *efficiency* η. In [Wiedemann89] a similar formula is obtained, with the same powers for the equivalent Young's modulus E_f' and for the structural index N_x/b, but without the efficiency η given explicitly here.

[†] In [Allen69] a formula similar to (101) is obtained, for $(t_f \ll t_c)$ (so that $(t_f + t_c)^2$ can be simplified to t_c^2):

$$\frac{t_f}{t_c} = \frac{\rho_c}{4\rho_f}$$

$$\text{or:} \quad m_c = 2m_f$$

The same result is also obtained by putting $\rho_c \ll \rho_f$ in (101).

Another formula for the equivalent stress σ' is found when not only buckling, but also material failure is considered. Then the following distinction in function can be observed in the panel: the faces carry the applied normal load with minimum thickness (and hence at the maximum allowable compressive stress $\overline{\sigma_c}$), while the core has a minimum thickness to provide the required bending stiffness against buckling. This can be called a *fully stressed design*, as all parts of the structure have the minimum allowed dimension in order to still satisfy the constraints. Below, a formula for the equivalent stress σ' indicating the performance of such panels is derived.

The material failure constraint associates the applied load with the face thickness t_f (the core is considered not to carry any load):

$$\overline{\sigma_c} = \frac{N_x}{2.t_f}$$

$$\text{or:} \quad t_f = \frac{N_x}{2.\overline{\sigma_c}}$$

(104)

For buckling (95) is again used. Solving for t_c yields:

$$p_x = \frac{E_f' k}{2ab} t_f (t_f + t_c)^2$$

$$t_c^2 + 2t_c t_f + t_f^2 - \frac{2 p_x ab}{E_f' t_f k} = 0.$$

(105)

This is a second order equation with two solutions:

$$[t_c]_1 = -\left(\frac{2p_x ab}{E_f' t_f k}\right)^{\frac{1}{2}} - t_f$$

$$[t_c]_2 = \left(\frac{2p_x ab}{E_f' t_f k}\right)^{\frac{1}{2}} - t_f$$

(106)

The first solution $[t_c]_1$ is discarded because it is always negative. The remaining solution $[t_c]_2$ becomes, after elimination of t_f with (104):

$$t_c = \left(\frac{4\overline{\sigma_c}ab}{E_f'k} \right)^{\frac{1}{2}} - \frac{N_x}{2\overline{\sigma_c}} \qquad (107)$$

Note that the core thickness t_c is decreasing as the load N_x increases, eventually becoming zero, when the load N_x has grown to its limit value N_x^*:

$$N_x^* = 4 \sqrt{\frac{ab\overline{\sigma_c}^3}{E_f'k}} \qquad (108)$$

Hence there are two formulae for σ', one for $N_x < N_x^*$ and another for $N_x \ge N_x^*$; substituting t_c from (107) or $t_c = 0$. respectively, and t_f from (104), the equivalent stress σ' becomes:

$$\text{for } N_x < N_x^* : \qquad \sigma' = \frac{1}{\dfrac{2\rho_f - \rho_c}{2\rho_f\overline{\sigma_c}} + \left(\dfrac{a}{N_x}\right) \dfrac{\rho_c}{\rho_f} \sqrt{\dfrac{4b\overline{\sigma_c}}{aE_f'k}}} \qquad (109)$$

$$\text{for } N_x \ge N_x^* : \qquad \sigma' = \overline{\sigma_c}$$

At this point two alternative formulae (103) and (109) are available for the equivalent stress σ' of sandwich panels in compression. As an example a square sandwich panel (with a=b=500.mm) is considered, with faces of CFRP $0°/90°$ laminate and a light honeycomb core, with the following material data:

face: $\rho_f =$ 1.60   g/cm^3 core: $\rho_c =$ 0.048   g/cm^3
         $E_f' =$ 76430.   MPa
         $\overline{\sigma_c} =$ -304.   MPa

Recall that the transverse shear deformation (covered in chapters 3 and 4), typical for the behaviour of sandwich panels, is not considered here. The following table gives the resulting face and core thicknesses t_f and t_c and the equivalent stress σ' for a given applied compressive load of N_x=300. N/mm, both when the sandwich panel is designed for highest buckling load, and when it is a fully stressed design.

Table 9 Performance of composite sandwich panels
designed for a compressive load of N_x=300. N/mm
(two equal faces of CFRP 0°/90° laminate; core of light honeycomb)

Design rule	t_f	t_c	m	σ'
	[mm]	[mm]	[g/cm^2]	[MPa]
highest buckling load	0.17	22.48	0.163	294.3
fully stressed design	0.49	12.90	0.220	218.4

Figure 25 shows the performance of sandwich panels designed according to the two *design rules* considered above (the two panels of table 9 are marked with a 'X' in Figure 25). Note that the design rule *highest buckling load* never yields a lower performance than the design rule *fully stressed design*. Therefore designing for 'highest buckling load' would be advantageous, but this design rule does not consider material failure and, as one can see in the table above, for some loads yields a face thickness so small that material failure does occur. This is confirmed by Figure 26 where the face thickness of sandwich panels designed according to the two design rules given above is plotted against the structural index. For a value of the structural index above $N_x/b \approx 0.1$ an optimum *fully stressed design* has a larger face thickness than an optimum panel considering only *buckling*; therefore, in that region of applied loads the faces of
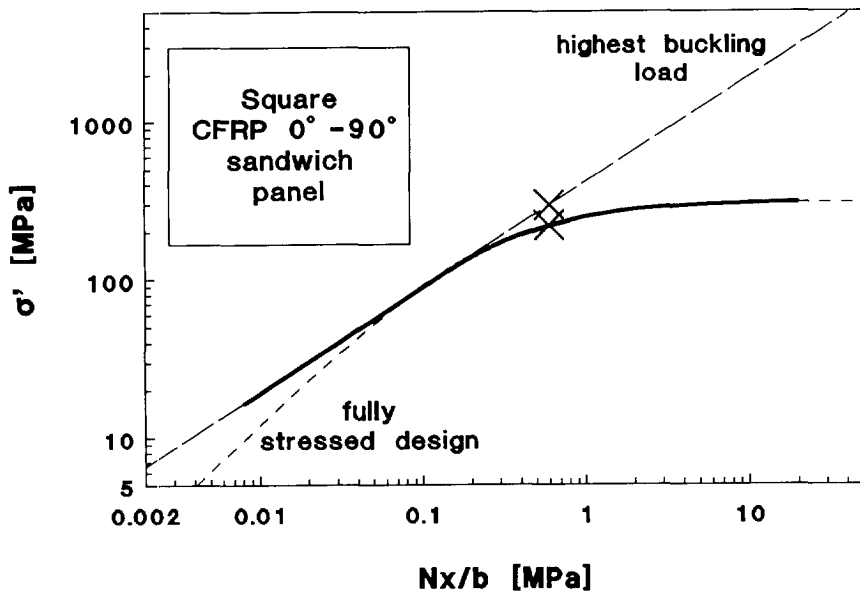

Figure 25 Performance of sandwich panels in compression

the *buckling* design will fail because of an excessive material stress. However, for loads below the limit value of $N_x/b \approx 0.1$, the face thickness of the *buckling* design is larger than that of the *fully stressed design*, and hence material failure will not occur. Because the performance of the *buckling* design is never worse than that of the *fully stressed design*, in the region $N_x/b \leq 0.1$ it is therefore better to apply the design rule *buckling*.

The somewhat surprising conclusion is that, in order to design the lightest possible panel considering *buckling* and *material failure*, for some loads it is best *not to consider material failure at all*, but to just look at the highest buckling load that can be achieved for a given mass. The same result can also be obtained by comparing the face thicknesses of the two design rules. Equating (102) (in which p_x is replaced by N_x) and (104) a numerical value for the limit value of the applied load N_x can be found, below which the *buckling* design has a sufficient face thickness to resist the stresses:

$$[t_f]_{(buckling \& mat. failure)} < [t_f]_{(highest buckling load)}$$

$$\frac{N_x}{2\overline{\sigma_c}} < \left(\frac{N_x a b}{2 E_f' k} \right)^{\frac{1}{3}} \left(\frac{\rho_c}{2\rho_f - \rho_c} \right)^{\frac{2}{3}} \tag{110}$$

$$N_x < \left(2\overline{\sigma_c} \right)^{\frac{3}{2}} \left(\frac{a b}{2 E_f' k} \right)^{\frac{1}{2}} \frac{\rho_c}{2\rho_f - \rho_c}$$
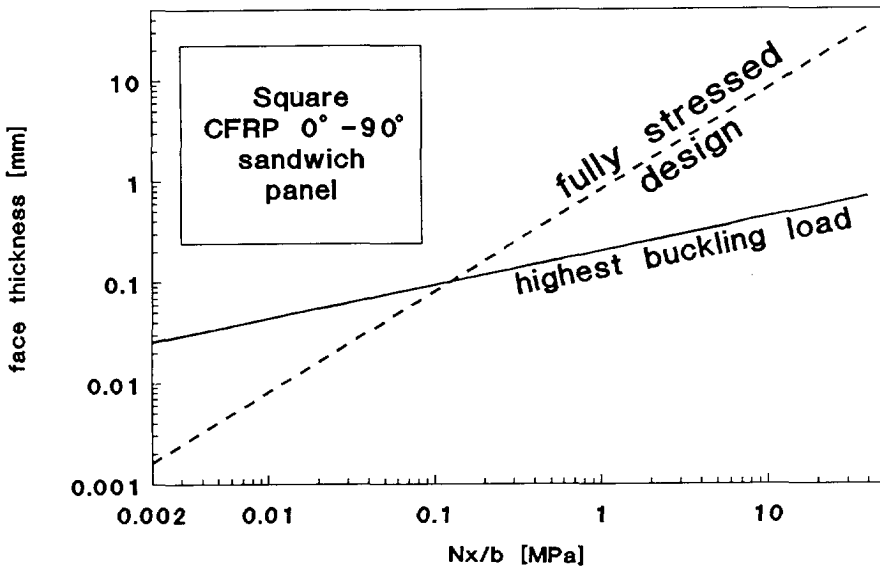

Figure 26 Sandwich panel face thickness for different design rules

For the sandwich panel in the example this limit value, calculated from (110), is N_x=62.0 N/mm. In Figure 25 this is the value for N_x at which the equivalent stress σ' of the two design rules is equal. Finally, Figure 25 shows the performance of the lightest possible panel (choosing whichever design rule yields the lightest panel that satisfies both buckling and material failure) with a solid line.

6.2   Performance of corrugated panels under shear

From the point of view of buckling, a corrugated panel loaded in shear is designed for coincident local and overall buckling. This condition is assumed to yield an optimum panel; the validity of this assumption is checked in part 4. The performance of the corrugated panel is given by the equivalent shear stress τ', defined as:

$$\tau' = \frac{q}{t'} = \frac{q}{Rt} \tag{111}$$

The equivalent thickness t' is here the thickness of a flat plate with the same mass as the corrugated panel. The aim, as in the previous paragraph, is to obtain a formula expressing the equivalent stress τ' in terms of the structural index (here this is q/h, the applied load divided by the panel height) and stiffness parameters, but not in terms of the laminate definition or the panel dimensions b_1, b_2 and β.

For simply-supported corrugated panels of *isotropic* material under shear load, [Rothwell85] has derived an efficiency formula based on coincident overall and local buckling, using an elementary formula for both buckling modes:

$$\tau' = \eta\ E^{7/15} \left(\frac{q}{h}\right)^{8/15}$$

$$\text{where:}\quad \eta = \frac{(k_L^3 k_O^4)^{1/15}}{R} \tag{112}$$

A maximum value η=1.73 was found by Rothwell.

A similar efficiency formula is derived for *composite* corrugated panels, again assuming coincident overall and local buckling, but now using the buckling formulae of chapter 5. These can be rewritten as follows:

$$q_L = \frac{k_L}{12} \frac{E_{short}^{1/4} E_{long}^{3/4}}{\mu^{1/4}} \frac{t^3}{b_2^2}$$

$$q_O = \frac{4 k_O}{12^{1/4}} E_{short}^{3/4} E_{long}^{1/4} \frac{R^{1/2}}{h^2} (t\omega b_2)^{3/2} \tag{113}$$

where $\omega.b_2$ is the radius of gyration (replacing ρ of chapter 5) and where μ is the Poisson's factor ($\mu = 1 - v_{xy}.v_{yx}$).
Substituting b_2 from q_L of (113) and t from (111) into q_O of (113) yields:

$$\tau' = \eta \left(\frac{E_{long}^{13} E_{short}^{15}}{\mu^3} \right)^{1/60} \left(\frac{q}{h} \right)^{8/15} \tag{114}$$

$$\text{where:} \quad \eta = \left(\frac{4^4}{12^3} \omega^6 \frac{k_L^3 k_O^4}{R^{13}} \right)^{1/15}$$

Formula (114) is somewhat more complicated than (112) due to the more elaborate buckling formulae, but its form is similar; note, for example, that the power of the *structural index* is the same in (114) and (112). Also, if an isotropic material is used (i.e. replacing E_{short} and E_{long} in (114) by E) the power of the Young's modulus E will be the same in (114) and (112). Unfortunately, unlike (92) for compression buckling of sandwich panels, here k_O and R depend on the design variables b_1, b_2 and β. The parameters k_O and R in (114) are therefore not constant as q/h increases. Therefore η also depends, even if only to a small extent, on q/h.

Figure 27 shows the performance of optimum composite corrugated panels, made of CFRP±45° laminate, with the following material data (that will be used in chapters 9 and 10 as well):

$$E_x = E_y = 11092. \text{ MPa} \qquad v_{xy} = .79$$

The line in Figure 27 labelled *coincident local & overall buckling* represents (114), using an efficiency value of $\eta = 1.73$. This value is of course approximative,

because it was obtained for isotropic material, while here orthotropic material is used. A second line in Figure 27 is that for material failure, because τ' can never be greater than the maximum allowable shear stress $\bar{\tau}$ (in Figure 27 a maximum allowable shear stress of $\bar{\tau}=566.$ MPa is used). In reality, the intersection point will not be reached, because as τ' reaches $\tau'=566.$ the curve will deviate from the sloping line towards the horizontal line.
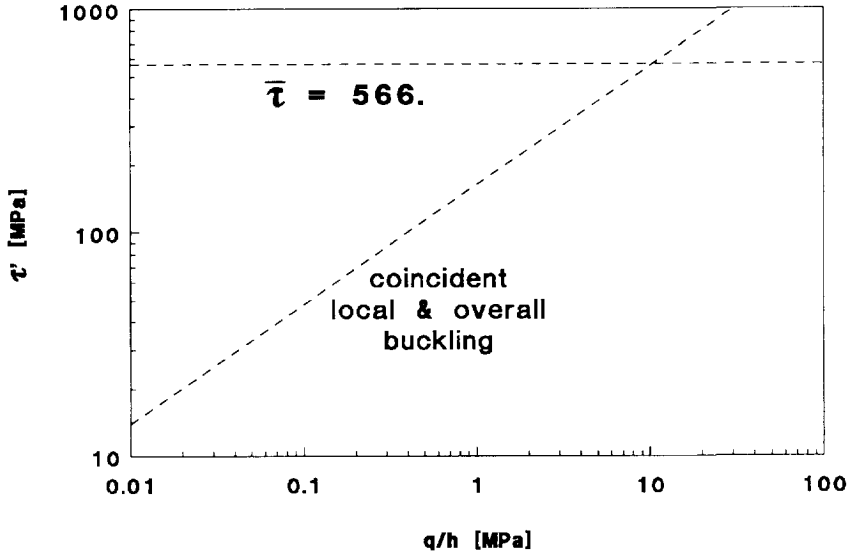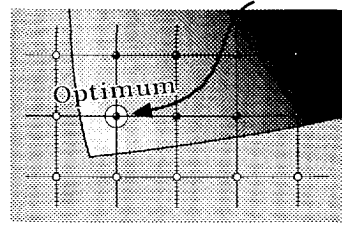

Figure 27 Performance of composite corrugated panels of CFRP±45°, with a height of 500. mm

7

Numerical Optimization

In the computer programs developed in this research for the design of composite panels, a numerical optimization method is provided to guide the user to an efficient design. While the previous chapter considered the optimum panel analytically, here an iterative, numerical procedure is used to locate the optimum. More specifically, the design problem of a composite sandwich panel or a corrugated panel is redefined here as a constrained, nonlinear optimization problem with *discrete* variables. The nature of the problem is examined, and a review is made of potentially suitable, discrete optimization methods. The Complex method selected is explained in some detail.

7.1   Definition of the numerical optimization problem

In summary, optimization is a process that searches for the extreme value of an *objective function* (in this case minimum mass) by varying some properties (the *variables*) of the subject under consideration. In principle this process can be performed with or without specified conditions (*constraints*) that have to be satisfied. Here the variables are the cross-sectional dimensions of the panel; for sandwich panels these are the thicknesses t_i of the different layers in the panel and their orientations ϕ_i with respect to the panel axes. For corrugated panels, as well as the definition of the laminate, the shape of the cross-section (lengths of the two faces b_1 and b_2 and the corrugation angle β) can also be varied. Typical constraints are material failure and buckling.

In contrast to the previous chapter, where the optimization was performed *analytically* to find formulae that define the performance of sandwich or corrugated panels satisfying some selected constraints, here the optimization is performed *numerically*, with an iterative process that searches to improve the quality of the solution (the panel) until an optimum (minimum mass) is found. First, the nature of the objective function, constraints and variables will be

examined. The objective function (the mass) of the *sandwich panel* is simply the sum over all layers of the density $\rho^{(k)}$ (typically in [kg/m^3]) multiplied by the thickness $t^{(k)}$:

$$m = \sum_{k=1}^{n} \rho^{(k)}.t^{(k)} \tag{115}$$

Note that m is the mass of the panel *per unit area*, as can be confirmed by the units [kg/m^2] of m in (115). Note further that this objective function is *linear* in the layer thickness $t^{(k)}$, but *independent* of the layer orientation $\phi^{(k)}$. For the *corrugated panel* the objective function is similar, but with an additional factor R representing the extra mass in the corrugated panel (per unit running length) because of the corrugation:

$$m = R. \sum_{k=1}^{n} \rho^{(k)}.t^{(k)}$$

$$= \frac{b_1 + b_2}{b_1 + b_2 \cos\beta} . \sum_{k=1}^{n} \rho^{(k)}.t^{(k)} \tag{116}$$

Here the mass m is linear in the layer thickness $t^{(k)}$, independent of the layer orientation $\phi^{(k)}$, and nonlinear in b_i and β.

The constraints to be considered in the optimization are very different in nature, and mostly nonlinear. For example, for the sandwich panel some of the constraints are:

♦ material failure: this constraint is given by the Tsai-Hill criterion of chapter 2 (Eq (14)), nonlinear in both layer thickness (but linear in the reciprocal of the thickness) and orientation.

♦ buckling: given by the buckling equations of chapter 3 or 4, nonlinear in both layer thickness and orientation.

♦ geometrical constraints (for example user-defined minimum thickness for some layers, or a maximum total panel thickness): these are linear in layer thickness and independent of the orientation.

For the corrugated panel, the constraints are similar.

The variables in sandwich panel optimization are different in character, as mentioned in chapter 1; the thickness of the layers of a composite panel is typically *discrete* (at least for aerospace applications) when *prepreg* material, i.e. thin layers (*plies*) of fibres *pre*-impregnated with a resin, is used because an integer number of plies have to be used. In theory, the orientation of the different layers in the laminate is a *continuous* variable, but manufacturing conditions limit the accuracy and the number of layer orientations in the

laminate. Therefore, the layer orientations can be treated as *discrete* variables as well, even if it would be perhaps more precise to consider the layer orientations to be continuous variables with some degree of uncertainty. This is an interesting matter, but not considered further here. For the corrugated panel, the laminate variables have, of course, the same character as the laminate variables of the sandwich panel. The shape variables b_i and β, on the other hand, are simple continuous variables.

The number of variables in the optimization depends on the complexity of the laminate at hand but, because of the way in which the laminate is defined in the following chapter, is generally small (say, five variables).

7.2 Numerical optimization methods for discrete variables

Structural optimization is a research area in its own right. However, discrete variable problems such as those considered in the previous paragraph remain part of this research area where high quality optimization methods for nonlinear problems are not available. The most elementary approach is, of course, to optimize with continuous variables, and afterwards to round the variables to the nearest available discrete value. However, this often results in a large increase in the objective function (especially when the 'grid' of possible discrete values is coarse in relation to the values themselves), so nullifying the perhaps very sophisticated achievement of a continuous optimization method. Moreover, when the grid is coarse, the true discrete optimum might not be located adjacent to the continuous optimum; then the rounding process cannot locate the true optimum of the original discrete problem. At first sight, the dual method [Fleury80] which optimizes in the dual space (which is continuous even for discrete variable problems) seems to eliminate this problem, but in the end merely provides a numerical scheme to locate the continuous optimum and perform the rounding within the optimization procedure. Yet another approach with continuous variables is an external penalty function formulation such that points not located on the 'grid' of discrete possibilities are penalized [Shin88], but even this method actually provides no more than an algorithm for rounding the continuous optimum.

Alternatively, it is possible to apply methods that use discrete variables directly. Many of these methods are heuristic by nature (i.e. a search method based on simple logic but not associated with some proof of convergence). The

Hooke and Jeeves' routine [Walsh75] is a simple improvement method for unconstrained optimization; hence the constrained problem has to be reformulated into an unconstrained one, by means of penalty functions. The method was initially developed for continuous variables, but can be used with discrete variables as well. 'Genetic search' [Hajela89] is a heuristic method based on the principles of genetics and natural selection; it is a discrete method by nature, able to overcome local minima and even disjoint design spaces. Its principal drawback is a large increase in the number of iterations necessary to locate an optimum, and it is not examined further. Other heuristic methods 'simulated annealing' and 'tabu search' [Glover93] share both the advantage (overcoming local minima) and drawback (large number of iterations) of genetic search, and are also rejected in favour of the Complex method described below. The latter is again a heuristic method, that has been proved to work well in the type of problem at hand (i.e. acceptable number of iterations, good convergence).

Note that in the discrete variable problems considered here (with a rather coarse grid of discrete variables) often many equivalent optima exist; for example [Bladel89c] reports a ten bar truss problem (10 variables, one constraint) for which at least 50 different optima with the same mass exist.

7.3   The Complex method

This optimization method is a heuristic that can be modified to apply to discrete value problems. It is a *direct, zero order* method (i.e. the constraints are not included in the objective function via a penalty function and no derivative information is required) first presented by Box [Box65] as a *con*strained *simplex* method. It uses a set of feasible points (the so-called complex) to assess the direction of improvement; repeatedly the worst point in the complex is moved to a better position. Because of its heuristic nature, references to this method (see [Bladel89c] for a comprehensive list) often present some modifications to the basic approach of Box. This is also so here, although in the first place only those modifications associated with the discrete nature of the variables are introduced. In this way a discrete Complex optimization method is obtained with good performance, especially for problems with few design variables (say, up to five). Some modifications are then examined to decrease the number of analyses involved.

A report by the author [Bladel89c] describes the discrete Complex method and its implementation in detail; here, its features are described by means of a simple two-variable problem, a two-bar truss (see Figure 28). This is a discrete optimization problem with linear objective function (minimum mass m) and one nonlinear constraint (maximum allowed displacement δ). The cross-sectional areas A_1 and A_2 of the bars are the variables. The problem is defined as follows:

Minimize $m = 10^{\frac{1}{2}}*A_1 + A_2$

subject to $\delta = \dfrac{10\sqrt{10}}{9A_1} + \dfrac{1}{9A_2} \leq 0.175$

where A_1, A_2 are *integer* variables
                within the bounds $A_1 \in [1,50]$, $A_2 \in [1,50]$

In Figure 29 the 2-dimensional design space is drawn. All trusses are represented by points X in this design space, with coordinates (A_1, A_2).

The Complex method has two parts; first a *setup phase* in which the set of feasible points (the *complex*) **C** is created, starting from a given feasible point, and a *move phase* in which the *complex* moves towards the optimum. Here, the starting point X_1 (40,20) (note that the subscript of X indicates its position in the set **C** and not the serial number within the optimization) is selected as
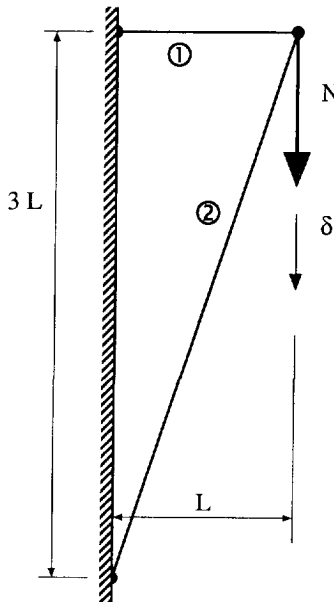

Figure 28 Two-bar truss optimization problem

starting point for the setup phase:

$A_1 = 40.$ $m = 146.5$
$A_2 = 20.$ $\delta = 0.093$

In the setup phase, repeatedly a new position is *generated* at random in a user-defined area of the design space; this new position is then analysed. If it satisfies all constraints, the point is accepted and added to the set; if not, it is moved (*retracted*) halfway towards the centroid of the previously accepted points and reanalysed. Notice the difference between the words *position* (a location in the design space) and *point* (a feasible position included in the complex set **C**). Because all points are feasible by definition it is likely that the retracted position will become feasible in the end. However, the design space is discrete in the application considered here, and when a retracted position is near the centroid of feasible points it might no longer move because of the discrete nature of the design space. Then the position is discarded and the process is repeated with another random generation. In the example under consideration, at the end of the setup phase, the following complex set **C** is obtained:
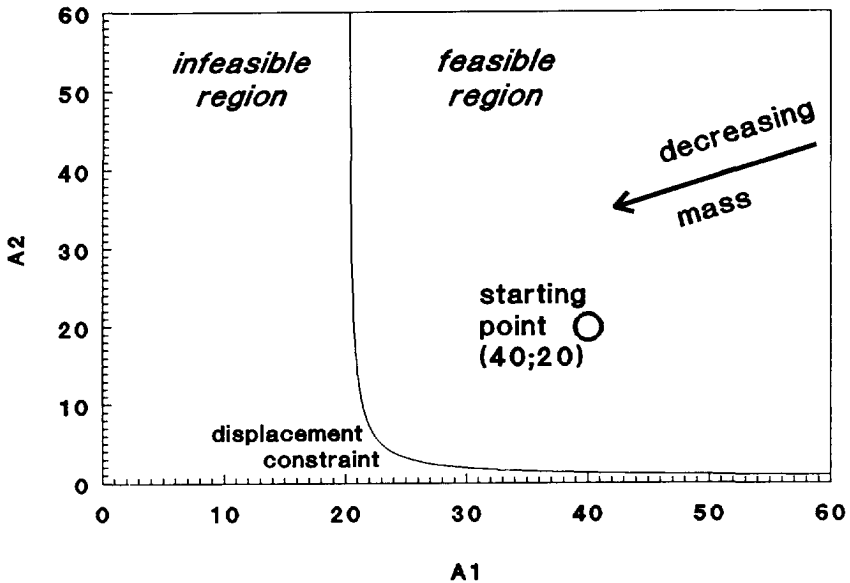

Figure 29 Design space of the two-bar truss problem

Table 10 the complex set **C** after the *setup* phase (two-bar truss problem)

point	X_1	$\mathbf{X_2}$	X_3	X_4	X_5	X_6
A_1	40.	**48.**	24.	28.	33.	26.
A_2	20.	**4.**	46.	35.	2.	11.
m	146.5	**155.8**	121.9	123.5	106.4	93.2

Then the method proceeds with the second or *move* phase, where repeatedly the worst point is moved to a better position. In Table 10 point X_2 (written in boldface) has the greatest mass and is thus the worst point. For the move a subset **C'** of the complex **C** is defined with all points except the worst point, and its centroid $X_{C'}$ is calculated:

Table 11 the subset **C'** of the complex **C**, and its centroid $X_{C'}$

point	X_1	X_3	X_4	X_5	X_6	$X_{C'}$
A_1	40.	24.	28.	33.	26.	30.2
A_2	20.	46.	35.	2.	11.	22.8
m	**146.5**	121.9	123.5	106.4	93.2	-

Note that the centroid need not be discrete. A trial position X_t to replace X_2 is generated on a discrete position at a certain distance beyond the centroid $X_{C'}$ on the line that connects X_2 with the centroid (called the *reflection* of X_2):

$$X_t = X_{C'} + \text{refl} * (X_{C'} - X_2) \tag{117}$$

where **refl** is the reflection factor that defines how far the trial position X_t is to be positioned beyond the centroid $X_{C'}$. Because X_2 was the worst point of the complex **C**, it is assumed that this trial position X_t has a smaller mass than the worst point X_1 of the *subset* **C'** (see boldfaced mass value in Table 11). X_t is analysed and if the position is feasible the complex **C** is updated replacing X_2 by X_t. The move process is then repeated with the definition of a new worst point (X_1). If, on the other hand, the position X_t is infeasible, it is *retracted* halfway towards the centroid, and analysed again. Note that it is also possible that X_t is located outside the user-specified bounds on the variables A_1 and A_2 (these bounds were also used in the *setup* phase for generation of the complex **C**); then X_t is positioned *on* the user-specified bound before analysis. In the

example under consideration Figure 30 and Table 12 illustrate this process:

Table 12 *Move* phase of the Complex method (refl=2.)

point	A_1	A_2	m	δ	Comment
X_2	48	4	**155.8**	.093	worst point
X_t	-5.4	60.4	-	-	after reflection out of user-given bounds
	1	50	53.16	**3.52**	positioned on bounds; constraint violation
	16	36	86.60	**0.223**	retracted; still constraint violation
X_2	23	29	101.7	0.157	retracted again; **feasible**; new position for X_2

In Figure 31 the optimization process is illustrated; in Figure 31a the optimization trajectory is drawn in the design space, by plotting the movement of the centroid of the Complex **C'**, while in Figure 31b the design history is shown with the evolution of the objective function of the best point in the Complex **C**.
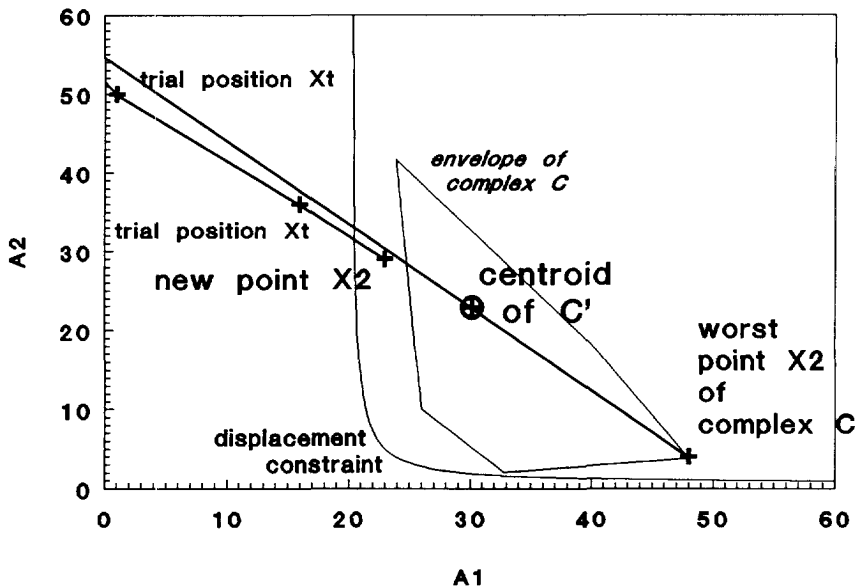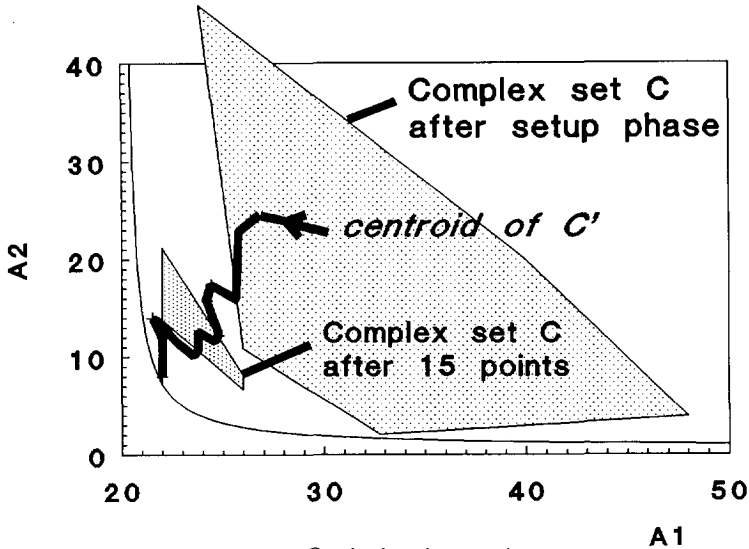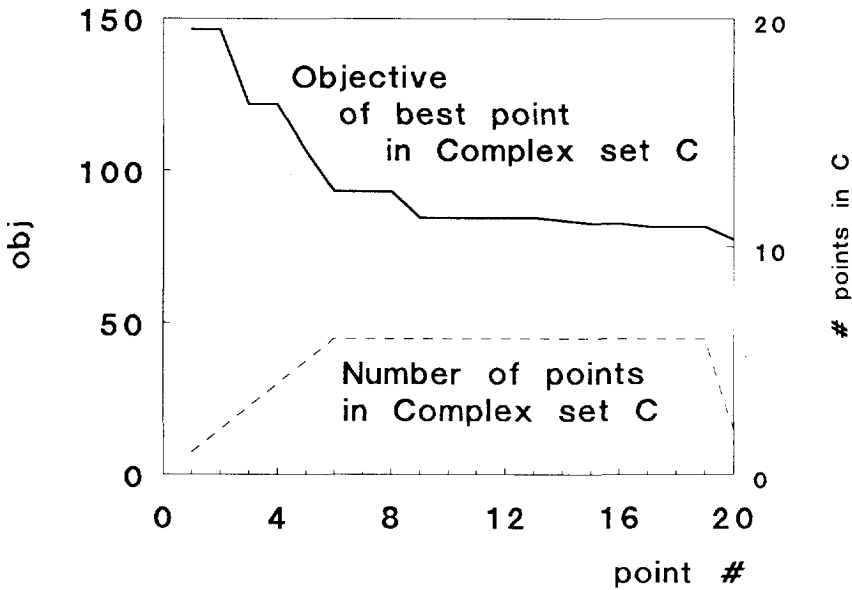

Figure 30 *Move* phase of the Complex method

Because of the discrete nature of the design space, at a certain point a *reflected* or *retracted* point may have not actually moved. As also done in the *setup* phase, this point is then removed from the Complex set and the *move* phase continues with one point less.

a. Optimization trajectory

b. Design history

Figure 31 Optimization with the Complex method of the two-bar truss problem

There are two stop criteria for the *move* phase; first, because the number of points can decrease (as described above) at a certain stage there may be only one point left. Furthermore, because of the discrete nature of the design space, it is possible that all points in the Complex are coincident. In both cases the optimization stops with the remaining point as optimum.

The procedure above describes the changes required for application of the Complex method to a discrete design space. There are two basic parameters involved, the number of points **npt** in the complex set **C** and the reflection parameter **refl**. In the original reference [Box65], for **nvar** *continuous* variables Box proposed:

npt = 2*nvar   refl = 1.3   (continuous variables)

For *discrete* variables, the author [Bladel89c] has proposed a larger number of variables, because points are deleted from the Complex set, and a larger value for **refl**:

npt = 2*nvar+2   refl = 2.   (discrete variables)

After 20 points and 52 analyses (including those yielding unfeasible points) the Complex method stops, having reached the discrete optimum $\mathbf{X}^*$:

$\mathbf{X}^*$: A_1 = 22.   m = 77.57
       A_2 = 8. δ = 0.161

However, sometimes the stop criterion can be satisfied before the optimum is actually found. Therefore, a *restart* feature is introduced; when the stop criterion is satisfied, another optimization run is done, starting from the current best point. When no improvement is obtained (i.e. when the end point equals the starting point of the restart) this point is accepted as optimum. With the *restart* the process of focusing on specific good points in the design space (during the *move* phase) is alternated with zooming out to check for the existence for other good points. In practice, it is found that restarts benefit from the use of a smaller design space. Therefore, at every restart, the interval in which the variables are generated is halved[†].

[†] At a *restart* only the bounds on the *setup* space are halved; the user-given bounds (used in the *move* phase) outside of which a point is not analyzed remain the same throughout.

For small problems (say, up to five discrete variables) the method first described (further called the *standard discrete Complex method* or SDC method) yields good results; the optimum is found in fewer analyses than, for example, Hooke and Jeeves' method. However, for larger problems the true optimum is not always found. Therefore it is best, at the end of an optimization, to repeat the optimization from the user given starting point. Then, because of the random aspect of the method (in the *setup* phase the Complex set **C** is generated randomly) *different* Complex sets **C** are obtained at the end of the *setup*, after which alternative optimization paths are followed to the optimum. Another possibility is to continue from the obtained optimum, to confirm whether the obtained optimum is indeed the global optimum. A further benefit of repeated optimizations from the user given starting point is the possibility of finding equivalent optima (recall from paragraph 5.2 that in this type of discrete optimization problem with a coarse discrete grid many equivalent optima often exist). A typical optimization with the discrete Complex method will therefore comprise some repeated optimizations from the obtained optimum, and some repeated optimizations from the user-given starting point.

This is a good optimization method for the discrete problems at hand, especially when few design variables are present. It differs from the approach of [Box65] only in the changes required for the use of discrete variables (i.e. removal of points when they do not move anymore, and the stop criterion). However, many 'useless' analyses are required; in the example above the optimum is reached after 52 positions have been analysed, to obtain 20 feasible points (before the restart); hence 32 analyses are done on infeasible points. This ratio of 52 to 20 is fairly constant, for various runs and different cases; before a next point is found, on average 2.5 analyses are needed. Two modifications were examined here to decrease this ratio; in the first approach it was tried to *estimate* the outcome of an analysis instead of performing one for every trial position. However, defining sufficiently reliable estimates is not easy and the estimation procedure also costs computer time. This approach was therefore abandoned (see [Bladel89c]). The second approach is to make the reflection factor **refl** variable. If the reflected position violates one or more constraints, at the end of this move **refl** is decreased by a certain amount. If, on the other hand, the position does not violate constraints and if it is not outside the user-given bounds, **refl** is increased. In this way less violating trial points are generated. In practice, this approach indeed decreases the overall number of analyses performed in an optimization, but often also results in a premature termination of the optimization because very low values of **refl** can occur. To balance this exaggerated focus on a specific good point the size of the setup space at a *restart*

should not be decreased.

With the second approach a *modified discrete Complex method* (MDC) is created, in which the number of analyses is indeed decreased significantly. The number of points before the optimum is reached is, on the other hand, increased. This indicates that the MDC method proceeds slower than the SDC method. The MDC method differs from the SDC method in the following aspects:

♦ at the beginning of a *move* phase, reset **refl** to the user-given value
♦ when a new point is found (or when the point is omitted from the complex set **C**), update **refl** as follows:
   ◊ when a trial position X_t has violated one or more constraints and has therefore been retracted **retr** times, decrease **refl**:

$$refl = refl \ / \ deltar^{retr}$$
where: $deltar = 2^{(1/npoint)}$

   ◊ when the trial position has not violated any constraint, and less than **(nvar/3)** variables are at their upper or lower bounds, increase **refl**:

$$refl = refl * deltar$$

The *modified discrete Complex method* (MDC) performs as well as the SDC method for small problems (for the two-bar truss problem the true optimum is found in as many analyses as in the standard discrete Complex method). For large problems, on the other hand, there is a clear advantage; optimizations from the user-given starting point arrive at optimum as good as those obtained by the SDC method, in half the number of analyses required in the SDC method. However, when the optimization is repeated from these optima, less improvement is on the whole found with the MDC method.
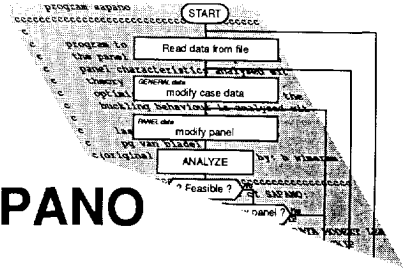
Concluding, the two variants of the Complex method each have their advantages and disadvantages; for small problems there is no difference in performance between the SDC and MDC method. For larger problems the SDC method can be described as *thorough but slower,* and the MDC method as *fast but less thorough.*

part III

Design Tools

8

The Computer Program SAPANO

8.1   Organisation of SAPANO

The computer program SAPANO (which stands for 'SAndwich Panel ANalysis and Optimization') is based on those aspects of the theoretical development in parts 1 and 2 of this thesis relevant to flat, rectangular laminates and sandwich panels. It is an interactive design tool to analyse and optimize such panels under in-plane loads, considering material failure and stability. The program COPANO (COrrugated Panel ANalysis and Optimization) on the other hand combines the aspects relevant to corrugated panels. This chapter describes the organisation of SAPANO and covers two optimization examples, while specific instructions for use are given in a separate user's manual ([Bladel94a]).
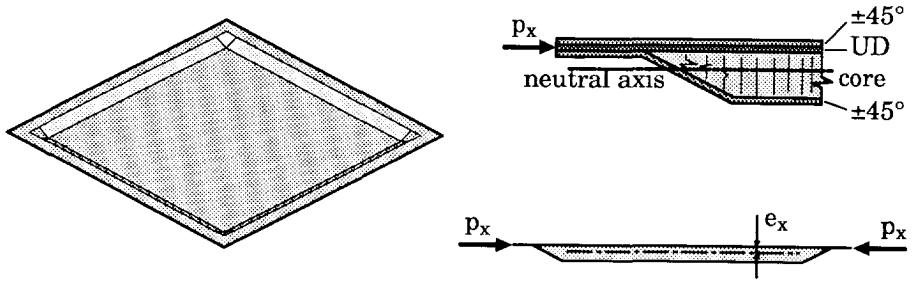

Figure 32 An example of a sandwich panel (in SAPANO also other materials and loads can be used)

8.1.1 Structural model in SAPANO

The structure, whether a laminate or sandwich panel, is considered to be flat, rectangular and simply-supported on all four sides, as shown in Figure 32. Note that the illustrated flattening of the edges (one of the possible methods of fastening) agrees well with the assumption of simple-support. Both sandwich panels and laminates are modelled as a stack of layers, each of a specific material and with a thickness and orientation with respect to the panel axes (both constant over the whole of the panel). In case of a sandwich panel one of the layers near the middle is made of a light but flexible material, creating in this way two distinct faces, separated by a core; typically this core layer constitutes more than three quarters of the thickness of the panel. In this way a high bending stiffness is obtained, but the relatively flexible core causes a significant reduction in transverse shear stiffness. Therefore, analyses incorporating transverse shear deformations are required (see chapters 3 and 4). The model in SAPANO is therefore defined by the size (length and width) of the panel and its layup, i.e. the material, thickness and orientation of the different layers. Different ways exist to model the layup; here the panel is considered to be a stack of up to 20 different layers; every layer is of one (user-defined) material and has a thickness and orientation with respect to the panel axes. The user defines the number of different layers in the panel and assigns a material to each of them. The orientation and thickness of every layer are then the variables that can be used in the optimization to find the panel of least mass (if the panel is symmetric, only half of the panel, up to the mid-plane, has to be specified). In the program the thickness is given as a multiple of the physical ply thickness of the material (this thickness is part of the data of the material). Further data for one case are the (up to 10) load combinations, each of which can have non-zero direct loads N_x, N_y and shear load N_{xy}. Only in-plane loads are considered.

When the panel is not symmetric it is possible to include the effect of the eccentricity of the applied load. Then it is necessary, of course, to specify the vertical position of the (in-plane) load at the edges. The loads are assumed to act at the middle of a given layer of the laminate, see Figure 32. The eccentricity is then given by the vertical difference between the position of the applied load and the neutral axis in cylindrical bending in that direction. In this way, as the thicknesses of the layers change during the optimization, the value of the eccentricity will change accordingly.

8.1.2 Panel analysis in SAPANO

Once the case is suitably defined by the appropriate data, an analysis can be

performed. The user can specify which aspects are to be examined, for example whether or not buckling and eccentricity effects are to be included. Then, within SAPANO, two different procedures for analysis are followed, depending on whether a single analysis is done, or a series of analyses (during the optimization). In the first procedure, all the aspects specified by the user are examined while in the second case aspects are examined in order of increasing complexity (and computer time) as long as no violations (i.e. non-compliance of the panel to the user-specified requirements) are encountered. In this way the first procedure provides a complete analysis of the panel, while the second discards generated designs that are infeasible as soon as the panel violates a requirement.

Every analysis begins with a calculation of the panel stiffnesses:
- ♦ the ABD-matrix is obtained by the classical laminate theory, as described in paragraph 2.1.1;
- ♦ transverse shear stiffnesses S_{xz} and S_{yz} (based on cylindrical bending) are obtained from paragraph 3.1.2;
- ♦ if the panel is not symmetric, reduced bending stiffnesses D^{**}_{ij} are calculated on the basis of cylindrical bending, see paragraph 2.1.2;
- ♦ if specified by the user, the bending stiffnesses of the individual faces of a sandwich panel are calculated (as required in the wrinkling analysis (see paragraph 4.3) and in the compression buckling analysis of paragraph 4.1).

Then various mechanical analyses are performed, as specified by the user, beginning with material failure:
- ♦ for static failure, the modified Tsai-Hill stress criterion of paragraph 2.2.1 is adopted;
- ♦ impact damage is covered based on a fibre strain criterion, as described in paragraph 2.2.2.

Next a number of buckling loads are calculated, if buckling is specified by the user:
- ♦ wrinkling analysis (if a sandwich panel is defined, with a core and two faces), as described in paragraph 4.3; the wrinkling load p_w in x- and y-direction is calculated, and for any given load case it is checked whether wrinkling occurs;
- ♦ basic buckling loads p_x, p_y and q (i.e. when only one of these loads is present):
    - ◊ direct buckling loads p_x and p_y are calculated with the formula of paragraph 4.1.1 (if required including face bending stiffnesses); the effect of moderate anisotropy can also be included (see paragraph 2.3.1);

◊ for buckling under shear loads, the formula of paragraph 2.3.2 is combined with the knock-down factor of 3.3.1.

♦ if within any load case different loads are present, it is examined whether buckling occurs for the following load combinations:

◊ combined p_x and q;

◊ combined p_y and q;

◊ combined p_x and p_y

(combined p_x, p_y and q cannot be analysed).

Finally, if required the stresses caused by the eccentricity are calculated, as given in paragraph 4.2.

8.1.3 Optimization in SAPANO

Optimization in SAPANO is performed by the Complex method, as described in paragraph 7.3. Recall that two alternative implementations are available; the *standard discrete Complex method* (SDC) and the *modified discrete Complex method* (MDC); the SDC can be described as *thorough but slower*, and the MDC as *fast but less thorough*. Note that an initial *feasible* point is required to initiate the optimization. All intermediate panels and the obtained optimum are feasible (i.e. the optimization proceeds *inside* the bounds of the feasible region of the design space).

The various calculations summarized in 8.1.2 can be selected by the user to be included or excluded as constraints during optimization, together with some geometrical constraints such as a user-specified minimum thickness for one or more layers, or a maximum overall thickness for the panel as a whole. Furthermore it is possible to add a condition by which the optimization process prefers orthotropic panels.

8.2   Some optimization examples

Two examples will be given here, considering a specific laminate optimization problem. They are presented here to show how such problems are modelled, the convergence of the optimization and the typical number of analyses involved. Furthermore, the results display characteristics that are typical of discrete optimization.

The examples treat the optimization of fibre orientation of a long, laminated

panel in compression, considering both buckling and material failure. On the basis of netting theory it is known ([Rothwell69]) that at low loading the fibres are best oriented at ±45° with respect to the direction of the applied load, while at high loading the optimum laminate contains only unidirectional material (UD) aligned with the applied load (in the 0°-direction), see Figure 33. Note that in both cases the laminate is balanced and orthotropic. The aim here is to see whether SAPANO, which uses classical laminate theory and a discrete optimization, reproduces these results. The panel dimensions are taken to be:

$$a = 5000. \text{ mm, } b = 200. \text{ mm}$$

representing a long laminated panel. Note that the compression buckling analysis of SAPANO deals accurately with long panels (while the shear buckling analysis is accurate only up to a/b≈5). Note also that the low transverse shear stiffness of the laminate (important at high loading) is taken into account in the buckling analysis. In [Rothwell69], this problem is modelled as a homogeneous two-fibre system where UD fibres and fibres at ±ϕ are distributed uniformly through the thickness. In [Rothwell69] for low loads the UD fraction in the laminate is zero and ϕ=45°, while for high loads the UD fraction increases to 100% as ϕ increases to 90°. In SAPANO it is not possible to model this homogeneous layup, because different orientations are in different layers, as in a real laminate. Furthermore, in the optimization in SAPANO only ϕ can vary, not ±ϕ together. Therefore layups are defined here with fixed orientation, (although in SAPANO it is possible to include the orientations as variables in the optimization). The following two examples are drawn from this case, showing the performance of SAPANO in both a large and a small problem.

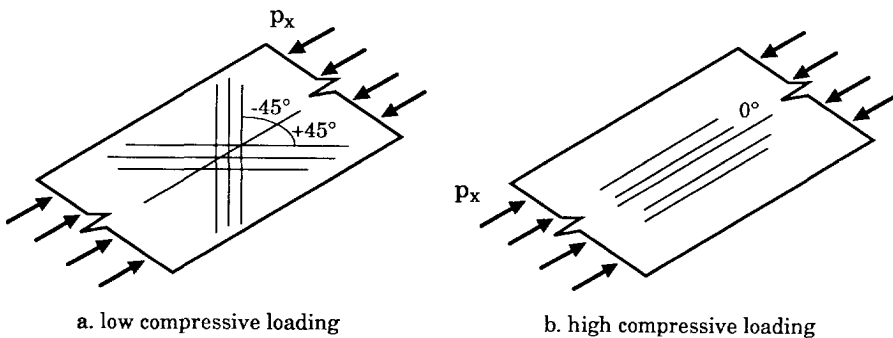a. low compressive loading   b. high compressive loading

Figure 33 Optimum fibre orientation of long laminates in compression, from netting theory

The first (large) example is a 7-layer symmetric laminate, defined as follows:

$$[90°/\pm75°/\pm60°/\pm45°/\pm30°/\pm15°/0°]_s$$

where the 's' stands for 'symmetric'. The following materials and mechanical properties are used:

Table 13 Material properties[†] for the laminate example

material		CFRP UD	CFRP ±15°	CFRP ±30°	CFRP ±45°
E_x	MPa	145000.	113550.	40309.	12860.
E_y	MPa	7000.	7050.	7780.	12860.
v_{xy}	-	0.34	1.35	1.66	.837
G_{xy}	MPa	3500.	11880.	28640.	37020.
G_{xz}	MPa	3500.	3000.	3000.	2500.
G_{yz}	MPa	1500.	2000.	2000.	2500.
σ_{tx}	MPa	1750.	1443.	385.	159.
σ_{cx}	MPa	-1350.	-1043.	-304.	-159.
σ_{ty}	MPa	63.	67.	87.	159.
σ_{cy}	MPa	-210.	-182.	-143.	-159.
τ_{xy}	MPa	80.	266.	618.	785.

[†] for all used materials the discrete ply thickness is 0.1 mm and the density is 1.6 g/cm^3

This laminate can be realized with the materials of Table 13, by defining the different layers as follows:

Table 14 Laminate definition for the 7-layer case

layer	1	2	3	4	5	6	7
material	CFRP UD	CFRP ±15°	CFRP ±30°	CFRP ±45°	CFRP ±30°	CFRP ±15°	CFRP UD
orientation	90°	90°	90°	0°	0°	0°	0°

Although seven different orientations are included in the laminate it is expected that the optimization will yield an optimum laminate with a high fraction of a few orientations. At first, optimizations are performed for Nx= -2000.N/mm, both with the standard discrete Complex method (SDC) and with the modified discrete Complex (MDC). The starting point is:

$$[90°_{10}/\pm75°_{10}/\pm60°_{10}/\pm45°_{10}/\pm30°_{10}/\pm15°_{10}/0°_{10}]_s$$

Because the laminate is symmetric, it has 140 plies of material in total. When the optimization is ended, it is restarted by the user, until SAPANO has returned three times the same optimum. This process is repeated five times from the starting point given above (note the random generation of points in the Complex method). In this way it is nearly certain that the overall optimum will be found. With the SDC method the following results are obtained:

Starting point $[10/10/10/10/10/10/10]_s$ (the numbers indicate the number of plies in that layer)

├ $[0/0/1/12/8/7/8]_s$ →[idem]→[idem] →$[0/0/0/11/16/1/7.5]_s$ →[idem]→[idem]→[idem]

├ $[0/0/5/3/14/3/11.5]$ →[idem]→[idem] →$[0/0/1/16/6/1/11.5]_s$ →$[0/0/0/21/3/2/9.5]_s$ → →[idem]→[idem]→[idem]

├ $[0/0/1/11/14/7/2.5]_s$ →[idem]→[idem]→[idem]

├ $[0/0/1/11/6/9/9]_s$ →[idem]→[idem]→[idem]

└ $[1/0/3/10/6/8/8.5]_s$ →[idem]→[idem] →$[0/0/0/21/2/3/9.5]_s$ →[idem]→[idem]→[idem]

In the optimization 'history' above the continued optimization from the last obtained optimum (until the same optimum is obtained three times) is clearly seen, as well as the five repeated optimizations from the same original starting point. At first sight, the optimization does not seem to perform well, as many different optima are found. However, many of these optima have the same thickness and are therefore equally good. This is clear from the following optimization record where the thickness of the optimum is given instead of its layup:

Starting point [t=14.mm]

├ [t=7.2mm] →[idem]→[idem] →[t=7.1mm] →[idem]→[idem]→[idem]

├ [t=7.3mm] →[idem]→[idem] →[t=7.1mm] →[t=7.1mm] →[idem]→[idem]→[idem]

├ [t=7.1mm] →[idem]→[idem]→[idem]

├ [t=7.2mm] →[idem]→[idem]→[idem]

└ [t=7.3mm] →[idem]→[idem] →[t=7.1mm] →[idem]→[idem]→[idem]

Not only do all the obtained final optima have a very similar efficiency, also many different optimum laminates exist with the same thickness of 7.1 mm. Furthermore it is clear that the first optimum (i.e. obtained after a single SAPANO run), even if it is not as good as the final optimum (after repeated

SAPANO runs until the same optimum is obtained three times), is already of a good quality. A final optimization record of this case shows the number of analyses required:

Starting point

⊢ [843 analyses] →[327 a] →[284 a] →[530 a] →[294 a] →[396 a] →[328 a]

⊢ [787 a] →[306 a] →[335 a] →[789 a] →[586 a] →[362 a] →[373 a] →[342 a]

⊢ [859 a] →[323 a] →[313 a] →[316 a]

⊢ [975 a] →[292 a] →[352 a] →[321 a]

⊢ [791 a] →[302 a] →[316 a] →[566 a] →[318 a] →[380 a] →[382 a]

Although many analyses are required, on a modern workstation this optimization can still be performed interactively (typically within a minute). Optimizing the same case again but using now the MDC method allows a comparison of performance between SDC and MDC. Below, the optimum thickness and number of analyses are compared for SDC and MDC, both for a single SAPANO optimization and for the same continued optimization (i.e. until the same optimum has been found three times):

Table 15 Performance[†] of SDC and MDC optimization of a 7-layer laminate for N_x=-2000. N/mm

SDC	single[‡] SAPANO run	continued[‡] SAPANO run	**MDC**	single SAPANO run	continued SAPANO run
t_{opti}	7.22 mm	7.12 mm	t_{opti}	7.24 mm	7.22 mm
# an.	851	2738	# an.	568	1417

[†] optimum thickness (t_{opti}) and the number of analyses (# an.) are averages over five optimizations from the starting point given by the user
[‡] 'single' means one SAPANO run from the user-given starting point; 'continued' means continuing the optimization until the same optimum is found three times

This confirms what was said about SDC and MDC in chapter 7: SDC can be considered as *thorough but slower* while MDC is *fast but less thorough*.

The obtained optima with t=7.1 mm do not reproduce the results of [Rothwell69]; here the results show only that layers with $\phi \leq \pm 45°$ are favoured

(see the first optimization history). This is examined in the second (small) example, with a 2-layer laminate, defined as follows:

$$[\pm\phi / 0°]_s$$

The first such case, $[\pm45°/0°]_s$, gives for both SDC and MDC even after one optimization run of SAPANO an optimum laminate thickness of t=7.1 mm (the thickness of the global optimum). While the quality of the optima is the same, the number of analyses still differs between SDC and MDC:

Table 16 SDC and MDC optimization of laminate $[\pm45°/0°]_s$
for N_x=-2000. N/mm

SDC	single SAPANO run	continued SAPANO run		MDC	single SAPANO run	continued SAPANO run
# an.	167[†]	350		# an.	89	206

[†] average over three optimizations

Note that now only three (not five) optimizations are performed from the user-given starting point, because the case is much simpler, and therefore the optimization more reliable. Note also that from here on, only results of SDC optimizations will be given (because of the smaller problem, here it is not necessary to use the faster MDC method). The optimizations and extra analyses show that a wide range of equivalent optima exist, all with a total laminate thickness of t=7.1 mm; in fact, all laminates with between 10% and 44% of the thickness made of UD material are equivalent optima. This confirms clearly what was said in chapter 7, that many equivalent optima exist in this kind of discrete optimization.

Optimizing other 2-layer laminates $[\pm\phi/0°]_s$ shows that for a compressive loading N_x=-2000. N/mm the laminate with $\pm45°$ gives the lowest optimum thickness:

Table 17 Optimum thickness of different two-layer laminates
at a compressive loading of Nx=-2000. N/mm

laminate composition	$[\pm30°/0°]_s$	$[\pm45°/0°]_s$	$[\pm60°/0°]_s$
optimum thickness	7.5 mm	**7.1** mm	7.6 mm

Performing similar optimizations for other compressive loads gives the results of Figure 34. In Table 18 the same results are given, with a column added with the percentage of UD-material in the optimum laminate:
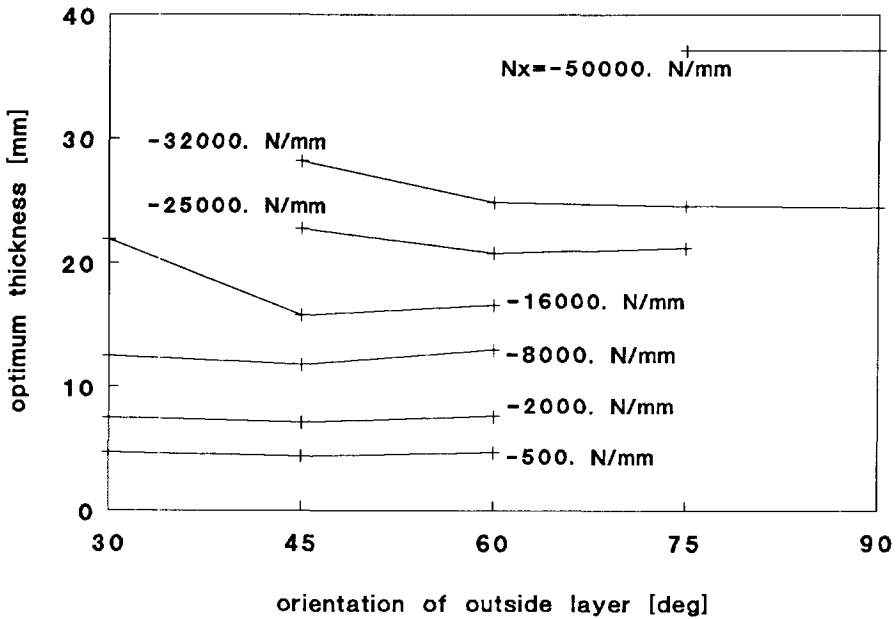

Figure 34 Optimum total thickness and orientation φ of two-layer laminates [±φ,0°]$_s$ for different loads

Table 18 Optimum thickness (in mm) of two-layer laminates
for various compressive loads

| compressive loading N_x [N/mm]	orientation $\pm\phi°$ of outside layer in $[\pm\phi°/0°]_s$ laminate					% 0° in optimum laminate
	±30°	±45°	±60°	±75°	±90°	
-500.	4.7	**4.4**†	4.7			0-41 %
-1000.	5.9	**5.6**	6.0			4-46 %
-2000.	7.5	**7.1**	7.6			10-44 %
-4000.	9.5	**9.0**	9.7			22-27 %
-8000.	12.5	**11.8**	13.			37-49 %
-16000.	21.9	**15.8**	16.6			62-66 %
-25000.		22.8	**20.8**	21.2		88 %
-32000.		28.2	24.9	24.6	**24.5**	98 %
-50000.				37.1	**37.1**	100 %

† boldface indicates the optimum (minimum) thickness

These results partially confirm the statement of [Rothwell69]; at high compressive loading the UD-fraction in the laminate is indeed dominant, at low loading the ±φ fraction. However, in this optimization there is only a small intermediate region where φ increases from ±45° to 90°.

A special property of the discrete optimization is the presence of many alternative optima. In other words the optimum thickness is often only weakly dependent on the layup. A general conclusion that can be drawn from this is that when the discrete thickness of the material is taken into account, 'simple' laminates (for example with the fibres only at 0°, ±45° and 90°) will often yield just as good results as more complex laminates (with many different orientations). Hence a designer may often limit his design to relatively few orientations, without much deterioration of the quality of the optimum.
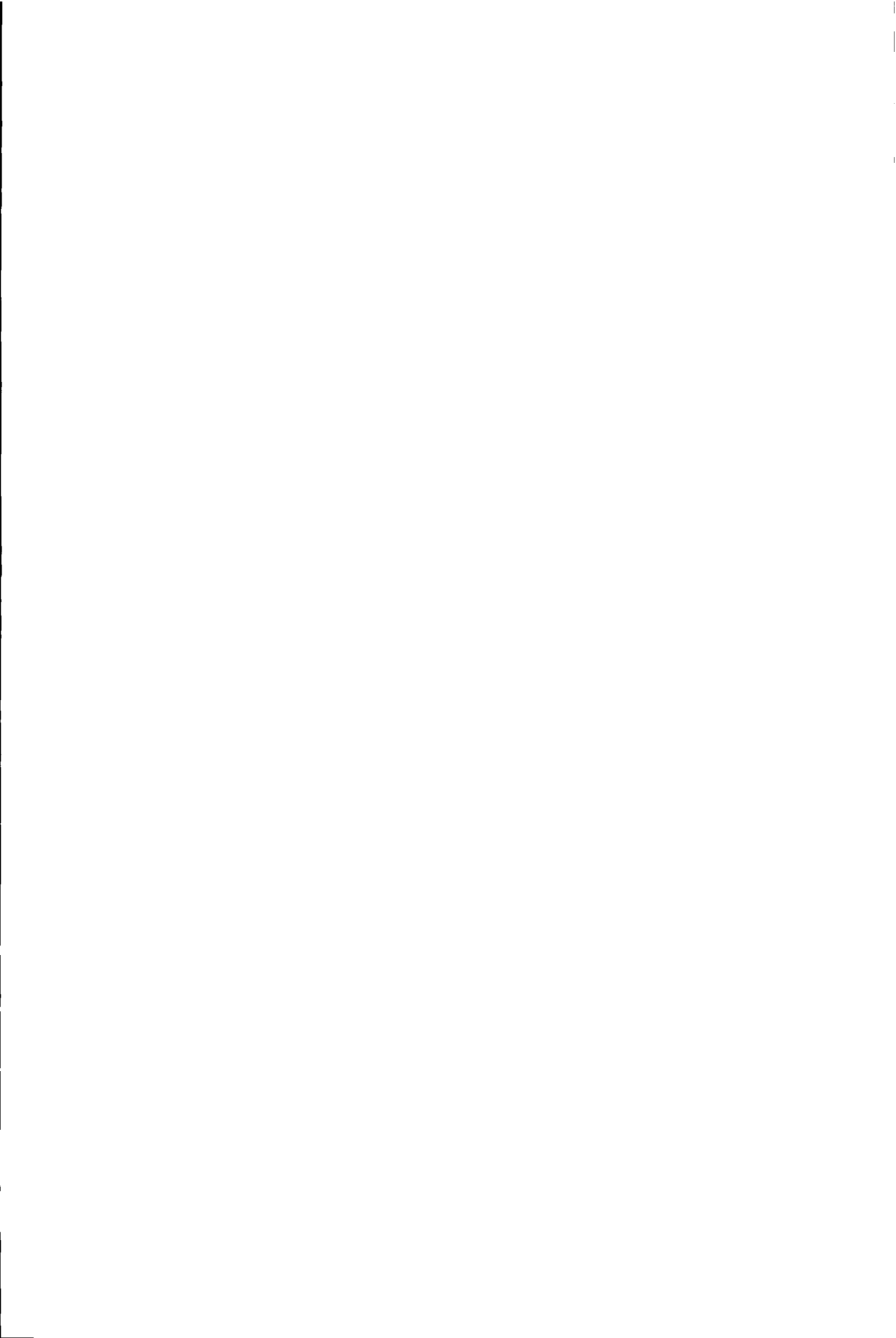
9
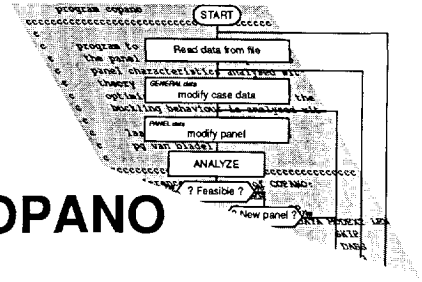
The Computer Program COPANO

9.1 Organisation of COPANO

This chapter describes how various aspects of parts 1 and 2 of this thesis are combined in the computer program COPANO (which stands for **CO**rrugated **P**anel **AN**alysis and **O**ptimization). The first paragraph describes the organisation of COPANO and the second presents an optimization example. Instructions for use can be found in a separate user's manual ([Bladel94b]). The computer program COPANO is based on those aspects of the theoretical development in parts 1 and 2 of this thesis relevant to composite corrugated panels. It is an interactive design tool to analyse and optimize long corrugated panels under in-plane loads. The shear buckling analysis (based on the results of chapter 5) has received special attention.
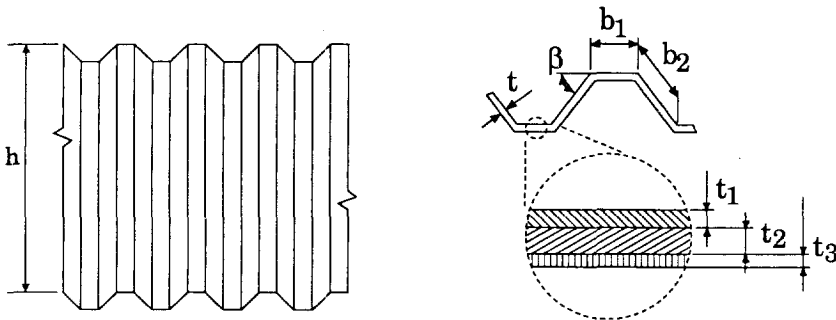

Figure 35 A typical corrugated panel of COPANO

9.1.1 Structural model in COPANO

The subject of the program is a corrugated panel with flat faces (recall that the term *face* is used here to denote the separate flat surfaces of the panel), as drawn in Figure 35. It is modelled as a long panel, hence the height h is the only relevant overall dimension. The corrugated cross-section is defined by the widths b_1 and b_2 of the two faces, and by the angle β between them. Both faces are made of the same laminate of up to 20 layers, defined in the same way as in SAPANO; each layer is made of one (user-defined) material and has a thickness and an orientation with respect to the panel axes. Here the term *laminate* is used, although it is of course possible to use only one layer of isotropic material. In COPANO, as in SAPANO, the laminate can be symmetric with respect to its mid-plane. The orientation and thickness of the layers are the laminate variables (next to the corrugation variables b_1, b_2 and β) that can be used in an optimization to find a panel of least mass (if the panel is symmetric, only half of the layup, up to the mid-plane, has to be specified). Further data for one case are the (up to 10) load combinations, each of which can have non-zero direct loads N_x, N_y and a shear load N_{xy}. Only in-plane loads are considered. Note that for the *stress analysis* all three in-plane loads are considered, while for *buckling* only N_x and N_{xy} are considered.

9.1.2 Corrugated panel analysis in COPANO

Once the case is suitably defined by the appropriate data, an analysis can be performed. As in SAPANO, two different procedures for analysis are followed, depending on whether a single analysis is to be done, or a series of analyses (during the optimization). In the first procedure, all the aspects specified by the user are examined, while in the second case aspects are examined in order of increasing complexity (and computer time) as long as no violations (i.e. non-compliance of the panel to the user-specified requirements) are encountered. In this way the first procedure provides a complete analysis of the panel, while the second discards infeasible designs as soon as the panel violates a requirement.

Every analysis begins with a calculation of the panel stiffnesses:
- ◆ the ABD-matrix of the laminate is obtained by classical laminate theory, as described in paragraph 2.1.1;
- ◆ if the panel is not symmetric, reduced bending stiffnesses D^{**}_{ij} are calculated based on cylindrical bending, see paragraph 2.1.2;
- ◆ the overall corrugated panel stiffness $\bar{D}_1$, $\bar{D}_2$ and $\bar{D}_{12}$ (to be used in the overall buckling analyses) are obtained from the formulae of paragraph 5.1.

Then various analyses are performed, as specified by the user, beginning with

material failure:

- ◆ for static failure, the modified Tsai-Hill stress criterion of paragraph 2.2.1 is adopted;
- ◆ impact damage is covered on the basis of a fibre strain criterion, as described in paragraph 2.2.2.

Next a number of buckling loads are calculated, if specified by the user and depending on which analysis procedure is being followed (i.e. one single analysis or an analysis during the optimization). Because of the corrugated shape, both local and overall buckling analyses are performed, for compression and shear loads. The shear buckling analyses (performed when $N_{xy} \neq 0$.) are taken directly from paragraphs 5.1 and 5.2 of this thesis. For compression buckling (performed when $N_x < 0$.), the case is somewhat more complex:

- ◆ first, local buckling analyses are performed on the faces separately, giving buckling loads p_{xl1} and p_{xl2}. Contrary to the local buckling analysis in shear, here the faces are considered separately (i.e. with no interaction between adjacent faces) and transverse shear effects are included;
- ◆ an overall compression buckling load p_{xe} is calculated, for which the panel is considered as a wide column, buckling in an overall 'Euler' mode.

Interaction between compression and shear buckling is analysed by means of the parabolic interaction formula, as discussed in paragraphs 3.4 and 5.4. Recall that paragraph 5.4 (on the interaction between overall compression and shear buckling) concludes that the formula is up to 10% conservative. For the local buckling mode, in principle the formula behaves well. However, the local compression and shear buckling modes considered here are not entirely similar; in *compression* the two faces are considered separately, while in *shear* two linked faces are considered. Still, the adopted formula is a good compromise between accuracy and simplicity.

Mode interaction of local and overall shear buckling, as discussed in chapter 5, can be checked by the stiffness parameter derived in paragraph 5.3; its value indicates whether interaction will occur.

9.1.3 Optimization in COPANO

Optimization in COPANO is performed by the Complex method, as described in paragraph 7.3. At the moment only the *standard discrete Complex method* (SDC) is available in COPANO. Note that an initial *feasible* point is required to initiate an optimization. All intermediate panels and the obtained optimum are feasible (i.e. the optimization proceeds *inside* the bounds of the feasible region of the design space).

The user can select the different calculations summarized in paragraph 9.1.2 to

be included or excluded as constraints during optimization, as well as a number
of geometrical constraints such as a user-specified minimum thickness for one
or more layers, or a maximum overall thickness for the panel as a whole.
Furthermore it is possible to add a condition by which the optimization process
prefers orthotropic panels.

9.2   An optimization example

Optimization in COPANO happens in much the same way as in SAPANO.
However, the Complex method has more difficulty in finding the optimum in
COPANO than it has in SAPANO. The average number of analyses required to
find a feasible point is greater here, and more often the optimization stops at a
local minimum. As an example, here the detail results of the optimization of the
second corrugated panel case of chapter 10 are given. The following materials
are used:

Table 19 Composite material data

	E_x [MPa]	E_y [MPa]	v_{xy} [-]	G_{xy} [MPa]	$\bar{\tau}$ [MPa]	ρ [g/cm^3]	t [mm]
CFRP ±45°	11092.	11092.	.79	24757.	566.	1.60	.23
CFRP 0°	145000.	7000.	.34	3500.	80.	1.60	.20

The corrugated panel has a height of h=1000.mm; it is made of a CFRP
laminate $[\pm 45°/0°]_s$ and is loaded by a shear loading q=50. N/mm. The
optimization proceeds as follows:

Starting point: laminate $[\pm 45°_5/0°_5]_s$, face widths $b_1=b_2=100.$mm,
corrugation angle β=90°, mass m=1.376 g/cm^2

├─ [m=.153] →[idem]→[idem]→[idem]

├─ [m=.174] →[idem]→[idem]→[idem]

├─ [m=.154] →[m=.153] →[idem]→[idem]→[idem]

├─ [m=.174] →[m=.174] →[m=.153] - [idem]→[idem]→[idem]

└─ [m=.204] →[idem]→[idem]→[idem]

The following intermediate optima are found in the process:
Starting point [5/5/100./100./90.]†

├─ [1/1/39./52./35.] →[idem]→[idem]→[idem]

├─ [1/1.5/57./66./18.] →[idem]→[idem]→[idem]

├─ [1/1/38./52./35.] →[1/1/39./52./35.] →[idem]→[idem]→[idem]

├─ [1/1.5/66./56./21.]→[1/1.5/57./66./18.]→[idem]→[1/1/39./52./35.]
│   →[idem]→[idem] →[idem]

└─ [1/2/82./73./12.] →[idem] →[idem] →[idem]

Contrary to the SAPANO results, here the different end results are not equally good, but are local optima with different performance. Other aspects of the optimization are similar to those of the optimization in SAPANO, and are therefore not covered here.

In summary, COPANO is very much like SAPANO (user interface, elements of the analysis), but the optimization process requires more effort from the user.

---

† [5/5/100./100./90.] is a condensed representation of the panel; first the symmetric laminate is described (on every half of the laminate: **5** plies of ±45° material, then **5** plies of 0° material); then the corrugation shape is given (face widths b_1=**100** mm, b_2=**100** mm, corrugation angle β=**90°**).
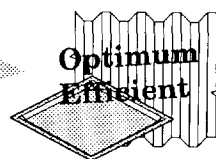
part IV

Application

10

Buckling
Eccentricity
Maximum thickness
Minimum thickness
Realistic layup

Optimum
Efficient

Efficiency of Optimum Panels

This chapter presents some results obtained with the computer programs SAPANO and COPANO, described in part 3 of this thesis. It must be noted that these results are not intended to show the limits of the developed software, but rather to present some interesting aspects of the design of sandwich panels and corrugated panels by comparing optimum panels designed with the computer programs with those obtained in chapter 6. In chapter 6 the design was done in an analytical way, which made it necessary to neglect some practical aspects essential to the real problem, that have been included in the programs SAPANO and COPANO.

10.1 Optimum sandwich panels under compression

The performance of optimum sandwich panels designed as in chapter 6 will always serve as an upper limit for the performance of optimum panels obtained with SAPANO, for two reasons: first, in chapter 6 the transverse shear effect is excluded; furthermore, the thicknesses of optimum panels of chapter 6 are continuous, not discrete values (note that by a suitable material definition it is possible to reproduce the analytical results with SAPANO, applying very high transverse shear stiffnesses G_{xz} and G_{yz}, and very small discrete material thicknesses).

A first interesting comparison is the effect of transverse shear on the efficiency, which is given in Figure 36. The dotted line represents the optimum design of chapter 6, while the full line shows the performance of the optimum sandwich panel designed with SAPANO, using normal transverse shear stiffnesses and a very small material thickness (of course, for best comparison, here eccentricity effects and face bending effects are excluded in the SAPANO design, leaving only material failure and buckling as constraints; later in this chapter these are included). The following data (elaborated from the material data of chapter 6)

are used for the CFRP 0°-90° material:

Table 20 Composite material data

	E_x [MPa]	E_y [MPa]	v_{xy} [-]	G_{xy} [MPa]	G_{xy} [MPa]	G_{xy} [MPa]	$\overline{\sigma_x}$ [MPa]	t [mm]
CFRP 0°-90°	76350.	76350.	.031	3497.	2500.	2500.	-304.	.10

Then:

$$E'_f = \frac{E_x}{1 - v_{xy}^2} = 76430.\,\text{MPa}$$

Note how in Figure 36 the difference between the two curves increases as the load is increased, showing an increasing transverse shear effect for higher loadings. Nevertheless, for this type of panel the effect remains small, even if at the edge of the graph (at Nx/b=4.N/mm^2) the optimum design of SAPANO buckles in a transverse shear mode, with $p_x=S_{xz}$ (hence with a pronounced influence of transverse shear). Also in Figure 36 the performance of sandwich panels with true discrete material thicknesses is drawn, showing a 'sawtooth' curve. The sawtooth appears because when the loading is increased, at a certain point the stress in the faces causes material failure, and an extra ply of
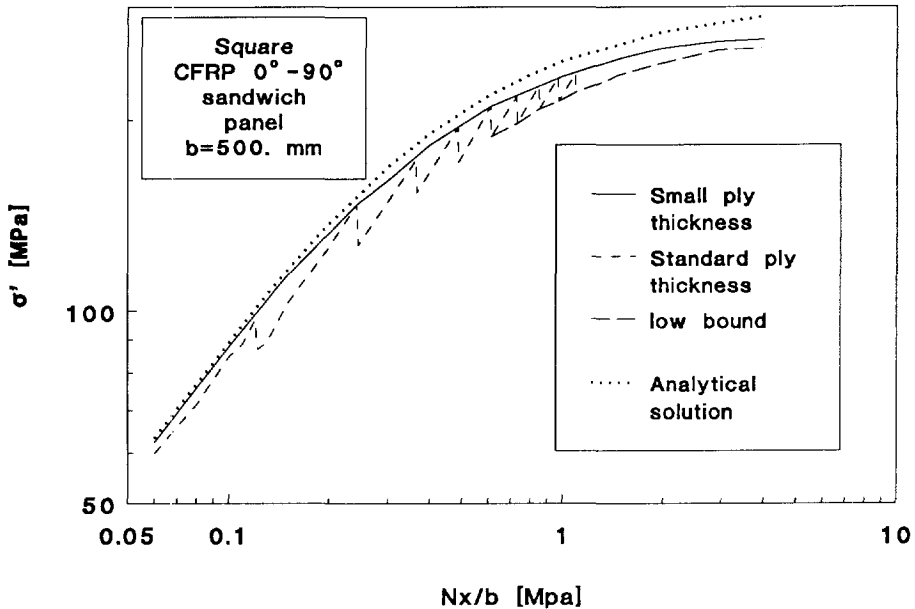

Figure 36 Efficiency of optimum sandwich panels in compression

material has to be added (to each face, because the panel is symmetric). The increased face thickness gives an increased out-of-plane stiffness, and therefore the core thickness can be decreased. Still, there remains a net increase in mass of the panel, and an associated decrease in equivalent stress σ'. Even when the face thickness is constant (eg. for Nx/b≈0.12) the sawtooth has no straight segments, because the core also has a discrete material thickness, of 1.mm (of course, for a honeycomb core material physically there is no such discrete material thickness, this is simply the procedure of SAPANO). Note that now, with the introduction of the discrete thickness, the graph is no longer generic, but applies only to panels with b=500.mm.

In chapter 6 for some (low) values of Nx/b sandwich panels with minimum face and core thickness (so called 'fully stressed designs') were heavier than panels designed for maximum buckling load (neglecting the stress in the faces). This effect is not present here because it applies only to the region below Nx/b≈0.1, and the face thickness (see Figure 26) of the associated optimum panels (as given in chapter 6) is always below 1.mm, the thickness of one ply of material. Figure 37 shows the composition of the discrete optimum panels of Figure 36; the double sawtooth is clearly visible.
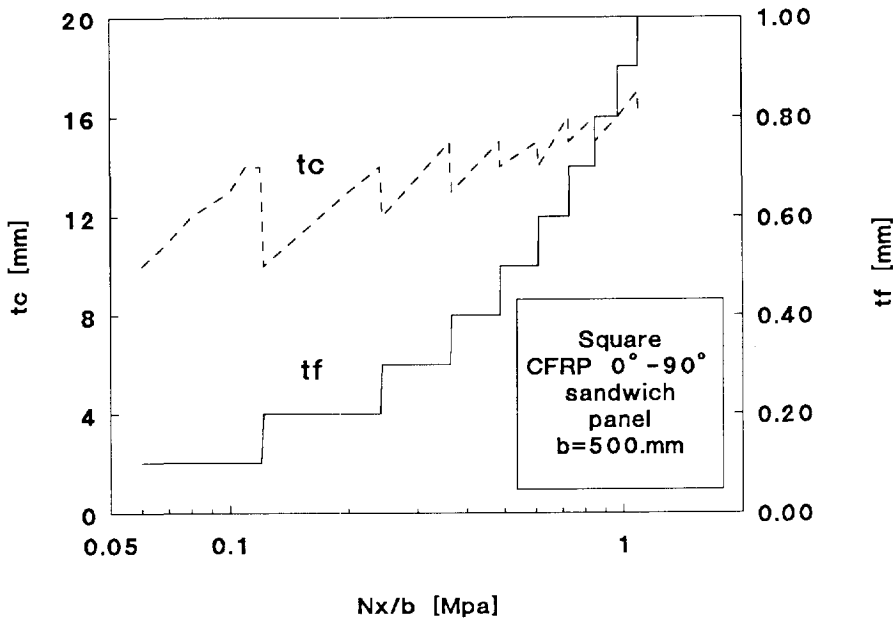

Figure 37 Optimum sandwich panels in compression

When the effect of face bending is included, for small loadings (up to $Nx/b \approx 3.N/mm^2$) the optimum design is equal to that without face bending. For higher loads only a small difference is found. This effect will increase, but for $Nx/b \geq 23. N/mm^2$ a massive CFRP plate performs best; of course at this stage the faces are no longer present. Note that in other cases the effect of face bending may be much more pronounced.

When the loading is applied at a face, the effect of eccentricity does have a significant influence on the performance of optimum sandwich panels, as can be judged from Figure 38. Although a discrete material thickness is used, the sawtooth is different because the optimum panel is now not designed by coincident buckling and material failure, but only on the basis of the eccentricity. This means that, because of the eccentric loading and the consequent out-of-plane deformation of the panel, the optimum panel always has the maximum allowable stress at the top or bottom surface. Figure 39 shows the composition of the optimum panel. Note that the panel is definitely asymmetric; the thickness of the face where the load is applied (face 1) increases much more than that of face 2 as the load is increased. In this way the neutral axis remains near to face 1, limiting the eccentricity.

Up to now, because of the comparison with the analytical results of chapter 6,
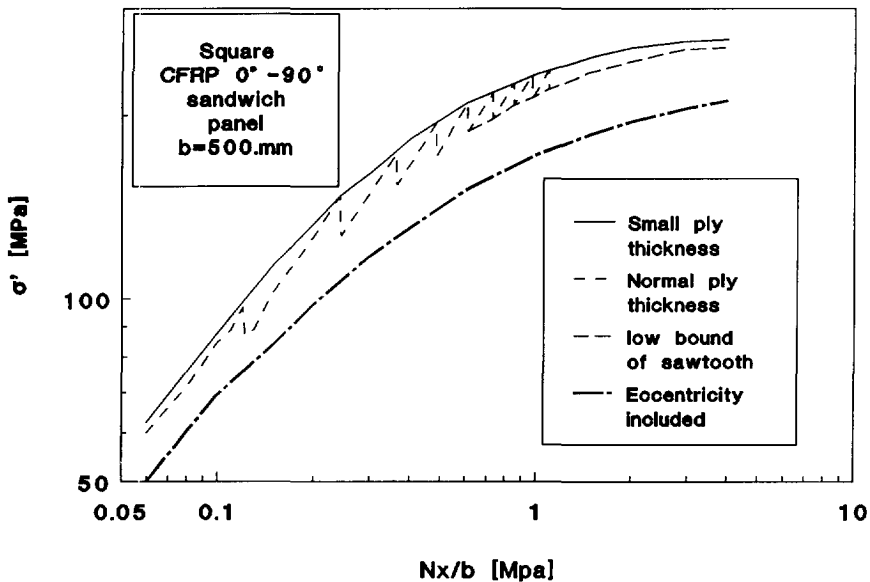
Figure 38 Efficiency of optimum sandwich panels, including the effect of eccentric loading

the faces of the sandwich panel have been of simple composition (0°-90° CFRP material). However, by combining different materials in the faces a more realistic sandwich panel can be obtained, with a much better performance. For example, the following layup could be used:

$$[\pm45°/0°/core/\pm45°]$$

where the compressive loading is considered to be applied at the 0°-layer. This is a typical asymmetric panel, where the second face carries little loading and only provides out-of-plane stiffness against buckling. For a loading of Nx=-500.N/mm (i.e. at Nx/b=1.) the following panel is optimum:

$$[3*0.1 \text{ mm} / 5*0.1 \text{ mm} / 28*1. \text{ mm} / 2*0.1 \text{ mm}]$$

This panel has a greater efficiency than the one with only 0°-90° material in the faces, as Table 21 shows, comparing all optimum panels at Nx/b=1. N/mm^2. The table shows 'reserve factors' (a reserve factor is the ratio between the failure load and the applied load) for the various constraints.
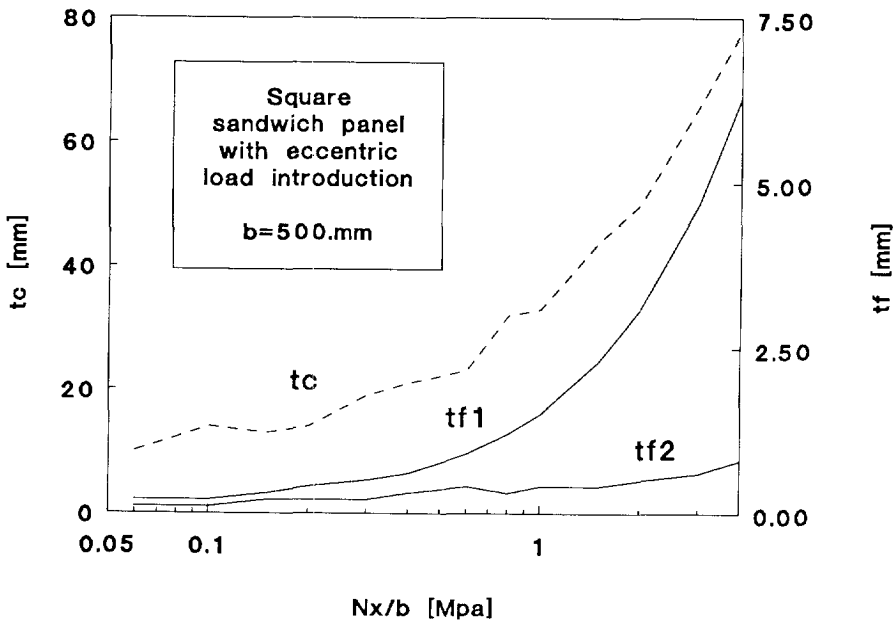

Figure 39 Composition of optimum sandwich panel, including eccentricity

Table 21 Optimum panels at Nx=-500.N/mm, a=b=500.mm

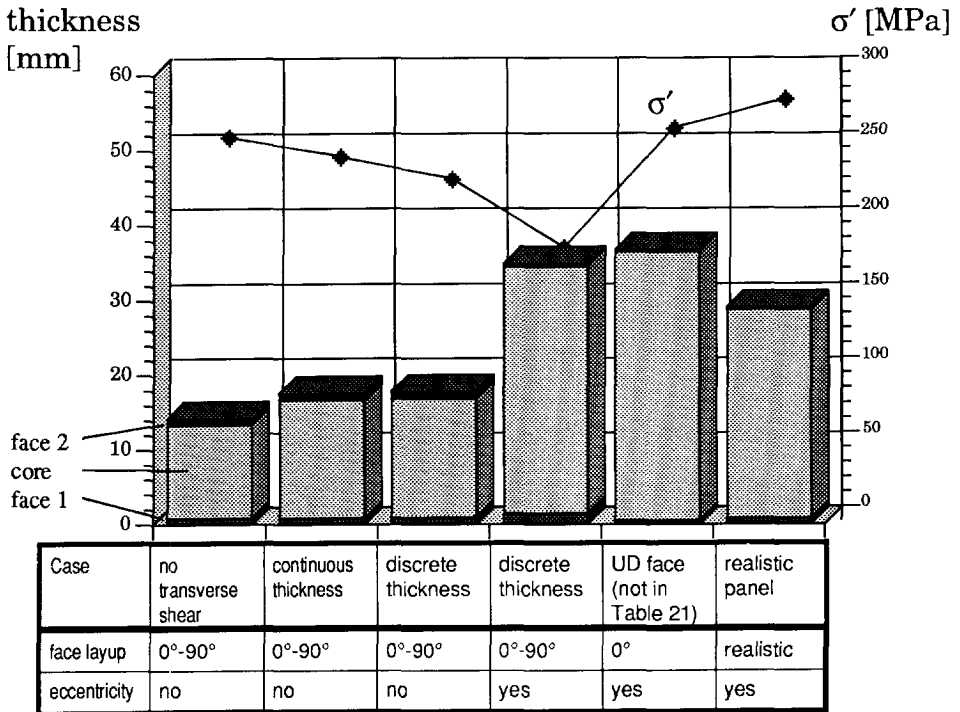| Case	t' [mm]	σ' [N/mm^2]	constraint value		
			res factor in-plane	res factor buckling	res factor eccentric
[0°-90°/core]$_s$ (no TS) (continuous thickness)	2.03	247.	1.00	1.00	-
[0°-90°/core]$_s$ (continuous thickness)	2.14	234.	1.00	1.00	-
[0°-90°/core]$_s$ (discrete thickness)	2.28	219.	1.09	1.07	-
[0°-90°/core/0°-90°] (discrete thickness)	2.89	173.	1.16	2.59	1.0005
[±45°/0°/core/±45°] (discrete thickness)	1.84	272.	1.72	1.66	1.07

Figure 40 Composition of optimum sandwich panels for Nx =-500.N/mm (a=b=500.mm)

Note that in the third case of Table 21 the reserve factor cannot be less than 1.07 or 1.09, because of the discrete thickness. The table shows that eccentricity is an important constraint, as it alone defines the optimum panel (the reserve factors of the other constraints are much higher than 1.00). In Figure 40 these results can be visualized, the composition of the different optimum panels and the equivalent stress σ' of that panel being given.

10.2 Optimum corrugated panels under shear

With COPANO the performance of the optimum corrugated panels, obtained in chapter 6 can be verified. Using the same CFRP ±45° material and using for the present a continuous thickness, the result of Figure 41 is obtained. The continuous line is associated with the analytical result of chapter 6, assuming an efficiency η=1.73 (the maximum value that can be obtained with an isotropic material according to [Rothwell85], see chapter 6). The difference between the
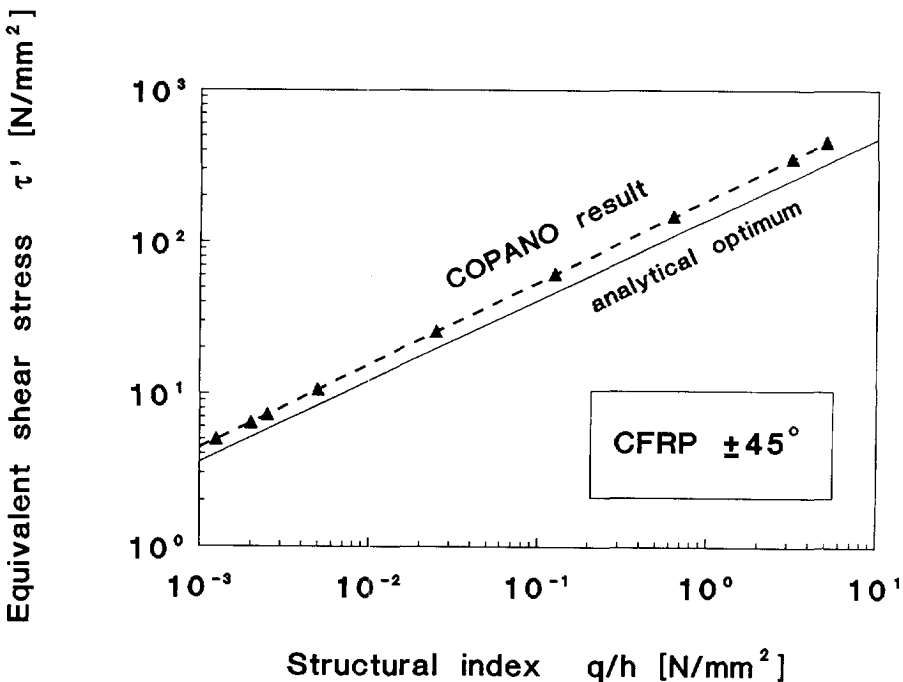

Figure 41 Optimum corrugated panels; comparison of analytical results of chapter 6 with optima of COPANO with continuous thickness

analytical and numerical result is not due (as in the previous paragraph) to differences in mechanical analysis, but only to approximations in Equation (114). First, the assumed efficiency $\eta=1.73$ is only valid for isotropic materials. Also, the power 8/15 (or .833) of q/h in (114) is only an approximation, as was pointed out in chapter 6.

The optimum panels of COPANO given in Figure 41 have a continuous thickness. When a discrete thickness is used, the results no longer form a straight line, as Figure 42 shows. However, there is no 'sawtooth' in the graph, like the graphs of the previous paragraph had; for every discrete thickness, the equivalent shear stress τ' forms a curve that in one point touches that of the optimum panel with continuous thickness. Another difference compared with the sandwich panel result is that, for increasing loading q/h, at the point where adding a layer to the laminate increases the equivalent shear stress τ' material failure is not active; this constraint only becomes active at much higher loads. The active constraints for all optimum designs of which the performance is plotted in Figure 42 are local and overall buckling.

At two loads (q/h=.05 and q/h=3.0) optimum panels are obtained for a more
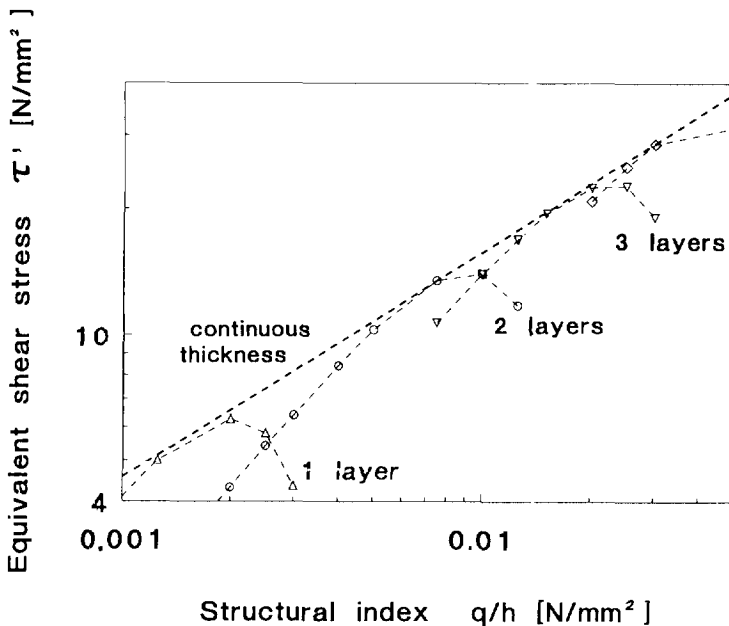

Figure 42 Effect of discrete ply thickness on the performance of optimum corrugated panels

realistic laminate, where 0° material is added to resist possible crushing loads:

$$[\pm45°/0°]_s$$

For a further comparison, a third case is examined in which the 2-layer laminate should have at least 60% of the ±45° material. Table 22 compares the optimum panels and the resulting performance:

Table 22 Optimum corrugated panels (h=1000.mm)

q/h [N/mm^2]	case	$n_{\pm45°}$	$n_{0°}$[†]	b_1 [mm]	b_2 [mm]	θ [deg]	τ' [N/mm^2]
	±45°	5	-	66.	82.	40.	37.9
.050	$[\pm45°/0°]_s$	2	2	39.	52.	35.	52.3
	$[\pm45°/0°]_s$ min 60% ±45°	4	1	69.	75.	23.	42.8
	±45°	32	-	144.	168.	42.	351.
3.0	$[\pm45°/0°]_s$	24	5	124.	137.	34.	419.
	$[\pm45°/0°]_s$ min 60% ±45°	24	5	124.	137.	34.	419.

[†] when the laminate has 2 layers, the 0° layer is at the centre of the symmetric laminate and is therefore the only layer that can have an odd number of material plies. Note that the number of plies is given for the whole of the laminate.

The table shows clearly that the optimum designs are very different to each other; COPANO uses all the variables to obtain the best possible design. Figure 43 shows the performance of these two new cases compared to that of the optimum corrugated panel made of only ±45° material. At q/h=.050 the introduction of 0° material in the laminate increases τ' by 38%. The subsequent constraint, on a minimum ±45° content of 60%, reduces the gain to 13%, which is still significant. At q/h=3.0 the introduction of 0° CFRP increases τ' by 19% in both cases (the constraint to have at least 60% ±45° is not active). Note that the stiffness parameter, defined in Equation (88) of chapter 5 to prevent interaction of the local and overall buckling modes, is not used in the optimization because it is not validated yet for composite materials (the optimum panels for q/h=0.05 all satisfy the constraint SP>1500., the optimum panels at q/h=3.0 do not).

In Figure 43 at the high end of the load range there is a change in the slope of the curve for the optimum panel made of only ±45° material; there the material failure constraint becomes active, that limits τ' to its maximum value equal to the maximum shear stress of the material.
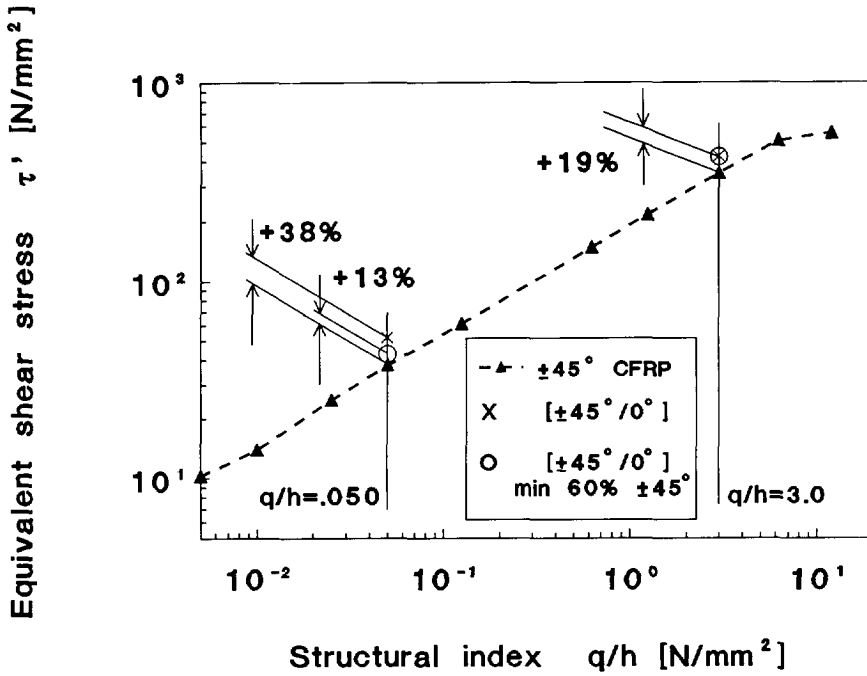

Figure 43 Performance of optimum corrugated panels

11

Conclusions

A number of general conclusions can be drawn with regard to various aspects of the work.

In the first part of the thesis various formulae have been presented, mainly on the stability analysis of composite panels. These are used in the design software developed in this work but are, of course, useful in their own right as well. They do not extend the level of accuracy of existing analysis methods; rather, they have the specific accuracy required in a design environment. Other products of this research are the two computer programs that have been developed, SAPANO and COPANO, for sandwich panels and corrugated panels respectively. Only a few applications of the programs are given in this thesis, but they are shown to be valid tools for the designer. They have, for example, allowed the author to generate very quickly the efficiency charts presented in this thesis.

In a computer program for use in design with composite materials an optimization method to guide the user towards panels with low mass is an essential feature. First of all this is because the design of composite panels can involve a large number of design variables. Even the optimization of the relatively simple layup [±45°/0°/core/±45°] of the sandwich panel of chapter 10 is probably beyond the reach of a designer without such a tool. An optimization method using discrete variables is employed. The primary benefit of using discrete variables is that results of direct practical use are obtained. An interesting feature of the design of composite panels, especially laminates, with discrete variables is the occurrence of many equivalent optima. This allows the user to select from a set of optima, with his own (subjective) constraints. Or the designer can at the outset start with a simple layup, knowing that the performance will in many cases differ little from that of a sophisticated layup.

Of course there are limitations to SAPANO and COPANO; some of these limitations can be removed by continued research leading to further development of the programs; for example, the use of curved panels in

SAPANO, or the use of the full ABD-matrix in the buckling analysis and in the eccentricity analysis. Further verification of the mode interaction in the corrugated panel buckling analysis is also required, especially for composite materials. Such improvements would certainly expand the capability of the programs. Other limitations are more difficult to overcome; for example, production requirements of the optimum designs are certain to introduce penalties (consider the additional material near the flattened edges of a sandwich panel and at the edges of a corrugated panel). But these are aspects that will always fall outside the scope of design tools for the first stage of the design process to assist the designer to make an initial design. In the later stages of design SAPANO and COPANO can be useful as well, because they can easily modify the panel at the level of the *layup* (having the orientations and thicknesses of the separate layers as variables), a feature that the computer codes currently used in those stages (i.e. finite element codes) generally lack.

The concept of a design program has been at the root of this research, where including all relevant types of analysis of the problem at hand coupled with an optimization procedure is more important than the highest degree of accuracy of the analyses. The success of this concept will ultimately be judged by the use made of the developed programs, and the extent to which their development can be continued to meet the changing needs of the designer.

References

[Allen69] H.G. Allen, Analysis and design of structural sandwich panels, Pergamon Press, 1969

[Ashton69] J.E. Ashton, Approximate solutions for unsymmetrically laminated plates, J Comp Mats, vol 3, 1969, pp 189-191

[Bijlaard52] P.P. Bijlaard, On the optimum distribution of material in sandwich plates loaded in their plane, Proc 1st US Nat Congr Appl Mech 1951, pp 373-380

[Bladel88] P.G. van Bladel, Review of formulae for the buckling of simply-supported, orthotropic plates under shear load, including transverse shear effects, TU Delft report LR-571, November 1988

[Bladel89a] P.G. van Bladel, A suitable transverse shear stiffness definition for buckling of laminates and sandwich plates, TU Delft Report LR-603, July 1989

[Bladel89b] P.G. van Bladel, The effect of eccentricities on sandwich plates under in-plane loads, TU Delft Memorandum M-612, August 1989

[Bladel89c] P.G. van Bladel, Discrete variable structural optimization by the complex method, TU Delft report LR-597, June 1989

[Bladel93] P.G. van Bladel, Formulae for the buckling of simply-supported corrugated panels of orthotropic material, TU Delft report LR-716, March 1993

[Bladel94a] P.G. van Bladel, User's manual of the computer program SAPANO, version 3.0, TU Delft memorandum M-696, January 1995

[Bladel94b] P.G. van Bladel, User's manual of the computer program COPANO, version 2.4, TU Delft memorandum M-697, January 1995

[Bleich52] F. Bleich, Buckling strength of metal structures, McGraw Hill 1952

[Box65] M.J. Box, A new method of constrained optimization and a comparison with other methods, Comp J, Vol 8, 1965, pp 42-52

[Chow71] T.S. Chow, On the propagation of flexural waves in an orthotropic laminated plate and its response to an impulsive load, J Comp Mats, vol 5, July 1971, pp 306-319

[ESA94] anon., Structural materials handbook, ESA PSS-03-203 Issue 01, February 1994

[ESDU73] anon., Buckling of flat rectangular orthotropic plates (computer program), ESDU data sheet 73003, Esdu Int London, 1973

[EDSU74] anon., Buckling of corrugated shear webs, ESDU data sheet 74022, Esdu Int London, 1974

[ESDU80] anon., Buckling of rectangular specially orthotropic plates, ESDU data sheet 80023, Esdu Int London, 1980

[Ewing88] M.S. Ewing et al., On the validity of the reduced bending stiffness method for laminated composite plate analysis, Comp Struct, vol 9, 1988, pp 301-317

[Fleury80] C. Fleury and L. Schmit, Dual methods and approximation concepts in structural synthesis, NASA CR-3226, December 1980

[Flügge51] W. Flügge,The optimum problem of the sandwich plate, J of Appl Mech, vol 19 no 1, March 1952, pp 104-108

[Glover93] F. Glover et al, A user's guide to tabu search, Annals of Operational research, vol 41, 1993, pp 3-28

[Hajela89] P. Hajela, Genetic search - An approach to the nonconvex optimization problem, AIAA paper 89-1177-CP

[Housner75] J.M. Housner and M. Stein, Numerical Analysis and Parametric Studies of the buckling of composite orthotropic compression and shear panels, NASA TN D-7996, October 1975

[Jong84] T. de Jong, Mechanica van composietmaterialen - theorie en toepassing, TU Delft report LR-431, June 1984

[Kovařík72] V. Kovařík, Optimum structure of sandwich plates under compressive loading, Acta Technica ČSAV, 1972 no 2, pp 113-136

[Kuenzi60] E.W. Kuenzi and J.J. Zahn, Shear stability of flat panels of sandwich construction, Forest Products Laboratory Report 1560, rev. May 1960

[Leissa87] A.W. Leissa, An overview of composite plate buckling, in Composite structures 4, Proc of ICCS4 (Jun 27-29, 1987), vol 1 Analysis and Design studies, pp 1.1-1.29

[Lekhnitskii68] S.G. Lekhnitskii, Anisotropic plates, Gordon and Breach 1968

[Libove48] C. Libove and S.B. Batdorf, A general small deflection theory for flat sandwich plates, NACA rep 899, 1948

[Middleton92] D.H. Middleton, Composite developments in aircraft structures, Aircraft Engineering 1992, May pp 2-8, June pp 6-11, August pp 10-14, September pp 6-10

[Noor75] A.K. Noor, Stability of multilayered composite plates, Fibre Science and Technology, vol 8, 1975, pp 81-89

[Noor89] A.K. Noor and W. Scott Burton, Assessment of shear deformation theories for multilayered composite plates, Appl Mech Review, vol 42 no 1, January 1989, pp 1-13

[Noor92] A.K. Noor, Mechanics of anisotropic plates and shells - A new look at an old subject, Computers & Structures, vol 44 no 3, 1992, pp 499-514

[Pearce72] T.R.A. Pearce and J.P.H. Webber, Buckling of sandwich panels with laminated face plates, Aeron. Quarterly May 1972, pp 148-160

[Peterson60] J.P. Peterson and M.F. Card, Investigation of the buckling strength of corrugated webs in shear, NASA TN D-424, June 1960

[Plantema66] F.J. Plantema, Sandwich construction, Wiley & Sons 1966

[Rothwell69] A. Rothwell, Optimum fibre orientations for the buckling of thin plates of composite material, Fibre Science and Technology (2) 1969, pp 111-121

[Rothwell85] A. Rothwell, On the efficiency of stiffened panels, with application to shear web design, in D.J. Dawe et al, Aspects of the analysis of plate structures, a volume in honour of W.H. Wittrick, Clarendon Press Oxford 1985

[Shin88] D.K. Shin et al, A penalty approach for nonlinear optimization with discrete design variables, in Discretization methods and structural optimization - procedures and applications (proc of a Gamm seminar, October 5-7 1988 Siegen FRG), Lecture Notes in Engineering, vol 42, Springer-Verlag

[Stamm74] K. Stamm and H. Witte, Sandwichkonstruktionen - Berechnung, Fertigung, Ausführung, Springer-Verlag Wien, 1974

[Sullins69] R.T. Sullins et al, Manual for structural stability analysis of sandwich panels and shells, NASA CR-1457, 1969

[Timoshenko63] S.P. Timoshenko and J.H. Gere, Theory of elastic stability, Mc Graw-Hill 1963

[Vlachoutsis92] S. Vlachoutsis, Shear correction factors for plates and shells, Int J for Num Methods in Eng, vol 33, 1992, pp 1537-1552

[Walden90] D.C. Walden, Applications of composites in commercial airplanes, Structural composites, design and processing technologies, Conference proc. 6th annual ASM/ESD advanced composites conf., Detroit (MI), October 8-11 1990, pp 77-82

[Walsh75] G.R. Walsh, Methods of optimization, Wiley London, 1975

[Whitney69] J.M. Whitney, The effect of transverse shear deformation on the bending of laminated plates, J Comp Mats, vol 3, July 1969, pp 534-547

[Whitney70] J.M. Whitney and N.J. Pagano, Shear deformation in heterogeneous anisotropic plates, J Appl Mech, vol 37 no 4, December 1970, pp 1031-1036

[Whitney87] J.M. Whitney, Structural analysis of laminated anisotropic plates, Technomic 1987

[Wiedemann86] J. Wiedemann, Leichtbau Band 1: Elemente, Springer-Verlag Berlin, 1986

[Wiedemann89] J. Wiedemann, Leichtbau Band 2: Konstruktion, Springer-Verlag Berlin, 1989

[Wiggenraad77] J.F.M. Wiggenraad, The influence of bending-torsional coupling on the buckling load of general orthotropic, midplane symmetric and elastic plates, NLR TR 77126 U, December 1977

[Wittrick52] W.H. Wittrick, Correlation between some stability problems for orthotropic and isotropic plates under bi-axial and uni-axial direct stress, Aero J, vol 4, August 1952, pp 83-92

[Zelst85] R.F.P. van Zelst, Hand calculation method for buckling of composite shell structures, in Proc. of Workshop Composites design for space applications Oct 15-18 1985, ESA SP-243 February 1986, pp 87-93

Samenvatting

Dit proefschrift is een van de resultaten van onderzoek op het gebied van de *synthese* (het ontwerpen) van constructies. Bij gegeven randvoorwaarden moet dan een ontwerp, een constructie gegenereerd worden. Dit vraagt een gedegen kennis van de *analyse* (het gedrag van de constructie), maar deze kennis is niet het doel van het onderzoek. De kennis wordt *toegepast* om nieuwe constructies te ontwikkelen bij gegeven randvoorwaarden. De concrete omgeving van het werk is het *begin* van het ontwerptraject, wanneer alleen nog de randvoorwaarden voor de constructie (belastingen, globale afmetingen) bekend zijn, terwijl de vorm van de constructie en de te gebruiken materialen nog bepaald moeten worden. In het bijzonder is de aandacht gegaan naar *composietconstructies*, omdat deze in toenemende mate gebruikt worden in lucht- en ruimtevaart. Met deze materialen kunnen constructies in het algemeen lichter gemaakt worden, en bevatten zij een kleiner aantal onderdelen. Composietmaterialen in lucht- en ruimtevaart zijn echter niet homogeen (het zijn vezels ingebed in hars) en ze zijn anisotroop (d.w.z. met verschillende eigenschappen in verschillende richtingen). Hierdoor wordt de analyse van deze constructies veel moeilijker. Bovendien is ook het ontwerpen moeilijker, omdat er veel meer vrijheden zijn in een composietconstructie. Niet alleen de uitwendige vorm, maar ook de samenstelling van het paneel zelf (ligging van de vezels in de verschillende delen van de constructie) moet bepaald worden.

Als concrete onderwerpen van het onderzoek zijn *twee types composietpanelen* gekozen die samen het dragende deel van een *vleugeldoos* kunnen vormen, een *sandwichpaneel* als normaalkrachtdragende constructie voor de boven- en onderhuid (met een gladde buitenkant blootgesteld aan de luchtstroming) en een *gegolfde liggerlijfplaat* die met name schuifbelasting draagt voor de voor- en achterligger van de doosconstructie in de vleugel.

De ontwikkelde computerprogramma's SAPANO[‡] en COPANO[‡] zijn, naast dit proefschrift, twee tastbare resultaten van het verrichte onderzoek. In deze programmatuur bestaat een zorgvuldig evenwicht tussen het *analytische* deel en het *synthetische* deel. De analyse moet de essentiële aspecten van het mechanische gedrag beschrijven, maar mag niet zo uitgebreid zijn dat detailinformatie overheerst. Het doel is immers een goed eerste ontwerp te genereren. Van de andere kant ondersteunen de programma's de ontwerptaak, allereerst door een

---

[‡] SAPANO betekent **SA**ndwich **P**anel **AN**alysis and **O**ptimization; COPANO staat voor **CO**rrugated **P**anel **AN**alysis and Optimization.

lage gebruiksdrempel zodat een ontwerper gemakkelijk de verschillende randvoorwaarden kan wijzigen om inzicht te krijgen in het probleem. Tevens is er een numerieke optimalisatiemethode in de programma's aanwezig, omdat het bepalen van het lichtste paneel door het grote aantal vrijheden al gauw buiten het bereik van een menselijke ontwerper ligt.

Deze aandacht voor een evenwicht tussen analyse en synthese heeft niet tot gevolg gehad dat enkel modellen en resultaten uit de literatuur zijn overgenomen. Veel bestaande modellen zijn uitgebreid of aangepast voor composieten. Dit proefschrift kan beschouwd worden als de theoretische handleiding bij deze programma's (voor het gebruik van SAPANO en COPANO bestaan aparte handleidingen, zie [Bladel94a] en [Bladel94b]). Toch zijn de ontwikkelde formules niet alleen van belang voor gebruikers van de programma's, maar zijn zij ook op zichzelf interessant.

Het eerste deel van dit proefschrift beschrijft het analytische deel van de ontwikkelde programmatuur, met formules voor het bezwijken en voor verschillende vormen van instabiliteit (knik) van de panelen. Steeds wordt de constructie als een vlak laminaat (stapeling van laagjes met verschillende eigenschappen) beschouwd. Het mechanische gedrag wordt beschreven met een model van de eerste orde (Reissner-Mindlin-Bollé). In het tweede deel van het proefschrift wordt de synthese van composietconstructies onderzocht. Het eerste hoofdstuk van dit deel bevat formules voor de efficiëntie van optimale sandwichpanelen en gegolfde platen, op basis van de analyse beschreven in het eerste deel. Het tweede hoofdstuk in dit deel beschrijft een numerieke optimalisatiemethode om met behulp van de computer dit zoekproces naar het optimale paneel uit te voeren. Een grote moeilijkheid bij dit zoekproces is dat composietconstructies een discreet optimalisatieprobleem opleveren. De dikte van de verschillende lagen in het paneel kan niet elke willekeurige waarde aannemen, maar enkel een waarde die een veelvoud is van de dikte van het materiaal. Twee concrete resultaten van het onderzoek, beschreven in het derde deel van het proefschrift, zijn de computerprogramma's SAPANO (voor laminaten en sandwichpanelen) en COPANO (voor gegolfde platen). In het vierde deel worden met SAPANO en COPANO een aantal panelen ontworpen. Vergeleken met de panelen ontwikkeld volgens de formules uit het tweede deel van het proefschrift zijn de panelen van de computerprogramma's van grotere waarde, omdat ze meer rekening houden met de concrete randvoorwaarden van het ontwerpprobleem (discrete dikte, accuratere analyse).

Curriculum Vitae

Patrick van Bladel was born in Deurne, near Antwerp (Belgium) on November 30th, 1963. In 1981 he graduated from pre-university education (*humaniora, wiskundige richting*) at the St. Xaverisucollege in Borgerhout, near Antwerp. From 1981 to 1987, together with the last group of students that received the five-year course, he studied Aerospace Engineering at the Delft University of Technology, the Netherlands. His final project for the Master's degree (*ingenieurstitel*) was carried out at the Structures' group, under supervision of prof.dr. A. Rothwell. This project later proved to be a first step towards the PhD thesis, that was started in 1987, as AIO (*assistent in opleiding*) in this same Group, again under supervision of prof.dr. A. Rothwell. The preparation of this thesis was interrupted twice, for a period of work and study at the International Centre *Mystici Corporis* in Loppiano, near Florence (italy) and for health reasons. The author has presented the results of his research work as author and co-author of papers, reports and presentations at several international conferences. Favourite pastimes are water sports and reading, but most of all collaborating to the Focolare Movement's activities promoting solidarity and unity.

Published Papers

Een programma voor optimalisatie van vezelversterkte sandwichpanelen SAPANO, Master's thesis[‡], June 1987

Calculation of the loads on the composite wing of a 105 passenger transport aircraft, P.G. van Bladel, LR[‡] memorandum M-595, April 1988

Review of formulae for the buckling of simply-supported, orthotropic plates under shear load, including transverse shear effects, P.G. van Bladel, LR[‡] report LR-571, November 1988

Discrete variable structural optimization by the complex method, P.G. van Bladel, LR[‡] report LR-597, June 1989

A suitable transverse shear stiffness definition for buckling of laminates and sandwich plates, P.G. van Bladel, LR[‡] Report LR-603, July 1989

The effect of eccentricities on sandwich plates under in-plane loads, P.G. van Bladel, LR[‡] Memorandum M-612, August 1989

Optimization of composite structures, an engineering application, P.G. van Bladel, conference paper, ICOTA'92 Singapore, proceedings p. 850-858

Formulae for the buckling of simply-supported corrugated panels of orthotropic material, P.G. van Bladel, LR[‡] report LR-716, March 1993

Computerized design of fibre composite panels for aerospace applications, P.G. van Bladel, conference paper, XI Polish conference on computer methods in mechanics, 1993, proceedings

User's manual of the computer program SAPANO, version 3.0, P.G. van Bladel, LR[‡] memorandum M-696, January 1995

User's manual of the computer program COPANO, version 2.4, P.G. van Bladel, LR[‡] memorandum M-697, January 1995

In preparation:

SAPANO: A computer program for the optimization of laminated composite sandwich panels, P.G. van Bladel and A. Rothwell

---

[‡] Delft University of Technology, Faculty of Aerospace Engineering